REPORT OF INVESTIGATION 65
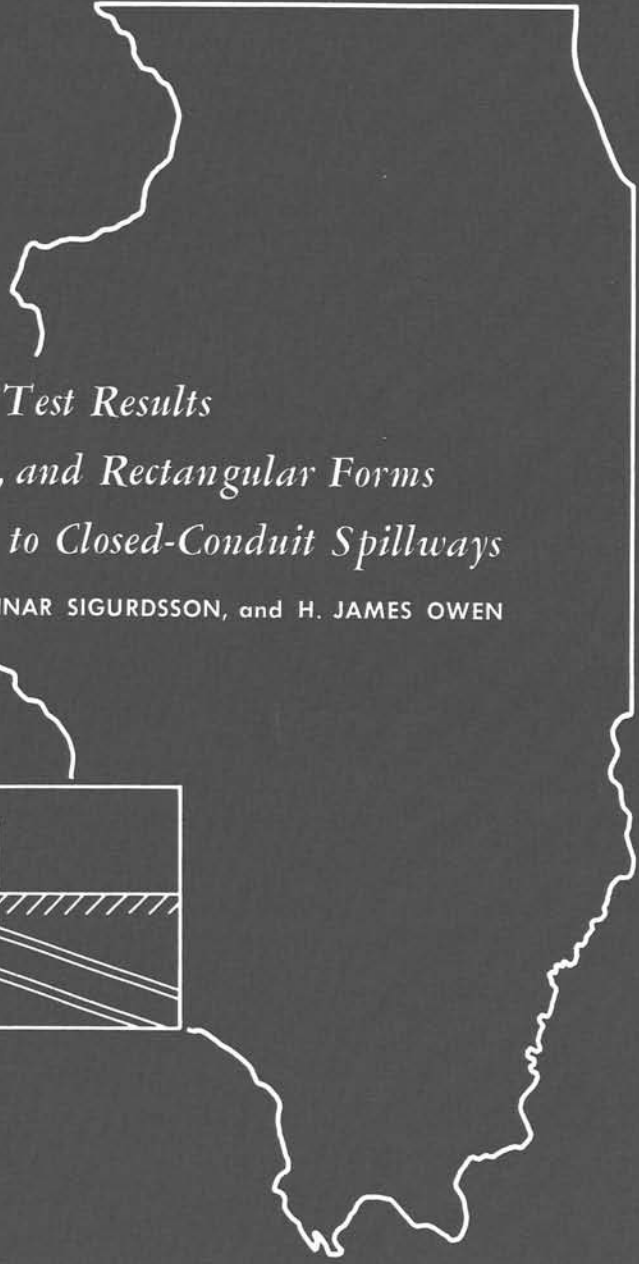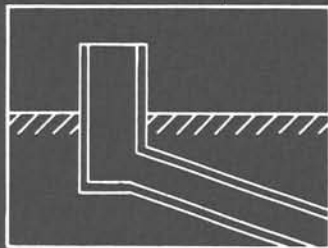
ILLINOIS

DEPARTMENT OF REGISTRATION AND EDUCATION

Model Test Results
of Circular, Square, and Rectangular Forms
of Drop-Inlet Entrance to Closed-Conduit Spillways

by HAROLD W. HUMPHREYS, GUNNAR SIGURDSSON, and H. JAMES OWEN

ILLINOIS STATE WATER SURVEY

URBANA

1970

REPORT OF INVESTIGATION 65

Model Test Results

of Circular, Square, and Rectangular Forms

of Drop-Inlet Entrance to Closed-Conduit Spillways

by HAROLD W. HUMPHREYS, GUNNAR SIGURDSSON, and H. JAMES OWEN

Title: Model Test Results of Circular, Square, and Rectangular Forms of Drop-Inlet Entrance to Closed-Conduit Spillways.

Abstract: Laboratory research studies were performed to develop closed-conduit spillways that have single-valued characteristics and to develop criteria for predicting the minimum hydraulic performance of drop-inlet spillways when vortex formation at the inlet is not controlled. When vortex formation is not controlled, the vortex can be erratic and its occurrence unpredictable. A method is presented for determining the minimum performance of a drop-inlet spillway when the vortex formation is uncontrolled. Also, a method is presented that can be used to determine when a drop-inlet spillway requires an antivortex device for satisfactory hydraulic performance. One effective antivortex device is a horizontal circular antivortex plate properly positioned above the drop-inlet crest. The influence of the antivortex plate on the spillway performance and capacity can be determined from the experimental equation presented. This study shows that the location of a drop-inlet entrance in a reservoir does not affect the spillway performance for normally developed circulation of the flow around the drop inlet when vortex formation is controlled. Experimental weir-flow coefficient equations and the coefficients for full-flow head-loss and nondimensional pressure are presented. Reversible single-valued head-discharge curves and the spillway hydraulic loading can be determined for prototype spillways geometrically similar to the models tested by using these coefficients.

Reference: Humphreys, Harold W., Gunnar Sigurdsson, and H. James Owen. Model Test Results of Circular, Square, and Rectangular Forms of Drop-Inlet Entrance to Closed-Conduit Spillways. Illinois State Water Survey, Urbana, Report of Investigation 65, 1970.

Indexing Terms: Circulation, closed conduit, drop inlet, head-loss coefficient, horizontal plate antivortex device, hydraulic performance, spillway, spillway pressure, surface water resources, vortex, water resource development, weir.

CONTENTS

Model Test Results of Circular, Square, and Rectangular Forms of Drop-Inlet Entrance to Closed-Conduit Spillways

by Harold W. Humphreys, Gunnar Sigurdsson, and H. James Owen

ABSTRACT

Laboratory research studies were performed to develop closed-conduit spillways that have single-valued characteristics and to develop criteria for predicting the minimum hydraulic performance of drop-inlet spillways when vortex formation at the inlet is not controlled. This report presents the results of model tests on circular, square, and rectangular forms of a drop-inlet entrance to a closed-conduit spillway.

When the formation of vortices at the entrance to a drop-inlet spillway is not controlled, the vortex can be erratic and its occurrence unpredictable. The vortex can be so strong that it seriously affects the spillway performance and reduces the spillway capacity, or the vortex can be so weak it has no effect on the spillway performance or capacity. Although the occurrence of the vortex is unpredictable, a method is presented that can be used to determine when a drop-inlet spillway requires an antivortex device for satisfactory hydraulic performance. Also, a method is presented for determining the minimum performance of a drop-inlet spillway when the vortex formation is uncontrolled.

A horizontal circular plate positioned above the drop-inlet crest of a circular drop-inlet spillway is shown to be an effective antivortex device. Also, a properly positioned plate can significantly reduce the head necessary for the spillway to prime and flow full of water when compared with the priming head at the intersection of the usual weir- and full-flow curves. The plate in this position will also influence the head on the drop inlet and the spillway performance in the normal weir-flow range. For a properly positioned plate large increases in spillway discharge can be obtained for very small increases in the reservoir level. The influence of the antivortex plate on the spillway performance and capacity can be determined from the experimental equation presented. The spillway flow conditions associated with the plate are described.

The full-flow head-loss coefficients and the equations for the weir-flow discharge coefficient are given so that prototype spillways similar to the models can be designed with reversible single-valued head-discharge curves.

The nondimensional pressure coefficients presented can be used to determine the prototype pressure distribution and the hydraulic loading on the component parts of the spillway.

The tests with forced circulation, normally developed circulation, and no circulation of the flow around the drop-inlet entrance show the circulation effect on the hydraulic performance of the spillway. When the formation of vortices at the drop-inlet entrance is controlled, the test results for the normally developed circulation are the same as those for no circulation. The test results for forced circulation show a significant effect in the weir-flow range for the flush approach but a very small effect for the deep approach when compared with the test results for normally developed circulation and for no circulation.

INTRODUCTION

Closed-conduit spillways with a drop-inlet entrance are used to convey excess water in a controlled and predictable manner from a reservoir to a channel below the dam. In the past this type of spillway has been called a pipe-drop spillway, closed-conduit spillway, drop-inlet culvert, trickle tube, etc. These spillways are used on the small- to medium-sized reservoirs that have watershed areas varying from a few acres to several thousand acres. The reservoirs are constructed for watershed protection, flood prevention, gully control, water quality improvement, water supply, and recreation. In 1966 there were 1466 dams and reservoirs constructed in Illinois and 49,807 in the United States. Although the number of drop-inlet spillways constructed in conjunction with these dams and reservoirs is unknown, this type of spillway would be applicable to many of them.

A closed-conduit spillway with a drop-inlet entrance is shown schematically in figure 1. The spillway has a horizontal inlet crest at the top of the drop inlet. The drop inlet shown has a uniform horizontal cross section although nonuniform cross sections have been used in the past. A transition joins the drop inlet to a barrel or pipe which conveys the water to an outlet below the dam. The barrel may be on a steep or mild slope.

The State Water Survey has been conducting a generalized
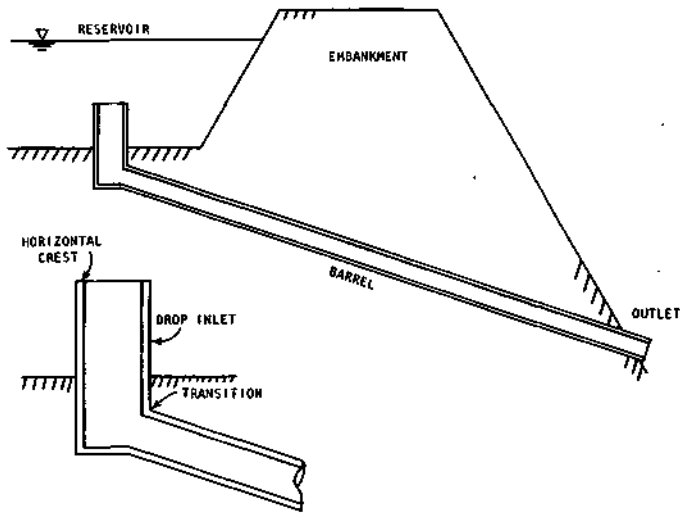
Figure 1. Components of a closed-conduit spillway with a drop-inlet entrance

research program on closed-conduit spillways with a drop-inlet entrance in cooperation with the Agricultural Research Service and the Soil Conservation Service of the United States Department of Agriculture and the University of Illinois Agricultural Experiment Station. The objectives were twofold: 1) to develop closed-conduit spillways that have single-valued hydraulic characteristics; and 2) to develop criteria for predicting the minimum hydraulic performance of drop-inlet spillways when vortex formation at the inlet is not controlled. The second objective required determining the limiting effects of vortices on the drop-inlet head and discharge.

The following dimensions are given to indicate the usual range in the size of the prototype. The prototype structures ordinarily have a barrel ranging from 2.5 to 6.0 feet in diameter. The reservoir level may be as high as 30 feet above the drop-inlet crest in a flood control reservoir. The difference in elevation between the drop-inlet crest and the barrel outlet

may be as small as 10 feet or as large as 100 feet.

The models used in this study do not represent specific spillways. However, the results are directly usable by the design engineer for spillways that are geometrically similar to these models.

This report describes the theory, test apparatus, test procedure, data reduction and analytical methods, model proportions, and test conditions, and presents the results of the tests. The test results include the effects on the spillway performance and capacity of weir control at the drop-inlet entrance of 1) vortices at the drop-inlet entrance, 2) a horizontal circular flat plate antivortex device, and 3) circulation around the drop-inlet entrance. In addition the weir-discharge coefficient, the energy-loss coefficients for the spillway component parts, the pressure distribution in the spillway, and the location of the hydraulic grade line at the barrel exit are presented. Notations for symbols used throughout this report are given in the back *(page 69)*.

Acknowledgments

Part 1. Theory

The basic theory for the hydraulics of a closed-conduit spillway with a drop-inlet entrance has been reported by Blaisdell.[1] In his analysis Blaisdell indicates the sections that control the flow head-discharge relationship may be 1) the inlet, resulting in weir control or orifice control at the drop-inlet crest, 2) the drop inlet, resulting in short-tube control, and 3) the barrel, resulting in pipe control. The flow conditions associated with these control sections are fully described by Blaisdell. Also, it should be noted that the formation of vortices at the entrance to the drop inlet was controlled by using an antivortex device.

The hydraulics of the above controls are also given in the analyses presented in this section. In addition the analyses include the effects of circular antivortex plates for circular drop inlets on the performance of drop-inlet spillways. The derived equations are presented in nondimensional form to make it more convenient to analyze the data and easier for a designer to apply the results.

Weir Control by Drop-Inlet Crest

The rectangular weir formula
$$Q = CL_c h^{3/2} \qquad (1)$$
was used to determine the weir coefficient of discharge. In equation 1, Q is the discharge in cubic feet per second, L_c is the weir crest length in feet, h is the head above the weir crest in feet as shown in figure 2, and C is the customary dimensional weir coefficient of discharge in $(feet)^{1/2}$ per second.

Replacing C in equation 1 by $C_w(2g)^{1/2}$ yields
$$Q = C_w(2g)^{1/2} L_c h^{3/2} \qquad (2)$$
where C^w is a nondimensional weir coefficient of discharge and g is the acceleration of gravity in feet per second per second.

The length of the weir crest, L_c, may be expressed as the product of a constant, k, and a characteristic dimension of the drop-inlet geometry, the constant k depending upon the drop-inlet geometry and the crest shape. For example, for a circular drop inlet with a square-edged crest, $L_c = \pi D_R$, where D_R is the inside diameter of the drop inlet in feet and $k = \pi$. For a square drop inlet with a square-edged crest $L_c = 4B$, where B is the inside dimension of a side of the drop inlet in feet and $k = 4$. The value of k for other crest and drop-inlet geometries would be computed from direct measurements of the crest and drop inlet.

Equation 2 is made nondimensional for a circular drop inlet with a square-edged crest by substituting πD_R for L_c and dividing both sides of the equation by $D_R^{5/2}(2g)^{1/2}$ to yield
$$Q/D_R^{5/2}(2g)^{1/2} = C_w \pi (h/D_R)^{3/2} \qquad (3)$$
Equation 3 was used for determining C_w. The parameters $Q/D_R^{5/2}(2g)^{1/2}$ and h/D_R were used for plotting the head-discharge curves for circular drop inlets.

For a square drop inlet with a square-edged crest $L_c = 4\,B$,

where B is the inside width of the drop inlet and $k = 4$. Using these quantities the nondimensional form of equation 2 becomes
$$Q/B^{5/2}(2g)^{1/2} = C_w 4(h/B)^{3/2} \qquad (4)$$
The general form of equation 4 for square or rectangular drop inlets with or without a square-edged crest is
$$Q/B^{5/2}(2g)^{1/2} = C_w k (h/B)^{3/2} \qquad (5)$$
where B is the inside width of a rectangular or square drop inlet.

The parameters $Q/B^{5/2}(2g)^{1/2}$ and h/B were used to plot the head-discharge curves for square and rectangular drop inlets.

Orifice Control by Drop-Inlet Crest

The discharge formula for orifice flow at the drop-inlet crest is
$$Q = C_0 A_0 (2g)^{1/2} h^{1/2} \qquad (6)$$
where C_0 is the orifice-discharge coefficient, A_0 is the horizontal area of the drop inlet in square feet, and h is the head or water surface elevation above the inlet crest as shown in figure 3. C_0 must be determined experimentally for the spillways that exhibit orifice control.

For a circular drop inlet $A_0 = \pi D_R^2/4$. Substituting this value for A_0 in equation 6 gives
$$Q = C_0(\pi/4)D_R^2(2g)^{1/2}h^{1/2} \qquad (7)$$
Equation 7 may be arranged in a nondimensional form by dividing both sides of the equation by $D_R^{5/2}$ and $(2g)^{1/2}$ to yield
$$Q/D_R^{5/2}(2g)^{1/2} = C_0(\pi/4)(h/D_R)^{1/2} \qquad (8)$$
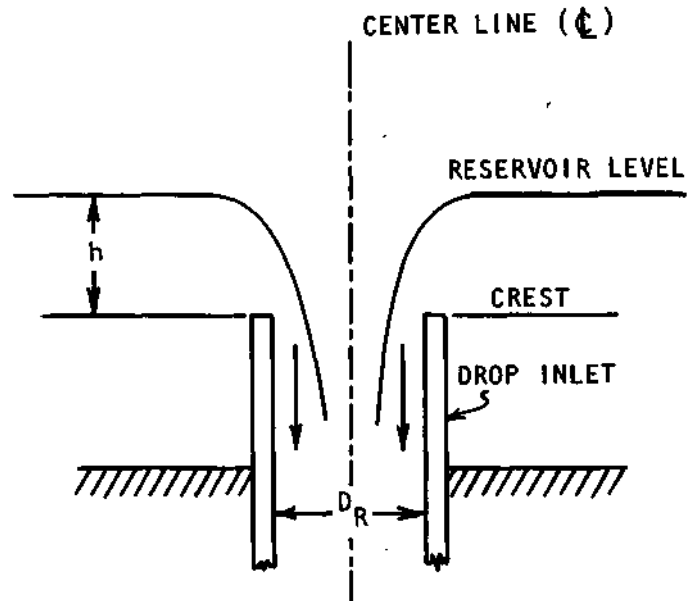
Figure 2. Definition sketch for weir control at the drop-inlet crest
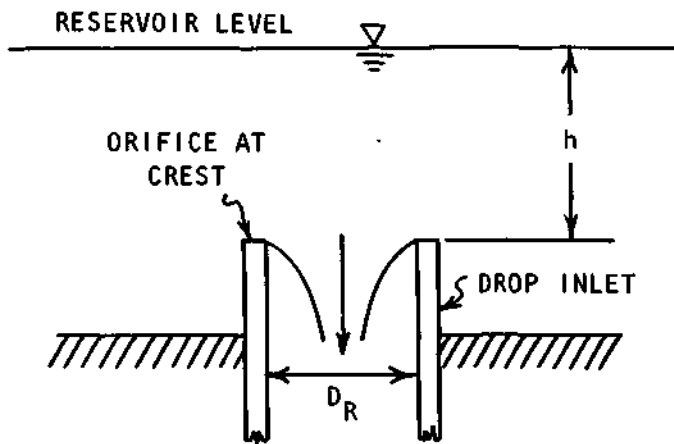
Figure 3. Definition sketch for orifice control at the drop-inlet crest
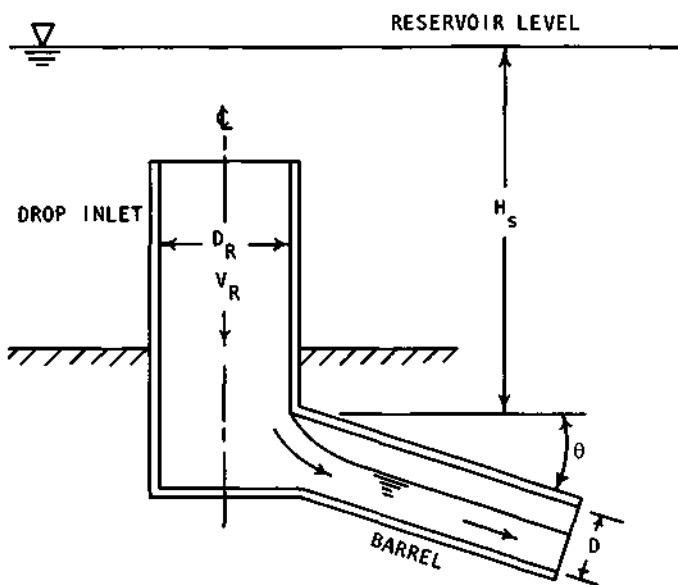
Figure 4. Definition sketch for short-tube control by drop inlet

For a square drop inlet $A_0 = B^2$. Therefore, substituting this relationship in equation 6 and rearranging in a manner similar to that for the circular drop inlet gives the nondimensional head-discharge equation for the square drop inlet:

$$Q/B^{5/2}(2g)^{1/2} = C_0(h/B)^{1/2} \qquad (9)$$

For a rectangular drop inlet the horizontal dimensions are the width B and the length cB, where c is a multiplying factor to obtain the horizontal length of the drop inlet. Therefore, $A_0 = cB^2$. Substituting this value for A_0 in equation 6 and rearranging as for the circular drop inlet gives the nondimensional head-discharge relationship for rectangular drop inlets as

$$Q/B^{5/2}(2g)^{1/2} = c_0 c(h/B)^{1/2} \qquad (10)$$

Short-Tube Control by Drop Inlet

The discharge equation for short-tube control by the drop inlet is

$$Q = C_8 A_R H_8^{1/2} \qquad (11)$$

which is the same as used by Blaisdell.[1] In equation 11 C_8 is the coefficient of discharge, A_R is the horizontal area of the drop inlet in square feet, and H_s is the distance from the reservoir surface to the point in the drop inlet where the water separates from the drop-inlet wall, in feet, as shown in figure 4. C_8 must be determined experimentally for spillways that exhibit short-tube control.

Equation 11 may be arranged in a nondimensional form for circular, square, and rectangular drop inlets by the same procedure used in the analysis for orifice control.

The resulting head-discharge equation for circular drop inlets is:

$$Q/D_R^{5/2}(2g)^{1/2} = C_8(\quad/4) \quad (H_8/D_R)^{1/2} \qquad (12)$$

For square drop inlets, the equation is:

$$Q/B^{5/2}(2g)^{1/2} = C_8(H_8/B)^{1/2} \qquad (13)$$

For rectangular drop inlets, the equation is:

$$Q/B^{5/2}(2g)^{1/2} = C_8 c(H_8/B)^{1/2} \qquad (14)$$

Full Flow

The following assumptions were made for the full-flow analysis:

1) The velocity head of approach is neglected because the velocity of approach in the test tank is very small.
2) The kinetic energy correction factor a is assumed to be 1.0.
3) The flow from the barrel outlet discharges freely into the atmosphere.
4) No air is passing through the spillway.

The equation for full flow is determined by selecting the datum at the centerline of the outlet (figure 5a) and applying Bernoulli's equation from the free surface in the approach channel to the point where the hydraulic grade line intersects the plane of the freely discharging outlet. This yields

$$h+Z=(V_B^2/2g)+(K_E V_R^2/2g)$$
$$+ \quad <f_R \quad \{[L_R + \quad (D_R/2) \quad - \quad (D/2)]/D_R\}(V_R^2/2g)>$$
$$+ \quad (K_T V_B^2/2g) \quad + \quad [f(L/D)(V_B^2/2g)]$$
$$+ \quad [\quad D-(D/2)]cos \quad 6 \qquad (15)$$

where h is the water surface elevation in feet above the drop-inlet crest, Z is the difference in elevation in feet between the drop-inlet crest and the center of the barrel outlet, V_B is the average velocity in the barrel in feet per second, V_R is the average velocity in the drop inlet in feet per second, K_E is the head-loss coefficient for the entrance to the drop inlet, f_R is the Darcy-Weisbach resistance coefficient for the drop inlet, L_R is the height of the drop inlet in feet, D_R is the circular drop-inlet diameter in feet, D is the barrel diameter in feet, K_T is the head-loss coefficient for the transition between the drop inlet and the barrel, f is the barrel resistance coefficient, L is the length of the barrel in feet, is the proportional part of the barrel diameter above the invert where the hydraulic grade line pierces the plane normal to the barrel axis at the barrel exit, 6 is the slope of the barrel in degrees, and g is the acceleration of gravity in feet per second per second.

The terms h, V_B, K_E, V_B, K_T, f and in equation 15 were computed from experimental measurements. The items Z, L_R,
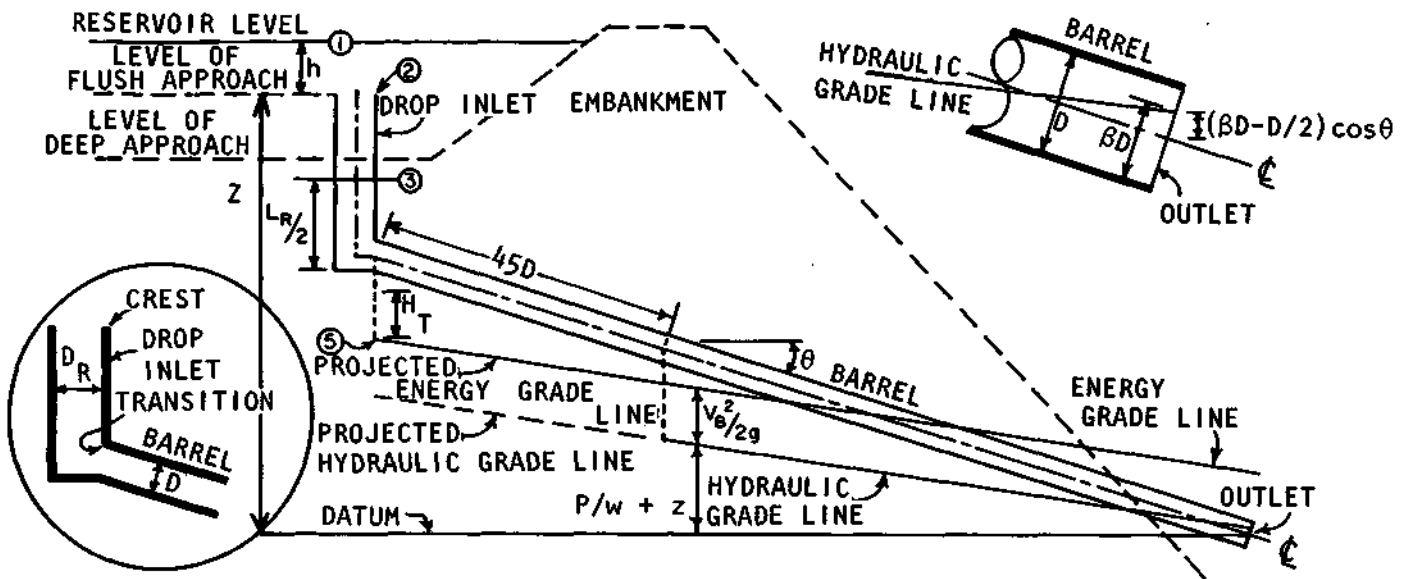
(a) DISTORTED CROSS SECTION
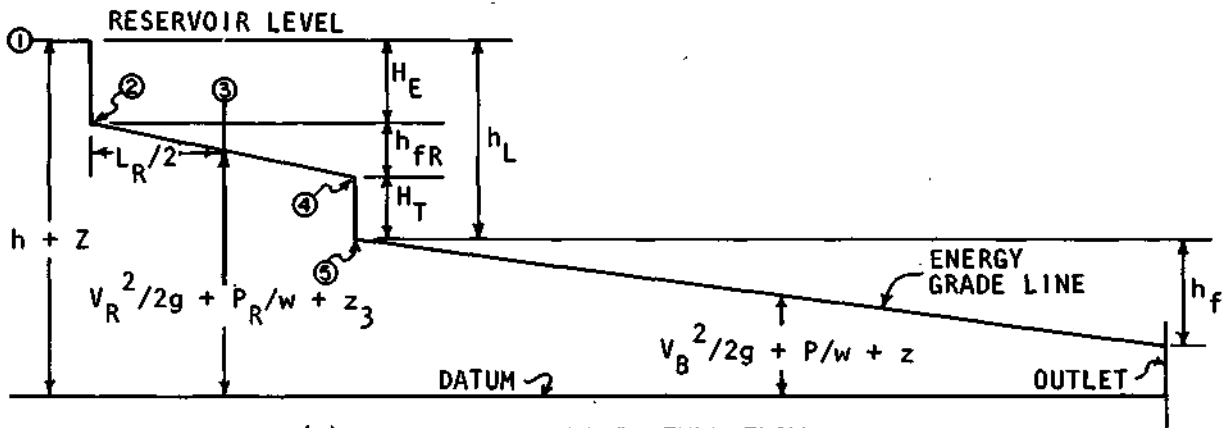
(b) ENERGY GRADE LINE, FULL FLOW

Figure 5. Definition sketch for full flow **for** a closed-conduit spillway with a drop-inlet entrance

D_B, L, and θ were determined by measurement of the spillway. The value of f_R was computed by assuming the drop inlet to be smooth and using the smooth pipe resistance equation [2]

$$1/(f_R)^{1/2} = 2\log \quad R_R(f_R)^{1/2} - 0.8 \qquad (16)$$

for turbulent flow. The term R_R is the Reynolds number for the drop inlet. The Reynolds number for a circular drop inlet is defined as $R_R = V_R D_R/\nu$ where ν is the kinematic viscosity in feet squared per second. The Reynolds number for square or rectangular drop inlets is $R_R = 4V_R R/\quad$ where R is the hydraulic radius in feet of the horizontal section of a drop inlet. The hydraulic radius is defined as the cross-sectional area divided by the wetted perimeter.

The circular drop inlet head-loss term

$$f_R\{[L_R + D_R/2) - (D/2)]/D_R \} \quad (V_R^2/2g) \qquad (17)$$

of equation 15 requires modification for square and rectangular drop inlets. For square and rectangular drop inlets the D_R in the denominator is changed to four times the hydraulic radius. The D_R in the numerator is the width B of a square drop inlet and one-half of the horizontal length of a rectangular

drop inlet. Therefore, the head-loss term for a square drop inlet is

$$f_R\{[L_R + (B/2) - (D/2)]/4R\}(V_R^2/2g) \qquad (18)$$

and for a rectangular drop inlet

$$f_R \quad [L_R + (cB/2) - (D/2)]/4R\} \quad (V_R^2/2g) \qquad (19)$$

where cB is the horizontal length of the rectangular drop inlet.

Head-Loss Coefficients

The head-loss coefficients for the entrance to the drop inlet, the transition between the drop inlet and the barrel, and the barrel Darcy-Weisbach resistance coefficient were determined separately. This was done so the designer could apply the results to drop inlets of heights that are different from those tested.

Entrance Head-Loss Coefficient. Determination of the entrance head-loss coefficient K_E necessitates establishing the energy grade line elevations in the drop inlet. The relatively

5

Figure 6. Definition sketch for variables associated with a horizontal circular plate above the drop-inlet crest

short length of the drop inlet precludes the establishment of uniform flow in the drop inlet and accurate determination of the energy grade line elevation therein. Therefore, the sum of the measured pressure head and the computed velocity head at the midpoint of the drop-inlet height was arbitrarily selected as a point on the energy grade line and as the reference elevation for determining the position of the drop inlet energy grade line (section 3 in figure 5b). Projecting the energy grade line from the energy grade line elevation at section 3 to the drop-inlet entrance, section 2, and subtracting this elevation from the reservoir elevation determines the entrance head loss H_E. The entrance head-loss coefficient was determined from

$$K_E = H_E/(V_R^2/2g) \qquad (20)$$

for each geometry of the entrance to a drop inlet. For example, a horizontal circular plate antivortex device shown schematically in figure 6 and described in the section on "Test Conditions" *(see page 15)* was used to control vortex formation at the drop-inlet entrance for circular drop inlets. For full flow it may be expected that the entrance head-loss coefficient, K_E, determined from equation 20 will depend upon the plate size, its elevation above the inlet crest, and the inlet crest thickness. Therefore, in nondimensional terms

$$K_E = H_E/(V_R^2/2g) = \emptyset \ (D_P/D_R, \ d/D_R, \ t/D_R) \qquad (21)$$

where D_P is the plate diameter in feet, d is the elevation of the bottom of the plate above the drop-inlet crest in feet, and t is the thickness of the drop-inlet crest in feet.

Transition Head-Loss Coefficient. Determination of K_T for the transition between the drop inlet and the barrel required the establishment of the barrel energy grade line elevation as shown in figure 5b. The difference between the barrel energy grade line elevation at section 5 and the drop inlet energy grade line projected from the energy grade line elevation at section 3 to section 4 determines the drop inlet transition head loss H_T. The coefficient of head loss K_T was readily determined from

$$K_T = H_T/(V_B^2/2g) \qquad (22)$$

Combined Entrance and Transition Head-Loss Coefficient. The head-loss coefficients K_E and K_T are combined into a single head-loss coefficient K_R by the equation

$$K_R = (H_E + H_T)/(V_B^2/2g) \qquad (23)$$

Barrel Resistance Coefficient. The Darcy-Weisbach resist-

ance coefficient, $/$, for the barrel was determined from

$$f = (h_f/L)D/(V_B^2/2g) \qquad (24)$$

where h_f/L is the slope of the measured energy and hydraulic grade lines shown in figure 5b and h_f is the head loss in the barrel in feet.

Hydraulic Grade Line Location at Barrel Exit

The location of the hydraulic grade line at the barrel outlet is required to apply equation 15 to the design of a drop-inlet spillway for full flow. The quantity   which relates the hydraulic grade line location to the barrel invert at the barrel exit was computed from experimental measurements. For this computation the hydraulic grade line in figure 5a was projected to the barrel exit and its elevation computed. The elevation of the barrel invert at the exit was subtracted from the hydraulic grade line elevation. The difference between these two elevations was divided by $D cos$ to obtain the value **of**   .

Spillway Pressure Distribution

Cavitation may develop in the prototype if the local pressures are low enough. This low local pressure may occur in the barrel, in the drop inlet, on the drop-inlet crest, or on the horizontal circular flat plate antivortex device. In order to compute the probability of cavitation occurring in the prototype, the local pressures in the barrel were determined at points where the hydraulic grade line deviated from the friction grade line. Also, the local pressures in the drop inlet, on the drop-inlet crest, and on the horizontal circular flat plate antivortex device were determined.

The prototype must be structurally capable of safely carrying all loadings imposed on it. One of these loads is the hydraulic loading which can be determined from the pressure distributions for the component parts of the spillway.

Pressure Distribution in Barrel. The local pressures in the barrel were determined at points where the hydraulic grade line deviated from the friction grade line. Disturbances in the flow due to the barrel entrance will persist for approximately $35D$ from the barrel entrance and cause the hydraulic grade line near the barrel entrance to deviate from the hydraulic grade line established in the zone of uniform flow when this grade line is projected as a straight line to the barrel entrance. The analysis of this variation for a piezometer located near the barrel entrance is based on Bernoulli's theorem. Referring to figure 7 and writing the energy equation from point 'a' to the barrel exit yields

$$(P/w) + (V^2/2g) + z = (P_0/w) + (V_B^2/2g) + z_0 + h_L + [pD-(D/2)]cos \qquad (25)$$

where P/w, $V^2/2g$, and z are the local pressure head, velocity head, and elevation head at point 'a', respectively; P_0/w, $V_B^2/2g$, and z_0 are the pressure head, velocity head, and elevation head at the barrel exit, respectively; h_L is the sum of all energy losses between point 'a' and the barrel exit; and   , D, and 6 are as defined for equation 15.

Rearranging equation 25 and dividing by the barrel outlet velocity head yields

$$[(P/w) + z - \{ D-D/2) \cos - (Po/w) -z_0 - h_L] / (V_B^2/2g) = 1 - (V/V_B)2 \quad (26)$$

The numerator of the left side of equation 26 is the local deviation, h_n, of the hydraulic grade line from the projection of the measured hydraulic friction grade line; therefore this equation may be rewritten in the abbreviated form

$$h_{,,}/(V_B^2/2g) = 1 - (V/V_B)^2 \quad (27)$$

Values of $h_n/(V_B^2/2g)$ were computed from experimental measurements for the entire length of the barrel.

Pressure Distribution in Drop Inlet without Circular Plate Antivortex Device. The local pressures in the drop inlet were computed from experimental measurements. Dimensional analysis was used to group the variables for presenting the pressure distribution. The following analysis is for circular drop inlets.

In figure 8 the datum is taken at the elevation in the drop inlet at which the drop-inlet pressure P is measured. The pressure distribution may be expected to depend upon a distance y below the drop-inlet crest, the drop-inlet diameter D_R, the average velocity V_R in the drop inlet, the unit weight w of the fluid, the acceleration of gravity g, the crest shape, a reference pressure P_1 in the reservoir, and the crest thickness t. The crest thickness was selected so that for full flow the drop-inlet entrance would act as a thick wall pipe for which t is not a pertinent variable. The crest shape was square-edged for all circular drop inlets. The head loss in the drop inlet is neglected as a first approximation.

Therefore, the pressure distribution in the drop inlet may be written as

$$P = (y, D_R, P_1, w, g, V_R) \quad (28)$$

These variables may be combined to yield

$$(P/w)/(V_R^2/2g) = [(y/D_R), \{P_1/w\}/\{V_R y 2g\}] \quad (29)$$

which gives the pressure distribution in the upper portion of the drop inlet. The constant 2 has been arbitrarily included to obtain velocity head.

Designating $AP=P_1—P$ allows rearranging equation 29 in the more convenient form

$$(P/w)/(V_R^2/2g) = (y/D_R) \quad (30)$$

which yields the difference in pressure between the reference pressure in the reservoir and the pressure at the same elevation in the upper portion of the drop inlet.

As the distance y increases downward from the crest the drop-inlet bottom and transition to the barrel may be expected to exert an influence on the pressure distribution. Referring to figure 8, the pressure distribution P near the drop-inlet bottom will depend upon the distance $L_R—y$ from the bottom, the barrel diameter D, the average velocity V_R in the drop inlet, the unit weight w of the fluid, and the acceleration of gravity g. These variables are combined nondimensionally to yield

$$(P/w)/(V_R^2/2g) = [(L_R-y)/D] \quad (31)$$

which gives the pressure distribution in the lower portion of the drop inlet.

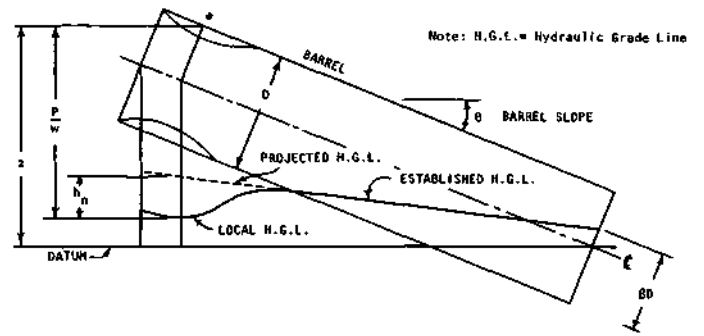The change in pressure AP for a single piezometer in the

Figure 7. Definition sketch for determination of local deviation of the hydraulic grade line in the barrel from the projected hydraulic friction grade line for full flow
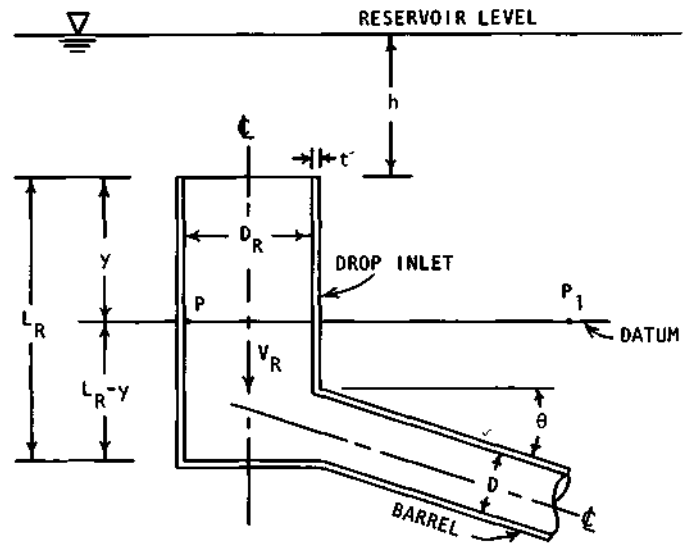

Figure 8. Definition sketch for drop-inlet pressure distribution for full flow

center of the drop-inlet crest may be written as

$$(P/w)/(V_B2/2g) =_0(t/D_R) \quad (32)$$

Equations 30, 31, and 32 are used to present experimental data for the pressure distribution in circular drop inlets with square-edged crests.

For square drop inlets with square-edged crests, the reference length D_R in equation 30 and 32 must be replaced with the inside width B of the drop inlet. Therefore, the pressure distribution functions for square drop inlets become

$$(P/w)/(V_R^2/2g)=_0(y/B) \quad (33)$$

for the pressure in the upper portion of the drop inlet and

$$(P/w)/(V_R^2/2g)=0(t/B) \quad (34)$$

for the pressure at the center of the crest. Equation 31 is applicable for the pressure distribution in the lower portion of the drop inlet.

For rectangular drop inlets, equations 31, 33, and 34 are applicable for presenting experimentally determined pressure distributions on the narrow sides of width B of the drop inlet. The pressure distribution on the long sides of length cB of the drop inlet will depend upon the position along the length. However, since the pressures in this study were measured at the center of the drop-inlet length, equations 31, 33, and 34 are used for presenting these distributions.

Pressure Distribution in Drop Inlet with Circular Plate Antivortex Device. When a horizontal circular plate antivortex device is positioned above the circular drop-inlet crest (figure 6), equations 30, 31, and 32 are insufficient to define the pressure distribution in the drop inlet since the plate can be expected to influence the pressure distribution. Therefore these equations must be expanded to include the circular plate diameter D_P and the plate clearance d above the drop-inlet crest. The effect of the plate size and position on the drop inlet pressure distribution may be expressed nondimensionally as

$$(P/w)/(V_R^2/2g) = [(y/D_R),(D_P/D_R),(d/D_R)] \quad (35)$$

for the pressure in the upper part of the drop inlet, as

$$(P/w)/(V_R^2/2g) = [(L_R-y)/D, (D_P/D_R), (d/D_R)] (36)$$

for the pressure in the lower part of the drop inlet, and as

$$(P/w)/(V_R^2/2g) = [(t/D_R), (D_P/D_R), (d/D_R)] \quad (37)$$

for the pressure for a single piezometer in the center of the drop-inlet crest.

Pressure Distribution on Circular Plate Antivortex Device. The local pressure on the underside of the circular plate antivortex device was computed from experimental measurements. Dimensional analysis was used to group the variables for presenting the pressure distribution.

In figure 6 the datum is taken at the elevation of the underside of the plate. The distribution of the local pressure P on the bottom of the plate may be expressed as

$$P = (V_R, w, g, D_P, d, r, P_1, t) \quad (38a)$$

where r is the radial distance from the plate center to where the local pressure P is measured. Designating $\Delta P = P_1 - P$ allows rearranging equation 38a in the more convenient form

$$(P/w)/(V_R z/2g) = [(r/D_R), (d/D_R),$$
$$(D_P/D_R), (t/D_R)] \quad (38b)$$

which yields the difference in pressure between the reference pressure in the reservoir and the pressure at the same elevation on the underside of the circular plate antivortex device. The constant 2 has been arbitrarily included to obtain velocity head.

Spillway Head-Discharge Curve with Circular Antivortex Plate

The horizontal circular antivortex plate can be placed close enough to the drop-inlet crest to influence the head-discharge relationship for the spillway in the normal weir-flow range. This has been reported by Blaisdell and Humphreys.[3] They noted that as the spillway discharge increased the reservoir level rose to the level of the antivortex plate and sealed the entrance to the drop inlet. Larger discharges resulted in an air-water mixture being discharged through the spillway with a very small increase in elevation of the reservoir water level. Air flow ceased when the discharge was sufficient to maintain full water flow in the spillway.

The effect of the circular flat plate shown in figure 6 on the head-discharge curve in the air-water flow range may be expressed as

$$h = (Q, D_R, d, L_0, g, t) \quad (39)$$

where the plate overhang L_0 is the horizontal distance the plate extends beyond the outer edge of the drop-inlet entrance. Equation 39 may be rearranged to yield nondimensionally

$$h/D_R = 0[(d/D_R), (L_0/D_R),(t/D_R), Q/D_R 5/2(2g)^{1/2}] \quad (40)$$

The constant $2^{1/2}$ has been arbitrarily included for convenience in plotting the head-discharge curves.

Size of Circular Plate for Vortex Control

To be effective for vortex control a horizonal circular antivortex plate must be large enough to close the air core of the free vortex. Using the plate to eliminate the air core should permit water to occupy this space and result in a larger spillway discharge for a given head on the drop inlet.

The diameter of the horizontal circular plate required to control the formation of vortices at the circular drop-inlet entrance was unknown. Therefore the following analysis was made to get an indication of a plate diameter that would probably prevent the vortex from forming.

Vortex Profile. Figure 9a shows a profile for the surface of a free vortex. The geometric variables are given in figure 9, and the datum is shown at the elevation of the inlet crest. Assuming no energy loss, the equation for a stream line on the free surface of the vortex is

$$z_1 + V_1^2/2g = z + V^2/2g \quad (41)$$

The elevation z_1 of the free surface of the vortex is at the limit of the vortex influence. Theoretically this limit of influence is at infinity, and the free surface of the vortex approaches the reservoir level asymptotically.[4] However, from
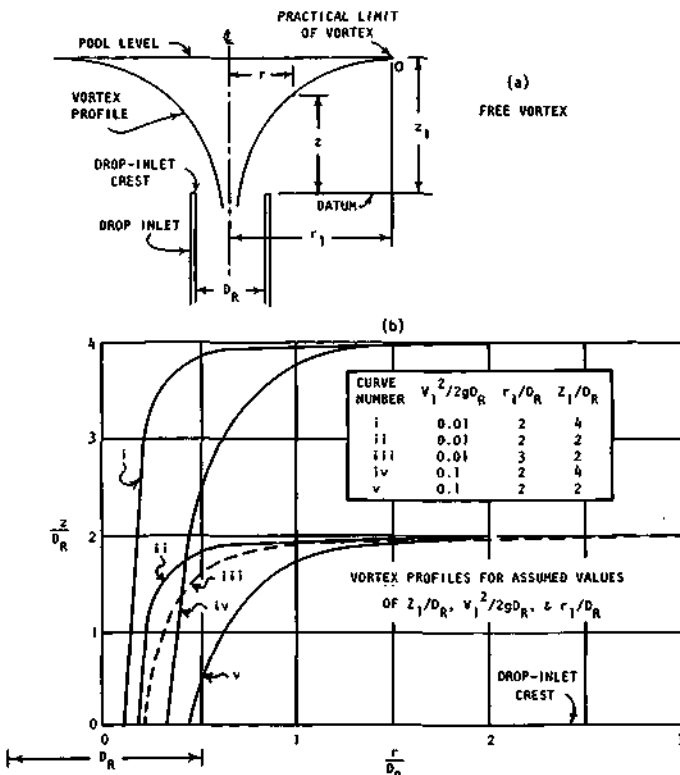

Figure 9. Definition sketch for free vortex above the drop-inlet entrance

a practical standpoint this limit is reached a few drop-inlet diameters from the vortex axis. V_1 is the tangential velocity of the vortex at elevation z_1 and a radial distance r_1 from the vertical axis of the vortex. The velocity V is the tangential velocity of the free surface at elevation z and at a radial distance r from the vertical axis of the vortex.

The velocity distribution for a free vortex is

$$V = T/r \tag{42}$$

where T is the circulation constant dependent upon the strength of the vortex.

The velocity at z_1 is $V_1 = r/r_1$. Elimination of T between this equation and equation 42 yields

$$V = V_1 \qquad\qquad r_1/r \tag{43}$$

Substituting equation 43 in equation 41 and solving for z gives

$$z = z_1 + \{V_1^2/2g\} - \{V_1^2/2g\}\ (r_1/r)^2 \tag{44a}$$

or

$$z = z_1 + (V_1^2/2g)\ [1-(r_1/r)^2] \tag{44b}$$

Dividing z, z_1, $V_1^2/2g$, r_1, and r in equation 44b by D_R yields

$$z/D_R = (z_1/D_B) + \{V_1^2/2gD_R\}$$
$$< 1 - [(r_1/D_R)/(r/D_R]^2 > \tag{45}$$

which is the nondimensional equation for the surface profile of a free vortex above the drop-inlet crest.

Antivortex Plate Diameter. The free vortex surface profile defined by equation 45 was used as a guide for determining the probable plate diameter D_P/D_R needed to control the vortex. To be useful in this determination the surface profile must be similar to those of vortices that form above a drop-inlet entrance.

The shape of the surface profile will depend upon the boundary values for the quantities $V_1^2/2gD_R$, z_1/D_R, and r_1/D_R. Since typical values for these quantities are unknown, values were assumed to determine the effect of each quantity on the shape of the vortex profile. The assumed quantities are shown in figure 9b along with the computed water surface profiles. If $V_1^2/2gD_R$ and r_1/D_R are constant, varying z_1/D_R moves the profiles vertically as shown in figure 9b curves i and ii and curves iv and v. Varying r_1/D_R for constant values of $V_1^2/2gD_R$ and z_1/D_R moves the profiles horizontally a slight amount as shown in figure 9b curves ii and iii. Examination of curves i and iv and curves ii and v in figure 9b shows that $V_1^2/2gD_R$ has the greatest effect in determining the vortex profile.

The profiles developed for $V_1^2/2gD_R = 0.01$, $r_1D_R = 2.0$, and $Z_1/D_R = 2.0$ or 4.0 (figure 9b curves i and ii) look reasonable when compared with the picture of a characteristic surface profile for an irrotational (free) vortex shown on page 88 of reference 2. These profiles are also similar to those formed above a drop-inlet entrance when compared with figures 19 and 20 in this report.

This analysis of the vortex profile indicates that the probable maximum diameter D_P needed for an antivortex plate is about *1.5r/D_R* or *$3D_R$*. The analysis, however, does not indicate the required elevation above the drop-inlet crest for the antivortex plate to effectively control the formation of vortices. The effect of the plate elevation and the plate diameter on the prevention of vortex formation at the drop-inlet crest must be determined experimentally.

Part 2. Test Procedure and Apparatus

TEST PROCEDURE

The basic test procedure developed by Blaisdell and Donnelly[5] was used in conducting these tests. Using this procedure permitted obtaining all the data required for a complete analysis covering the entire range of flow conditions at a considerable savings in laboratory time. Tests covering the complete range of flow conditions were usually completed in 2 to 3 hours. Conventional methods would have required a minimum of 1 day and probably 2 to 3 days to obtain comparable data.

Tests of this nature are usually conducted by setting a rate of flow, waiting until the reservoir water level has stabilized, and then recording the data. This procedure is satisfactory for weir control since the reservoir level stabilizes rapidly. However, for full-pipe flow a relatively long time is required to stabilize the flow. In the procedure used for these experiments all the data were taken simultaneously "on the run," that is, before the flow conditions were fully stabilized. To do this, the reservoir water level was continuously recorded, and at the instant the manometer measurements were photographed an event pen indicated the time of the run on the water-level recorder chart. The heads on the drop-inlet crest were taken from the water-level recorder chart. Discharges through the spillway were determined by correcting the inflow to the reservoir by ΔQ, the rate of change in reservoir storage. This procedure for taking data "on the run" was a necessity when vortices formed at the drop-inlet entrance because many times this flow condition would not stabilize.

Prior to beginning a series of test runs the test tank was filled to an elevation just below the drop-inlet crest, and the water level was allowed to come to rest. At this elevation, a base line was established on the water-level recorder chart. Also, the elevation of the drop-inlet crest above this water level was established using the point gage in the reference well and a point gage temporarily located over the spillway crest.

in figure 12, when visual observation indicated this was desirable. The bend meter water-air manometer was read and the value recorded along with the water temperature. The inflow control valve was then adjusted for the next run at a slightly higher discharge and the above procedure was repeated. For each successive run the inflow was increased until the spillway flowed full of water. The time required for each run in the weir-flow range was about 5 minutes.

After the spillway flowed full of water, the inflow was greatly increased to fill the test apparatus rapidly to the maximum desired water level. At this water level the inflow was adjusted so the trace on the water-level recorder chart was approximately horizontal, although the trace would generally be slowly rising or falling. To obtain a trace from which the rate of change of storage in the approach channel could be computed, the model was permitted to operate for about 5 minutes, after which the data were taken "on the run." The event pen on the water-level recorder chart was activated simultaneously with the data cameras to photograph the barrel and the drop-inlet manometer boards. The run number was marked on the chart, the bend meter water-air manometer was read, the water temperature was determined, and the spillway flow conditions were recorded. Then a drain valve connected to the bottom of the test section was opened to lower the water level to the elevation desired for the next run. The inflow control valve was adjusted, if necessary, to keep the reservoir water-level trace approximately horizontal. The above procedure was repeated for each successive run at decreasing discharges until the spillway ceased to flow full of water. Each run required approximately 8 to 10 minutes to complete.

For the very small weir flows the inflow control valve was closed and the water in the test apparatus was drained through the spillway. The discharge for these low flows was determined from the slope of the water-level recorder trace.

Vortex Formation at Drop-Inlet Entrance, Controlled

The following test procedure was used when the formation of vortices at the drop-inlet entrance was controlled.

After establishing the base line, a typical series of test runs began in the weir-control range by adjusting the inflow control valve to obtain a small discharge. The trace on the water-level recorder was observed until the trace appeared to be level, which indicated essentially steady-flow conditions. Flow conditions in the spillway were observed and descriptive notes recorded. The event pen on the water-level recorder was actuated and the chart marked to identify the run. At the same time, flow conditions at the drop-inlet crest and part way down the drop inlet were photographed, using the model camera shown

Vortex Formation at Drop-Inlet Entrance, Not Controlled

The following test procedure was used when the formation of vortices at the drop-inlet entrance was not controlled.

A typical series of test runs began in the same manner described for the controlled vortex formation, and the same data were taken and recorded. However, at an indeterminate inflow and head on the spillway the flow condition would change from weir flow to vortex flow. When this occurred, the water level in the test tank would rise and fall in an unpredictable manner, indicating a continuing change in the spillway discharge. Therefore, once the vortex formed it was necessary to operate the model for approximately 15 to 30 minutes without changing the inflow control valve to obtain the head-

discharge data necessary to determine the varying influence of the vortex on the discharge through the spillway. During this time period the inflow rate to the reservoir was assumed to be constant. This assumption of constant inflow was checked for the initial tests by reading the bend-meter manometer several times to determine if the fluctuating reservoir had any effect on the manometer reading. At times no difference in manometer readings was observed, and at other times a small difference in manometer readings, always less than 1 percent, was noted. This small percentage difference would cause the assumption of constant inflow to be in error by 0.5 percent or less since the flow rate through the bend meter varies as the square root of the manometer reading. Therefore, the assumption of a constant inflow rate to the reservoir for any valve setting was considered satisfactory.

The discharge through the spillway was calculated in the same manner as described for full flow when the vortex formation at the drop-inlet entrance was controlled. For identification, the water-level recorder chart was marked at the beginning and end of the 15-30 minutes period. The water-level chart was also ma'rked during this time period. At the instant the bend-meter manometer reading was observed and recorded, flow conditions at the drop inlet were photographed, the water temperature was recorded, and notes of the observed flow conditions were recorded. At the time of each successive inflow valve adjustment to increase the inflow rate the water-level recorder chart was marked. This procedure continued until the vortex effect was insignificant.

After the vortex effect became insignificant, the inflow was greatly increased to fill the test apparatus rapidly to the maximum desired water level. At this water level the inflow control valve was adjusted until the trace on the water-level recorder chart was approximately horizontal. Although a long slender vortex could form at the high heads and carry small amounts of air through the spillway, there was no effect on the spillway capacity and care was taken to insure that no air was in the spillway when the piezometric data were photographed. The procedure for taking the data for these full-flow runs was identical to that previously described for the full-flow runs when the formation of vortices was controlled. The above procedure was repeated for each successive run at decreasing discharges until the formation of vortices had a significant effect on spillway discharge.

It was not necessary to continue the test at successive decreasing discharges until the spillway flow was weir control.

Early in the program tests were made that began with weir control and continued for increasing discharges to significant vortex effects, insignificant vortex effects, and full flow; then at decreasing discharges from full flow to significant vortex effects and weir control. The test results were the same for both sequences.

Reduced Full-Flow Spillway Capacity

The tailgate at the barrel outlet was used for several series of tests to reduce the spillway full-flow capacity to values below the ungated capacity. The purpose was to determine the effect of spillway capacity on the performance of the spillway. The test procedure was the same as described above.

Conducting reduced full-flow capacity tests on closed-conduit spillways by using a tailgate at the barrel outlet is a quick and efficient method to simulate the effect of various barrel slopes on the spillway performance without actually reducing the barrel slope. However, the researcher should be cautioned against the indiscriminate use of the tailgate. The tailgate can reduce the spillway full-flow capacity to such an extent that the flow conditions in the barrel will not represent the barrel-flow conditions for an ungated spillway. When this occurs, the abnormal flow conditions in the barrel will have an uncertain influence on the flow conditions at the drop inlet.

In the weir-flow range for an ungated spillway with the barrel on a mild or steep slope, hydraulic jumps or slugs form in the barrel and move in the downstream direction to discharge freely at the barrel outlet. These moving hydraulic jumps suck air through the spillway to the outlet. When the tailgate at the barrel outlet is used to reduce the spillway capacity a small amount, the hydraulic jumps formed in the barrel move toward the outlet and carry the air in the spillway to the outlet in the same manner as with an ungated spillway. Continuing to reduce the spillway capacity by closing the tailgate will result in a tailgate position which traps air in the barrel. Also, the hydraulic jumps may no longer move in the downstream direction and remove the trapped air from the barrel. In fact, they may move in the upstream direction, as was observed in several tests. The upstream movement of the hydraulic jumps with the trapped air will affect the head on the spillway crest. This head effect on the head-discharge curve is in the transition between the weir and full-flow curves and is not predictable. The head-discharge results are also different in this transition for rising and falling heads.

<div align="center">

TEST APPARATUS

</div>

The test apparatus was designed specifically for making model studies of closed-conduit spillways with a drop-inlet entrance. The design was based on the test program requirements and past experience of Blaisdell and Donnelly[5] in the development of similar test apparatus at the St. Anthony Falls Hydraulic Laboratory.

The test apparatus is shown in figures 10, 11, and 12. The test section is rather large and the water enters quietly from a stilling basin to provide excellent approach conditions. Glass side and end walls of the test section permit observation of the flow conditions in the model. The barrel is supported on a steel beam that has slope adjustments. The laboratory recirculation
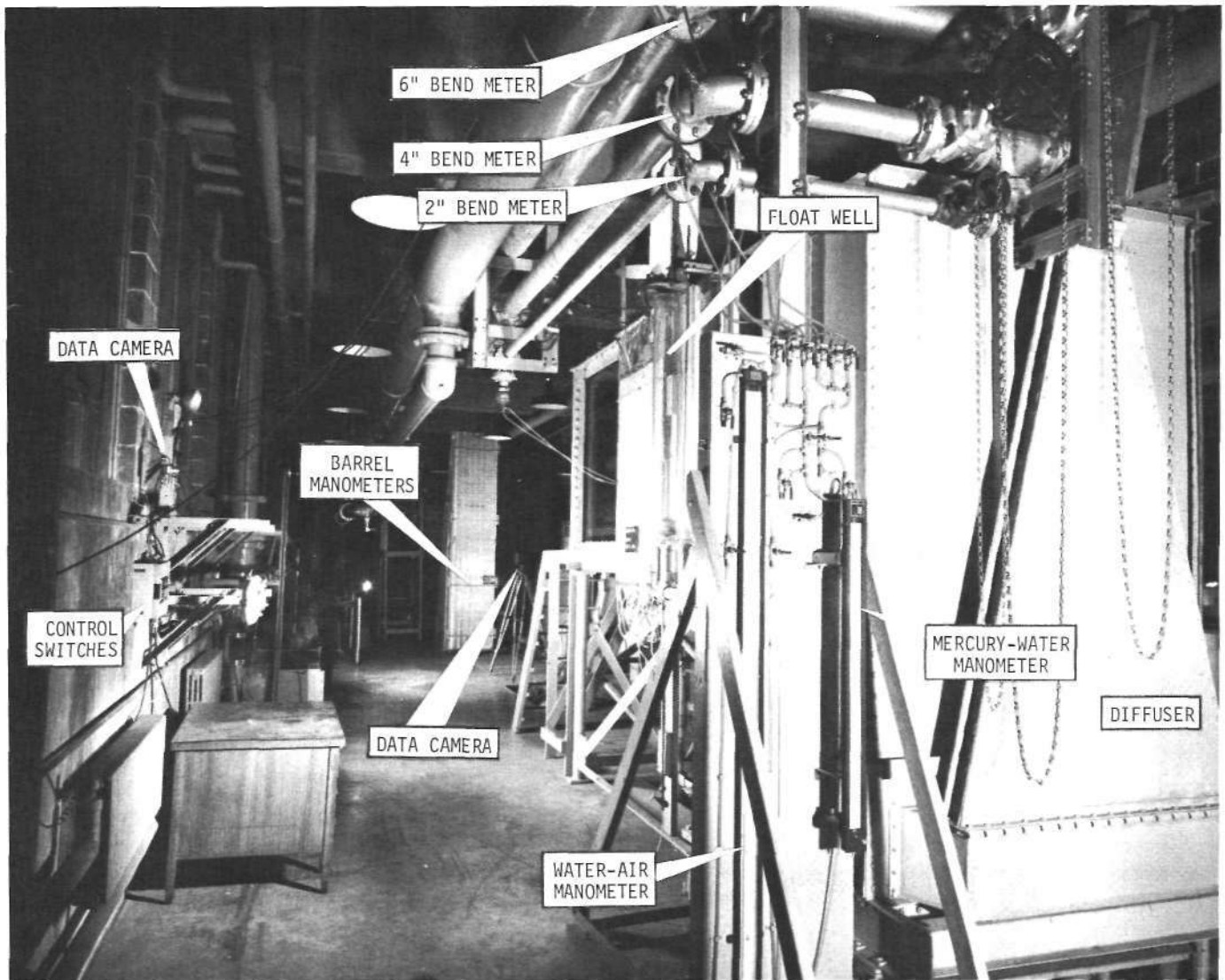
Figure 10. Test apparatus looking downstream

system supplies water to the test apparatus. Flows are measured with calibrated bend meters. Water levels in the test section are continuously recorded on a chart. Piezometric heads within the drop inlet and barrel are recorded by photographing the manometers, and flow conditions in the drop inlet are also photographed.

The steel test tank supported on steel pipe columns consists of a stilling basin, a transition section, and a test section with glass side walls and a glass end wall. The stilling basin is 5 feet wide, 4 feet long, and 8 feet 10 inches deep. The bottom of the stilling basin is 4 feet 4 inches below the bottom of the test section. A transition section 5 feet wide and 1 foot 3 inches long joins the stilling basin and the test section. The bottom of the transition section joining the downstream vertical side of the stilling basin and the bottom of the test section has a radius of 1 foot 3 inches. The test section is 5 feet wide, 9 feet long, and 4 feet 6 inches deep. The test section floor has an opening 2 feet by 2 feet centered 2 feet 6 inches from the downstream glass end wall. The well beneath this opening is 1 foot 2 inches deep and has clear plastic side walls on the

two sides parallel to the length of the test section.

Figure 10 is a view looking downstream from upstream of the stilling basin. Water is supplied from the laboratory recirculation system[6] through one of three parallel galvanized steel pipes, each with a bend meter and a control valve, to the diffuser outside the tank. The bend meters are 2. 4. and 6 inch standard black cast iron flanged elbows, cadmium plated for corrosion protection. An 80-inch water-air differential manometer is used to measure the piezometric head difference between the inside and outside curves of the elbows.[7] Each bend meter was calibrated in place by measuring the discharge volumetrically. The indicated precision is between 1 and 2 percent. Periodic checking of the bend meters shows their constants remained within $+0.5$ percent of their original value after 3 years.

The diffuser shown in figure 10 expands from a section 4 by 8 inches at the top to 4 by 48 inches at the bottom in a vertical distance of 6 feet 10 inches. The bottom of the diffuser has a connection to the stilling basin which permits the water to enter through an opening 1 foot high and 4 feet 7.5

inches wide into the lowest 1 foot of the upstream side of the stilling basin. A perforated plate with 1-inch diameter holes covering this opening, combined with the relatively deep stilling basin and the rounded floor transition into the test section shown in figure 11, results in the flow leaving the stilling basin and entering the test section quietly and uniformly. The glass panel at the downstream end of the test section can be seen in figure 12. The upper portion of the drop inlet can be seen through the glass panel.

The barrel of the spillway shown in figure 12 is a polished lucite pipe having a nominal inside diameter of 3 inches and a length of 25 feet (100D). The pipe passes through a 0-ring sealed connection in the end of the well in the test section. Sections of the lucite pipe are connected with couplings that also have 0-ring seals. The entire pipe is supported on a steel beam 25-feet long which in turn is supported on three adjustable supports. The barrel slope can be adjusted from 0 to 32 percent.

The flow from the barrel outlet discharges freely into a laboratory floor channel and is returned to the laboratory recirculation system. An adjustable tailgate at the barrel outlet permits the spillway capacity to be reduced to any desired discharge that is less than the normal ungated full-flow capacity.

The water-level stage in the test section is continuously recorded on a Stevens Type M water-level recorder chart. The stage is recorded at full-stage scale and the chart speed is 36 inches per hour. A border pen at the bottom of the chart marks each minute and is also used to mark events such as the run number and the taking of photographs. The 6.5-inch diameter recorder float well shown in figure 11 is connected to the test section with a 2-inch diameter pipe to insure rapid response of the recorder to changes in the water surface level.

The reference point gage well is installed parallel with the float well, but all heads were taken from the recorder chart. To determine the pressures in the drop inlet, piezometers are located on the drop-inlet crest, in the side wall, and at the bottom of the drop inlet. These piezometers are connected by clear tygon tubing to the 0.5-inch diameter glass manometer tubes grouped together in front of the ruled manometer board shown in figure 11. The ruled lines on this manometer board are scribed at 0.02-foot intervals.

Clear water is used in the glass manometer tubes, but is made to appear colored for ease of identification by attaching a narrow strip of colored plastic tape lengthwise to the back of the glass tubes. This manometer board is also used to measure the pressure on the underside of the circular horizontal antivortex plate.

Piezometers are located at equally spaced intervals along the barrel to determine the pressure in the barrel and to determine the hydraulic grade line. At each station along the barrel, except for the single-crown piezometer near the barrel entrance, four piezometer holes are drilled at 90-degree intervals around the barrel periphery. A sleeve sealed by 0-rings and having a machined interior groove is located at each station to manifold the four piezometer holes to obtain the average piezometric head. The manifolds are connected by clear tygon tubing to the 0.5-inch diameter glass manometer tubes grouped together in front of the barrel manometer board as shown in figure 10. The meniscus of the water in these manometers is sharp, clear, and easily identified. Therefore it is not necessary to use coloring in the water. The manometer board is milk white lucite with lines scribed at 0.02-foot intervals. These
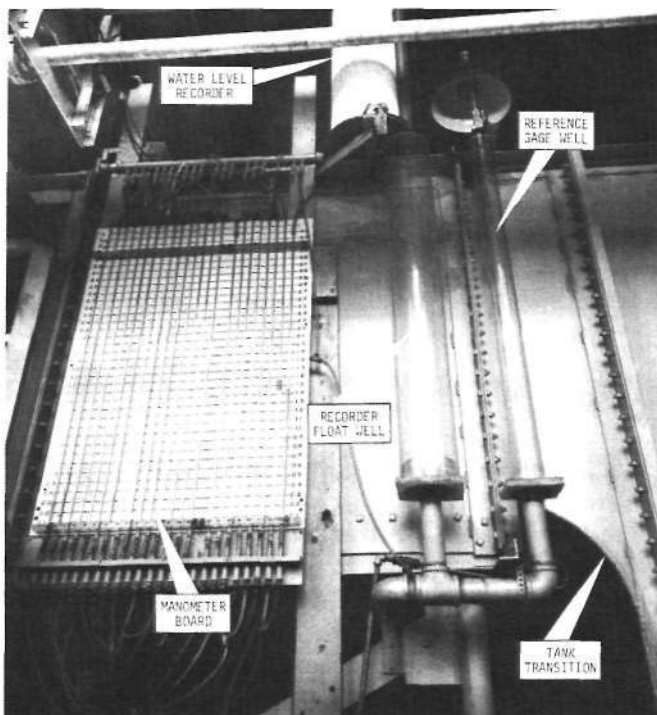

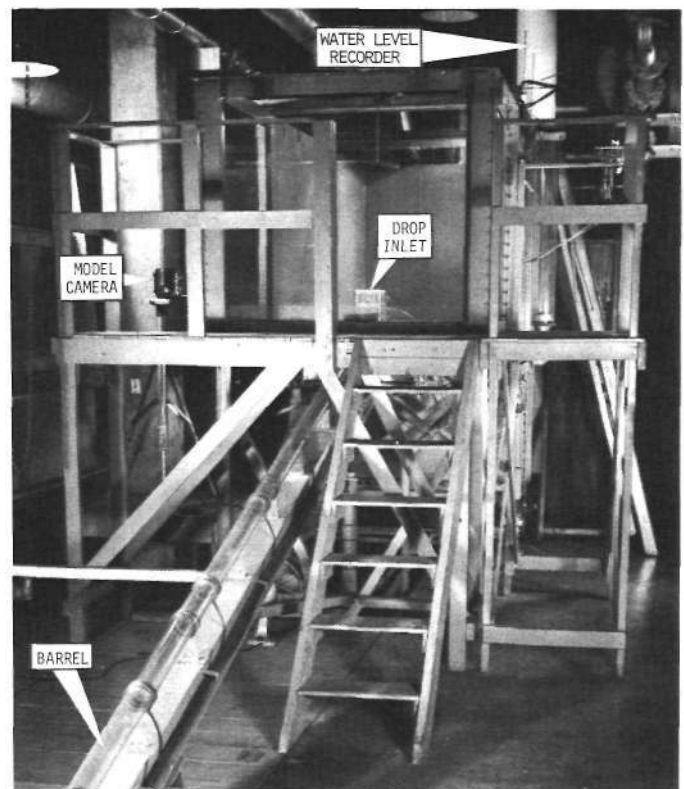Figure 11. Instrumentation on side of the test tank

Figure 12. Test apparatus looking upstream

13

scribed lines are dyed black using black enamel diluted with chloroform.

The piezometric data and the flow conditions are recorded photographically. Piezometric data are recorded only for the full-flow runs. Flow conditions in the drop inlet are photographed when it is desirable. The drop-inlet manometer board shown in figure 11 is illuminated by flood lights in front of the board. The lucite manometer board for the barrel pie-zometers is back lighted using fluorescent lights. The drop inlet is lighted from below through the plastic side of the test section described above. The cameras shown in figures 10 and 12, and the event pen on the water-level recorder are tripped simultaneously from a single control switch. All data are permanently recorded on films or a chart except the bend meter readings, water temperature, and the notes made by the observer of flow conditions in the spillway.

DATA REDUCTION AND ANALYTICAL METHODS

Most of the analyses of the data were performed on an electronic digital computer. However, the calculations for the pressure distributions in the drop inlets and under the horizontal antivortex plates were made with a desk calculator.

The first step in preparing the data for analysis was to take the data from the water-level recorder chart. The drop-inlet crest elevation on the chart was established, then the instantaneous head, h, for each run was measured vertically on the chart from the drop-inlet crest elevation to the water-level trace. The rate of change in storage in the test tank, AQ in cubic feet per second, was determined by measuring the slope of the water-level trace. The slope was obtained directly as AQ by using a template on which lines were scribed for various values of AQ. The second step was to read the piezometric heads by projecting the photographic negatives on a screen and tabulating the readings.

The values of h and AQ obtained from the charts, the piezometric readings, viscosity, run numbers, and the bend meter water-air differential manometer readings recorded during the test constituted the raw data. These data along with a number of constants describing the physical characteristics of the model spillway were assembled in the proper form for the computer program.

The computer program converted the input data into:
1) The nondimensional parameters for plotting head-discharge rating curves for the entire range of discharges.
2) The nondimensional weir-discharge coefficient, C_w, for the weir-flow range.
3) The nondimensional values of K_E, K_T, K_B, f, , R_B, RR, and $h_n /(V_B^2/2g)$ for the spillway flowing full of water.
4) The values of $V_R^2/2g$ and $V_B^2/2g$ for full flow.

Standard computational procedures were programmed for the computer to obtain the output items listed above. However, since K_T, K_B, f, , and $h_n /(V_B^2/2g)$ were dependent upon the barrel hydraulic grade line, a description of how the hydraulic grade line was established is in order.

The hydraulic grade line was determined for a barrel having a diameter equal to the average diameter of the barrel. Therefore, since the actual barrel diameter at each piezometer station was slightly different from the average diameter, a velocity head correction to the actual piezometer reading was necessary to obtain the piezometric head for a barrel of uniform diameter. The corrected piezometric head for each station was determined from:

$$[(P/w)+z]_{av} \quad = \quad [(P/w)+z] + (V_B^2/2g) \quad [(D_{av}/D)^4 - l]$$

(46)

where $[(P/w)+z]_{av}$ is the piezometric head at the station for a barrel of uniform diameter, $[(P/w)+z]$ is the actual piezometric head at the station, V_B is the average velocity for the barrel of uniform diameter, D_{av} is the average barrel diameter, and D is the actual diameter of the barrel at the station.

The corrected piezometric heads determined from equation 46 for stations 45D, 55D, 65D, 75D, 85D, and 95D from the barrel entrance were used in establishing the hydraulic grade line by the method of least squares to obtain the "best fit" straight line.

MODEL PROPORTIONS

The model proportions for the drop inlets and barrels are given in table 1. The models were constructed of clear polished lucite with one exception; the barrel for drop inlet A was a standard 2-inch diameter galvanized steel pipe positioned on the horizontal. The barrel slope for all other models was 17.5 degrees below the horizontal.

The horizontal inlet crests to the drop inlets are either square or quarter round. The square crests have sharp edges around the outside and inside peripheries of the drop inlet. The quarter-round crests have a radius equal to one-half the crest thickness, and the rounding tangent to the top of the crest and the inside vertical surface of the drop inlet whereas the outside periphery of the drop-inlet crest is sharp-edged.

Each drop inlet has a uniform horizontal cross section with the dimensions given in table 1.

The inverts of the circular drop inlets A through G, the square drop inlets H through K, and the rectangular drop inlet 0 were horizontal with the dimensions of each invert being the same as those of the drop inlet horizontal cross section. The rectangular drop inlets L and N each had a half-round bottom with the horizontal invert parallel to the horizontal length of each drop inlet and the radius of each half-

Table 1. Model Drop-Inlet Spillway Proportions

Drop inlet	Nominal dimensions (inches)	Actual dimensions (ft)	Horizontal length	Crest Shape	Radius	Thickness t/D_R or t/B	Length L_c/D_R or L_c/B	D_R/D	B/D	L_R/D	L_R/D_R or L_R/B	Transition Shape	Radius	D (ft)	Z/D	L_B/D	Remarks
	Circular D_R	D_R															
A	3	0.2486		Square		0.0838	π	1.443		33.90	23.45	Round	0.121D	0.172	33.4	53.2	Horizontal barrel, steel
B	3	0.2507		Square		0.0824	π	1.007		5.022	4.986	Round	0.167D	0.2489	34.68	100.36	
C*	3.5	0.2882		Square		0.0752	π	1.158		5.017	4.333	Round	0.167D	0.2489	34.60	100.11	
D*	4	0.3310		Square		0.0625	π	1.330		5.022	3.776	Round	0.167D	0.2489	34.68	100.37	
E*	5	0.4150		Square		0.0750	π	1.667		5.022	3.012	Round	0.167D	0.2489	34.73	100.50	
F	6	0.4943		Square		0.0880	π	1.986		5.022	2.529	Round	0.167D	0.2489	34.68	100.34	
G	8	0.6611		Square		0.0468	π	2.656		8.035	3.025	Round	0.167D	0.2489	37.71	100.42	
	Square B	B															Barrel slope 17.5° below horizontal for drop inlets B--O
H*	4.5	0.3763		Square		0.0454	4.00		1.512	5.022	3.322	Round	0.167D	0.2489	34.67	100.35	
I*	5.25	0.4370		Quarter round	t/2	0.0929	4.381		1.756	5.001	2.849	Sharp edge		0.2489	34.68	100.43	
J	6	0.5017		Square		0.0380	4.00		2.016	5.022	2.492	Round	0.167D	0.2489	34.67	100.35	
K	7.5	0.6222		Quarter round	t/2	0.0668	4.268		2.500	7.512	3.005	Sharp edge		0.2489	37.18	100.41	
	Rectangular B		Horizontal length														
L	3x6	0.2528	0.5010	Quarter round	t/2	0.3983	7.601		1.016	4.970	4.893	Sharp edge		0.2489	34.65	100.44	Half-round horizontal bottom
M	3x6	0.2524	0.5017	Quarter round	t/2	0.4122	7.619		1.014	4.980	4.911	Sharp edge		0.2489	34.66	100.44	Half-round bottom, same slope as barrel L_R/B & L_R/D based on drop-inlet height at transition to barrel
N	3x12	0.2463	1.0006	Quarter round	t/2	0.2568	11.191		0.990	4.998	5.050	Sharp edge		0.2489	34.64	100.31	Half-round horizontal bottom
O	3x6	0.2471	0.5007	Square		0.3360	6.057		0.993	5.022	5.059	Top half round Bottom half sharp edged	0.167D	0.2489	34.66	100.30	Square posts at corners Side of square = c, post height = $\frac{5}{8}B$
O-t																	Drop inlet O without corner posts

*Models tested with deep and flush approach-

Note See table 4 for circular antivortex plate proportions for circular Drop inlets

round bottom being one-half the width of each drop inlet. The invert for the half-round bottom of drop inlet M was an extension of the barrel on the same slope as the barrel invert.

The transitions between the drop inlets and the barrels were either well-rounded or sharp-edged. Each well-rounded transition had the radius given in table 1 with the rounding tangent to the inside vertical surface of the drop inlet and the inside barrel surface. For each sharp-edged transition the entrance to the barrel was flush with the inside vertical surface of the drop inlet. The barrel invert for each transition inter-sected the drop-inlet invert at the inside edge of the drop-inlet vertical surface.

The barrel was connected on the downstream side of each drop inlet with the barrel aligned so its extended center line intersected the drop-inlet vertical center line in a vertical plane of symmetry. This plane of symmetry was perpendicular to the short side of the rectangular drop inlets.

The proportions of the horizontal circular antivortex plates used for testing with circular drop inlets A, C, and E are given in table 4.

TEST CONDITIONS

Test conditions are presented for: 1) deep approach channel, 2) flush approach channel, 3) horizontal circular antivortex plates, and 4) circulation around the drop-inlet entrance. Test conditions and test results are given in tables 2, 3, 4, 5, and 6. A detailed description of each of the four test conditions is given below.

Deep Approach

Test conditions and results for the deep approach channel are given in table 2. The drop-inlet crest was located at a distance equal to or greater than *2D* above the approach channel. The flow approached the drop-inlet entrance from all directions, and the circulation around the drop inlet was permitted to develop freely. The sheet metal cross vanes were used to inhibit the formation of a vortex at the drop-inlet

entrance for each series indicated. The orientation of the vanes on the inlet crest is also shown. The downstream end of the test tank is on the right of the vane orientation sketch.

Flush Approach

The drop-inlet crest was located at the same elevation as the approach channel. Only the drop inlets shown in table 3 were selected for testing with a flush approach. The flow approached the drop-inlet entrance from all directions, and the circulation around the drop inlet was permitted to develop freely. The sheet metal cross vanes were used to inhibit the formation of a vortex at the drop-inlet entrance for each series indicated. The orientation of the vanes on the drop-inlet crest is also indicated in table 3. The downstream end of the test tank is on the right of the vane orientation sketch.

Table 2. Test Results for Deep Approach

Drop inlet* Circular	Series	K_E	K_T	K_R	$R_B \times 10^{-5}$	$h_n/(V_B^2/2g)$	Barrel crown pressure minimum observed Barrel station	Average percent $\frac{f_{meas} - f_{smooth}}{f_{smooth}}$ Barrel	Approach depth	Remarks**
A	58	0.48							2D	No antivortex device
	59	0.60							2D	12x12x6-inch vanes on crest ⊠
B	64	0.64	0.46	1.15	3.17	-0.23	0.53D	0.7	2D	12x12x6-inch vanes on crest ⊠
	70A	0.69	0.51	1.23	1.34	-0.40		2.4	2D	Series 70A--70E, same vanes
	70B	0.63	0.51	1.19	2.10	-0.13		-0.6	2D	as for series 64, tailgate
	70C	0.63	0.50	1.18	2.32	-0.18		-0.7	2D	used to change full-flow
	70D	0.63	0.50	1.18	2.49	-0.18		-0.7	2D	capacity
	70E	0.64	0.46	1.16	2.64	-0.14		0.0	2D	
C	43	0.61	0.28	0.65	3.53	-0.32	0.49D	1.4	2D	12x12x6-inch vanes on crest ⊠
	44	0.52	0.27	0.59	3.76	-0.34		1.4	2D	No antivortex device
	45	0.59	0.36	0.73	1.15	-0.50		3.4	2D	No antivortex device, tailgate used to reduce full-flow capacity
D	24	0.56	0.21	0.41	3.54	-0.24	0.46D	1.4	2D	12x12x6-inch vanes on crest ⊠
	25	0.50	0.23	0.39	3.72	-0.10		1.4	2D	No antivortex device
	26	0.55	0.29	0.48	1.28	-0.42		2.3	2D	No antivortex device, tailgate used to reduce full-flow capacity
	69A	0.56	0.23	0.43	3.35	-0.22		0.0	2D	Series 69A--69H and 69J, 12x12x6-inch vanes on crest, tailgate used to change full-flow capacity
	69B	0.56	0.22	0.42	3.17	-0.25		0.7	2D	
	69C	0.56	0.24	0.44	3.03	-0.23		0.0	2D	
	69D	0.56	0.23	0.43	2.97	-0.69		0.0	2D	
	69E	0.57	0.23	0.43	2.83	-0.30		0.7	2D	
	69F	0.56	0.23	0.43	2.74	-0.33		0.0	2D	
	69G	0.55	0.23	0.42	2.46	-0.29		-0.7	2D	
	69H	0.56	0.23	0.43	2.24	-0.34		-2.0	2D	
	69J	0.54	0.24	0.43	1.93	-0.34		-1.3	2D	
E	2	0.56	0.12	0.20	3.72	0.09	0.43D	4.3	2D	12x12x6-inch vanes on crest ⊠
	3	0.49	0.10	0.17	3.95	0.07		3.7	2D	No antivortex device
	38	0.56	0.12	0.20	3.15	0.04		1.4	2D	Series 38--40, 12x12x6-inch
	39	0.55	0.14	0.22	2.25	0.10		0.7	2D	vanes on crest, tailgate
	40	0.45	0.24	0.31	0.76	-0.12		3.2	2D	used to change full-flow capacity
	89	0.53	0.13	0.21	4.01	0.14		0.0	2D	12x12x6-inch vanes, 2x2-foot well in test tank covered ⊠
	182	0.52	0.10	0.18	4.00	0.10		1.4	2.84D	No antivortex device
	183	0.77	0.07	0.18	3.94	0.10		1.4	2.84D	15x15x6-inch vanes ⊠
F	41	0.72	0.13	0.18	3.72	0.15	0.51D	1.4	2D	12x12x6-inch vanes ⊠
	42	0.65	0.13	0.17	3.86	0.15		2.2	2D	No antivortex device
	127	0.74	0.15	0.20	2.84	0.16		0.7	2D	Tailgate used to change full-flow capacity
G	67	0.99	0.11	0.13	3.73	0.10	0.39D	1.4	5D	No antivortex device
	68	0.86	0.10	0.12	3.82	0.05		1.4	5D	15x15x6-inch vanes ⊠
	71A	0.73	0.11	0.13	2.92	0.12		0.0	5D	Series 71A--71E, 15x15x6-
	71B	0.77	0.11	0.12	2.83	0.12		0.0	5D	inch vanes, tailgate used
	71C	0.72	0.11	0.12	2.74	0.11		0.0	5D	to change full-flow capacity ⊠
	71D	0.74	0.11	0.13	2.50	0.12		-0.7	5D	
	71E	0.75	0.20	0.22	1.46	0.13		-1.8	5D	

Table 2. (Continued)

Drop inlet*	Series	Average values K_E	K_T	K_R	$R_B \times 10^{-5}$	Barrel crown pressure minimum observed $h_n/(V_B^2/2g)$	Barrel station	Average percent $\frac{f_{meas} - f_{smooth}}{f_{smooth}}$ Barrel	Approach depth	Remarks**
Square										
H	65	0.75	0.20	0.29	3.6<1	0.14	0.46D	0.0	20	15x15x6-inch vanes
	66	0.60	0.19	0.27	3.88	0.11		0.0	2D	No antivortex device
	124	0.75	0.21	0.30	1.81	0.07		0.6	2D	No antivortex device, tailgate used to change full-flow capacity
I	78	0.29	0.43	0.^5	3.74	-0.36	0.42D	-0.7	2D	12x12x6-inch vanes
	79	0.24	0.42	0.44	3.75	-0.49		0.7	2D	No antivortex device
	80	0.27	0.43	0.45	3.05	-0.50		-0.7	2D	Series 80 and 81, no anti-vortex device, tailgate used to change full-flow capacity
	81	0.26	0.45	0.47	2.31	-0.42		-0.7	2D	
J	62	0.92	0.18	0.21	3.69	-0.02	0.46D	0.7	2D	15x15x6-inch vanes
	63	0.77	0.17	0.21	3.83	0.19		1.4	2D	No antivortex device
	126	0.86	0.16	0.20	3.41	0.16		0.7	2D	No antivortex device, tail-gate used to change full-flow capacity
K	76	0.54	0.42	0.43	3.75	0.18	0.43D	0.0	2D	15x15x6-inch vanes
	77	0.51	0.42	0.42	3.75	0.19		0.0	2D	No antivortex device
Rectangular										
L	82	0.09	0.25	0.27	3.80	-0.80	0.40D	1.4	2D	15x15x6-inch vanes
	83	0.06	0.24	0.26	3.94	-0.79		0.7	2D	No antivortex device
	84	0.14	0.30	0.33	1.44	-0.77		2.4	2D	Series 84 and 85, no anti-vortex device, tailgate used to reduce full-flow capacity
	85	0.07	0.26	0.28	2.49	-0.78		0.7	2D	
M	86	0.10	0.32	0.34	3.84	-1.03	0.40D	0.0	2D	15x15x6-inch vanes
	87	0.10	0.39	0.41	1.42	-1.02		1.8	2D	No antivortex device, tail-gate used to reduce full-flow capacity
	88	0.08	0.32	0.33	3.98	-1.02		0.0	-2D	No antivortex device
N	72	0.18	0.24	0.25	3.85	-0.86	0.46D	1.5	2D	No antivortex device
	74	0.17	0.24	0.25	2.98	-0.86		0.7	2D	No antivortex device, tail-gate used to reduce full-flow capacity
	75	0.22	0.23	0.24	3.68	-0.86		0.7	2D	23x12x6-inch vanes
O-1	123								2D	No antivortex device, corner posts removed, rating curve data only

*See table 1 for drop inlet and barrel dimensions

**The downstream end of test tank is on the right of each cross vane orientation sketch

(a)

TANK WITH DIKE

SERIES 28, 29, 92 & 93

24"   18"

18-1/4"

12-5/8"

FLOW

60"

$11\frac{3}{4}$"

23-1/2"

DIKE

3'6" TALL

18-1/4"

(b)

TANK WITH GUIDE WALL

SERIES 30, 31, 94 & 95
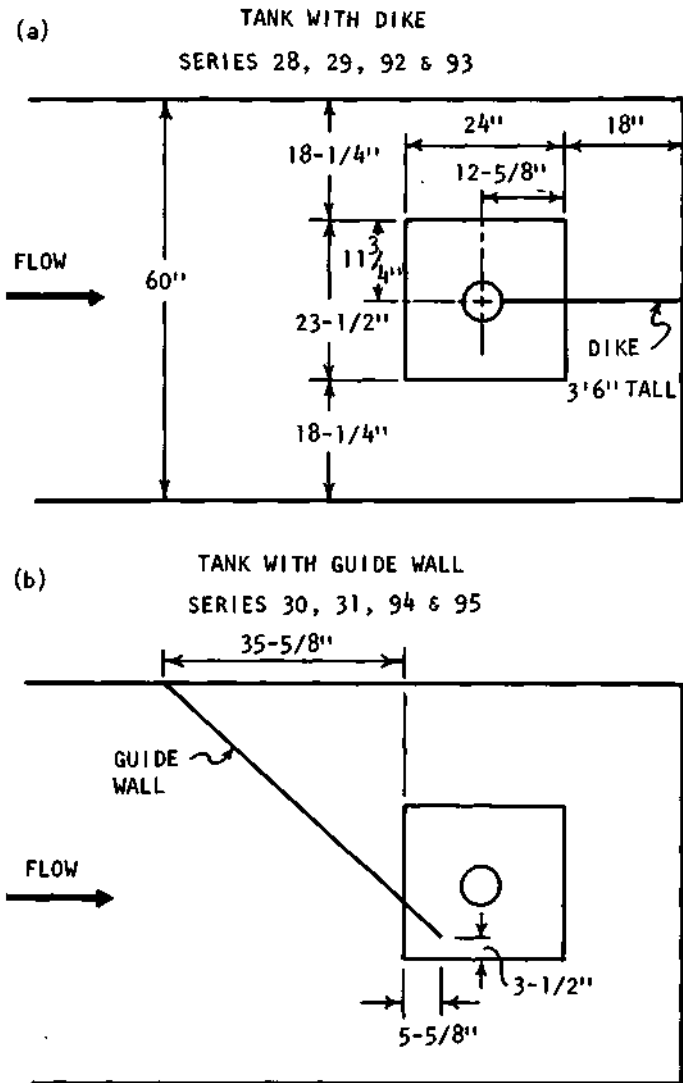
35-5/8"

GUIDE WALL

FLOW

3-1/2"

5-5/8"

Figure 13. Approach conditions for dike and guide wall

Deep Approach with Horizontal Circular Antivortex Plate

The deep approach was used for the series of tests with horizontal circular antivortex plates on the selected models listed in table 4. Each model had its inlet crest at a distance of *2D* above the approach channel. The flow approached the drop-inlet entrance from all directions, and the circulation around the drop inlet was permitted to develop freely. The horizontal circular antivortex plate was positioned at a height of d/D_R above the inlet crest for each series as shown. The vanes indicated in the sketches were attached to the plate. The downstream end of the test tank is on the right of each orientation sketch.

Circulation around Drop-Inlet Entrance

The circulation tests listed in tables 5 and 6 were conducted using drop inlet E *($D_B = 1.667$ D).* One set of five test series used the deep *(2D)* approach and another companion set used the flush *(0D)* approach. The test series for which sheet metal cross vanes (12x12x6 inches) were used to control vortex formation at the drop-inlet entrance are indicated in tables 5 and 6 for each of the approach depths. Table 6 lists the series for each approach depth in which either a guide wall was used to force circulation or a dike was used to prevent circulation around the drop-inlet entrance. The size and location of the guide wall and dike are shown in figure 13.

Each series for which the adjustable tailgate at the barrel outlet was used to reduce the full-flow spillway capacity to a value below the ungated capacity is shown in tables 2, 3, 4, 5, and 6.

Each series for which no antivortex device was used is shown in tables 2, 3, 5, and 6.
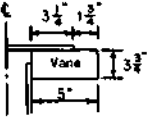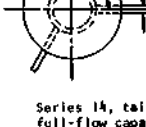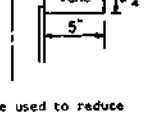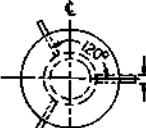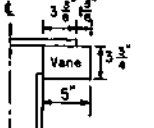
Table 3. Test Results for Flush Approach
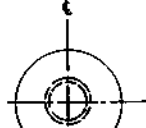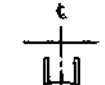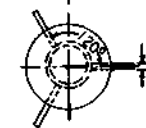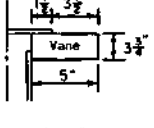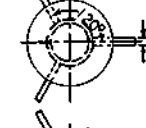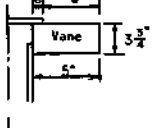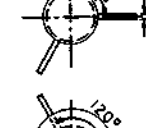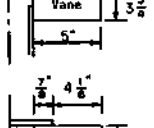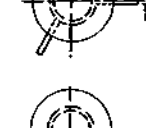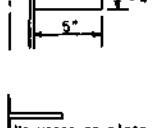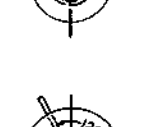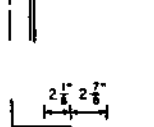
Drop inlet*	Series	Average values				Barrel crown pressure minimum observed $h_n/(V_B^2/2g)$	Barrel station	Average percent $\dfrac{f_{meas} - f_{smooth}}{f_{smooth}}$ Barrel	Remarks**	
		K_E	K_T	K_R	$R_B \times 10^{-5}$					
Circular										
C	96	0.55	0.29	0.63	3.90	-0.16	0.49D	0.0	12x12x6-inch vanes	⊠
	97	0.47	0.29	0.59	4.09	-0.19		0.7	No antivortex device	
	98	0.53	0.38	0.71	1.17	-0.62		-1.1	Series 98, 99, 110, 111, 112, and	
	99	0.49	0.40	0.71	0.66	-0.74		4.6	113, no antivortex device, tail-	
	110	0.58	0.43	0.79	0.68	-0.54		1.5	gate used to change full-flow	
	111	0.49	0.47	0.78	0.72	-0.55		0.5	capacity	
	112	0.62	0.40	0.78	0.70	-0.39		5.7		
	113	0.57	0.41	0.76	0.65	-0.41		-2.0		
D	114	0.49	0.25	0.42	3.63	-0.11	0.46D	-0.7	12x12x6-inch vanes	⊠
	115	0.42	0.23	0.38	3.80	-0.27		0.0	No antivortex device	
	116	0.47	0.30	0.46	1.67	-0.57		0.6	Series 116 and 117, no antivortex	
	117	0.47	0.28	0.45	1.37	-0.65		1.8	device, tailgate used to change full-flow capacity	
E	90	0.53	0.13	0.20	4.00	0.12	0.43D	0.7	12x12x6-inch vanes	⊠
	91	0.47	0.12	0.19	4.23	0.09		0.7	No antivortex device	
Square										
H	100	0.59	0.18	0.25	4.09	0.13	0.46D	2.2	No antivortex device	
	101	0.66	0.19	0.28	3.39	0.15		-2.1	12x12x6-inch vanes	⊠
	102	0.58	0.20	0.27	2.05	0.06		-1.9	Series 102 and 103, no antivortex	
	103	0.61	0.19	0.27	2.62	0.07		0.0	device, tailgate used to change full-flow capacity	
I	104	0.30	0.43	0.45	3.65	-0.43	0.42D	-0.7	12x12x6-inch vanes	⊠
	105	0.26	0.44	0.46	2.61	-0.41		-0.7	No antivortex device, tailgate used to change full-flow capacity	
	106	0.26	0.43	0.45	4.00	-0.44		0.0	No antivortex device	
	107	0.32	0.44	0.45	3.14	-0.52		0.0	Series 107, 108, and 109, no	
	108	0.22	0.41	0.53	0.69	-0.42		3.6	antivortex device, tailgate used	
	109	0.31	0.46	0.52	0.67	-0.45		0.5	to change full-flow capacity	

*See table 1 for drop-inlet dimensions.
**The downstream end of test tank is on the right of each cross vane orientation sketch.

Table 4. Test Results and Circular Horizontal Antivortex Plate Proportions for Circular Drop Inlets

Drop Inlet	Series	Nominal diameter (inches)	D_P/D_R	L_o/D_R	t_P/D_R	d/D_R	K_E	K_T	K_R	$R_B \times 10^{-5}$	Barrel crown pressure minimum observed $h_n/(V_B^2/2g)$	Barrel station	Average percent $\frac{f_{meas}-f_{smooth}}{f_{smooth}}$ Barrel	Remarks*
A-1	60	3.0	4	1.416	0.0838	0.25	0.87							
	61		4	1.416	0.0838	0.25	0.89							No vanes on plate
C-1	46	3.5	3.0364	0.943	0.1086	0.325	0.77	0.29	0.75	3.43	-0.311	0.49D	1.3	
	47		3.0364	0.943	0.1086	0.250	1.05	0.30	0.92	3.33	-0.251		1.3	
	48		3.0364	0.943	0.1086	0.175	2.00	0.26	1.41	3.13	+0.042		1.9	
	49		3.0364	0.943	0.1086	0.125	4.43	0.17	2.67	2.64	+0.016		2.8	
C-2	50	3.5	2.038	0.434	0.0722	0.125	4.62	0.14	2.74	2.57	-0.503	0.49D	3.3	
	51		2.038	0.434	0.0722	0.175	1.85	0.23	1.29	3.12	-0.087		2.6	
	52		2.038	0.434	0.0722	0.250	0.99	0.27	0.85	3.37	-0.301		2.1	
	53		2.038	0.434	0.0722	0.325	0.74	0.27	0.78	3.48	-0.330		1.5	
C-3	54	3.5	1.518	0.184	0.0722	0.325	0.74	0.26	0.80	3.46	-0.281	0.49D	2.1	
	55		1.518	0.184	0.0722	0.250	0.85	0.24	1.03	3.41	-0.262		1.3	
	56		1.518	0.184	0.0722	0.175	1.31	0.23	1.87	3.23	-0.080		1.5	
	57		1.518	0.184	0.0722	0.125	4.46	0.31	2.63	2.78	0.073		1.9	
E-1	32	5.0	1.15	0	0.0501	0.325	0.97	0.14	0.27	3.58	-0.137	0.43D	2.4	
	33		1.15	0	0.0501	0.125	5.71	0.13	0.87	3.33	+0.138		3.5	
E-2	34	5.0	1.50	0.175	0.0501	0.325	0.79	0.15	0.26	3.64	+0.124	0.43D	2.5	
	35		1.50	0.175	0.0501	0.250	1.04	0.15	0.29	3.64	+0.146		2.1	
	36		1.50	0.175	0.0501	0.175	2.17	0.17	0.45	3.67	+0.209		1.9	
	37		1.50	0.175	0.0501	0.125	5.66	0.17	0.91	3.38	+0.326		2.6	
E-3	1	5.0	2.008	0.425	0.0501	1.00	0.54	0.12	0.19	3.65	+0.098	0.43D	2.5	
	4		2.008	0.425	0.0501	0.25	0.95	0.12	0.25	3.82	+0.085		4.3	
	5		2.008	0.425	0.0501	0.125	6.30	0.09	0.91	3.59	+0.142		5.5	
	6		2.008	0.425	0.0501	0.500	0.59	0.12	0.20	4.00	+0.092		5.1	No vanes on plate
E-4	7	5.0	2.008	0.425	0.0501	0.500	0.55	0.13	0.20	4.06	+0.107	0.43D	1.2	
	8		2.008	0.425	0.0501	0.125	5.76	0.14	0.89	3.52	+0.225		4.8	
	10		2.008	0.425	0.0501	0.050	40.6		5.11	2.27			4.3	
	11		2.008	0.425	0.0501	0.400	0.62	0.15	0.22	3.98	+0.112		0.1	
	12		2.008	0.425	0.0501	0.025								
	13		2.008	0.425	0.0501	0.250	0.99	0.14	0.27	3.98	+0.110		0.9	
	14		2.008	0.425	0.0501	0.250	0.97	0.12	0.26	2.61	+0.094		0.9	
	27		2.008	0.425	0.0501	0.175	2.26	0.17	0.46	3.47				Series 14, tailgate used to reduce full-flow capacity
E-5	119	5.0	2.912	0.692	0.0754	0.200	1.38	0.17	0.36	3.46			1.7	
	120		2.912	0.692	0.0754	0.400	0.63	0.15	0.24	3.66			1.3	
	121		2.912	0.692	0.0754	0.400	0.61	0.16	0.24	3.93	+0.128		0.4	
	122		2.912	0.692	0.0754	0.200	1.38	0.18	0.36	3.17	+0.203		-3.1	Series 121 and 122, plate waxed

*The sketches on the left show the plan view with the vanes attached to the plate.
The sketches on the right show the elevation view of the plate and vane.

Table 5. Circulation Test Conditions

Series and approach depth Deep	Flush	Circulation around inlet	Flow in approach channel	Antivortex device	Tailgate position
2	90	Normal	Full width	Cross vanes	Open
28	92	Eliminated by dike (figure 13a)	Full width	Cross vanes	Open
29	93	Eliminated by dike (figure 13a)	Full width	None	Partially closed
30	94	Forced by guide wall (figure 13b)	Guided to one side	None	Partially closed (same as series 29 6 93)
31	95	Forced by guide wall (figure 13b)	Guided to one side	Cross vanes	Open

Note: Dike and guide wall (figure 13) extended from test tank floor to well above all water levels.
Cross vanes on drop-inlet crest were 12x12x6-inch sheet metal.

Table 6. Circulation Test Results for Drop Inlet E

Series	K_E	K_T	K_R	$R_B \times 10^{-5}$	$h_n/(V_B^2/2g)$	Barrel station	Average percent $\frac{f_{meas} - f_{smooth}}{f_{smooth}}$ Barrel	Number of runs in average	Approach conditions*	Approach depth**	Tailgate position
2	0.56	0.12	0.20	3.72	0.09	0.43D	4.3	11		Deep	
90	0.53	0.13	0.20	4.00	0.12	0.43D	0.7	10		Flush	
28	0.58	0.13	0.21	3.58	0.12	0.43D	1.1	12		Deep	Fully open
92	0.52	0.13	0.21	4.14	0.12	0.43D	0.4	8		Flush	
31	0.56	0.10	.0.18	3.72	-0.02	0.43D	1.1	4		Deep	
95	0.50	0.12	0.19	4.15	0.10	0.43D	0.8	10		Flush	
29	0.55	0.21	0.29	1.26	-0.18	0.43D	1.7	10		Deep	
93	0.44	0.20	0.26	1.49	-0.17	0.43D	1.5	9		Flush	Partially closed
30	0.70	0.20	0.30	1.28	-0.13	0.43D	1.7	6		Deep	
94	0.48	0.24	0.31	1.50	0.04	0.43D	1.7	7		Flush	

*   Dike   Cross vanes   Guide wall
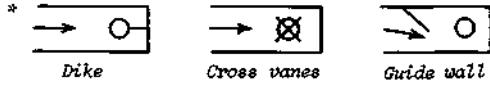
**Deep approach depth = 2D for series 2, 28, 29, 30, and 31.*

Part 3. Test Results

SPILLWAY PERFORMANCE

A designer must be acquainted with the performance of a closed-conduit spillway with a drop-inlet entrance to properly design this type of spillway. This requires that the flow conditions be known for each type of control such as weir control at the drop-inlet entrance. Therefore, the observed flow conditions for weir control, vortex effect, and a horizontal circular plate antivortex device are described.

Weir Control by Drop-Inlet Crest

In the weir-flow range the weir nappe can be either free or clinging. However, the clinging nappe predominated in the tests presented in this report. A description of the flow conditions observed in the drop inlet for ventilating the free nappe follows.

When the nappe was free for very low discharges, there was a free passage of air up through the barrel and into the pocket under the nappe. As the discharge was increased the transition between the drop inlet and barrel was sealed by a mixture of air and water buildup in the lower portion of the drop inlet, thereby eliminating all ventilation through the barrel. This air-water mixture or boil in the drop inlet was saturated with large bubbles of air. Most of these bubbles were trapped by the water and carried through the barrel. Some bubbles, however, found their way under the nappe to release their air content there and free the nappe. This indirect way of ventilating the nappe was the one most frequently observed.

The balance of air under the nappe was unstable which resulted in the nappe changing at times from free to clinging and vice versa. These changing nappe conditions influenced slightly the head or the weir, causing a higher head for the free nappe than for a clinging nappe. Quite frequently, for intermediate conditions, the air pocket under the nappe was nearly full of water. No attempt was made to measure the pressure in the air pocket under the free nappe. Figure 14 shows weir flow with a clinging nappe and figure 15 shows weir flow with a free nappe.

The flow conditions in the barrel, while it is filling, is also considered important to understanding the spillway performance. For very low discharge there is open channel flow in the barrel and a free passageway of air all the way through the spillway. As the discharge was increased a mixture of air and water built up in the bottom of the drop inlet and sealed the entrance to the barrel. This seal extended initially only 1 or $2D$ into the barrel. There the water broke away from the barrel crown and flowed with a free surface down the barrel. With a further increase in the discharge the water surface in the barrel at first became wavy. Still further increases in the discharge caused hydraulic jumps to form. These jumps completely filled the barrel for approximately $10D$. The jumps or slugs of water traveled down the barrel like a piston in a cylinder. As the discharge increased the jumps formed more
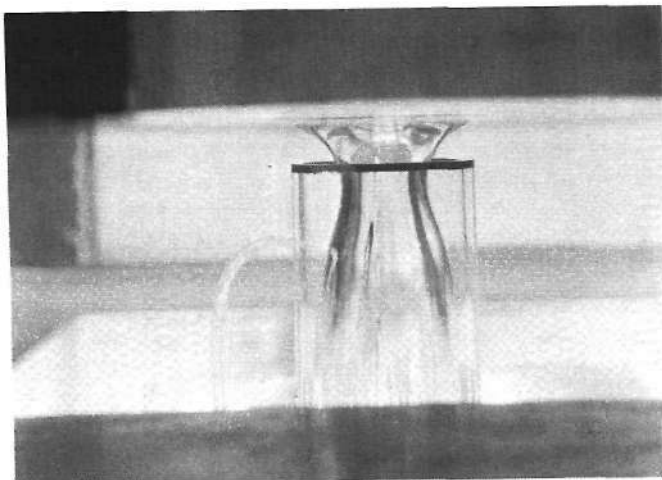
Drop inlet E, series 3

$Q/D_R^{5/2}(2g)^{1/2} = 0.265$, $h/D_R = 0.284$

Figure 14. Weir flow, clinging nappe
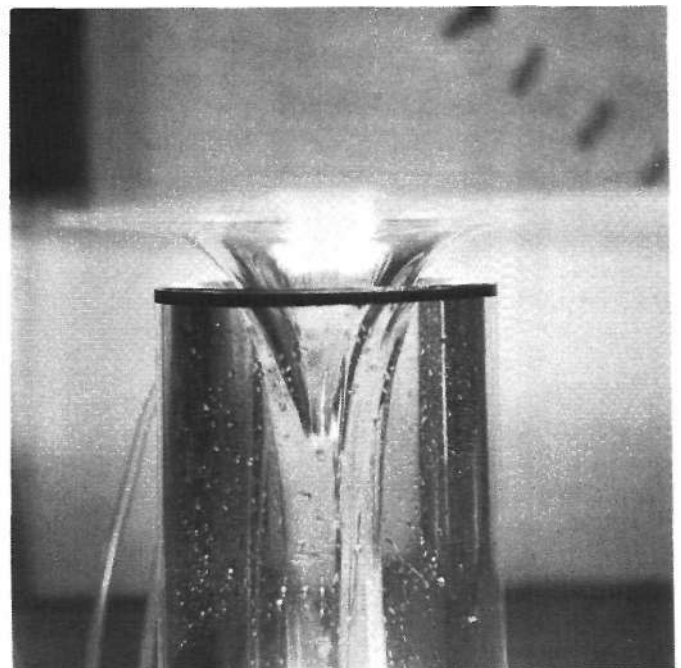
Drop inlet G, series 67

$Q/D_R^{5/2}(2g)^{1/2} = 0.141$, $h/D_R = 0.20$
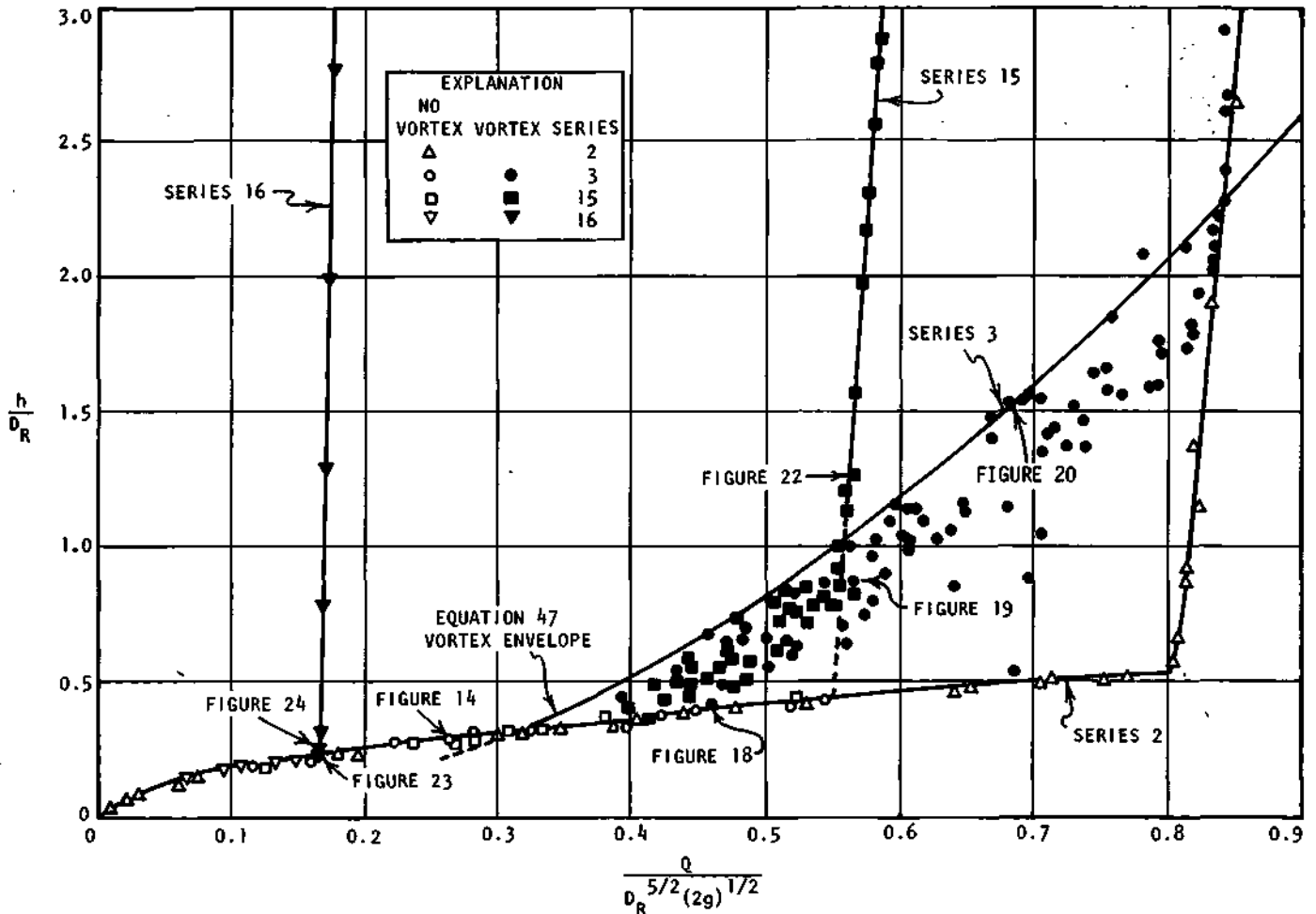
Figure 15. Weir flow, free nappe

Figure 16. Effect of vortex on spillway performance and discharge for drop inlet E with deep approach

and more frequently and several jumps would be traveling down the barrel at the same time. Eventually all distinct jumps disappeared and the barrel flowed full of an air-water mixture. Finally, the spillway inflow became sufficient to displace the air and completely fill the spillway with water.

As the hydraulic jumps traveled down the barrel a vacuum was created behind them which noisily sucked in great amounts of air. This sucking caused a rapid drop in the level of the air-water mixture in the drop inlet. However, the water level would rise as the next jump was formed in the barrel. The resulting violent action of the air-water mixture in the drop inlet did not have any noticeable effect on the weir control at the drop-inlet entrance.

Orifice Control by Drop-Inlet Crest

Orifice control by the drop-inlet crest was not observed at any time for the drop-inlet models listed in table 1.

Short-Tube Control by Drop Inlet

Short-tube control by the drop inlet was not observed at any time for the drop-inlet models listed in table 1.

Vortex Effect and Flow Descriptions

The formation of vortices at the drop-inlet entrance was a natural flow phenomenon, and was neither inhibited nor forced. Initially four series of tests were conducted to learn the effect of vortices on the performance of drop-inlet spillways:

1) For series 2, the formation of a vortex was prevented by placing the sheet metal cross vanes on the inlet crest.
2) For series 3, the cross vanes were removed and the vortex was free to form.
3) For series 15, the full-flow capacity of the spillway was reduced by partially closing the tailgate located at the barrel outlet. The cross vanes were omitted from the inlet crest to permit the vortex to form.
4) For series 16, the full-flow capacity of the spillway was reduced to a value well below the capacity for series 15 by further closing the tailgate. The cross vanes were omitted to permit the vortex to form.

Each of the tests was conducted using circular drop inlet E. This $5D/3$ diameter drop inlet was $5D$ high and its inlet crest was $6D_R/5$ above the approach channel floor. The flow approached the inlet from all directions.
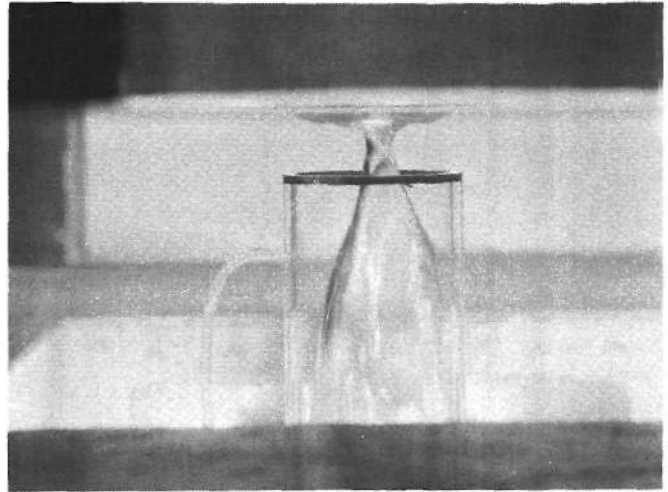
The instantaneous head-discharge data obtained for this spillway are shown in figure 16.

23
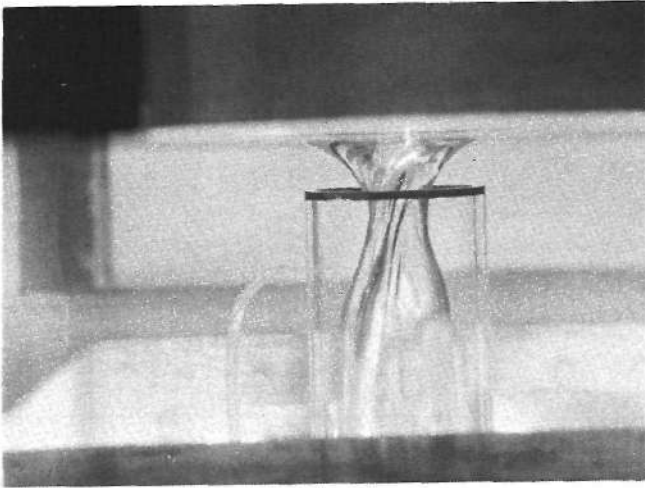
Drop inlet E, series 3

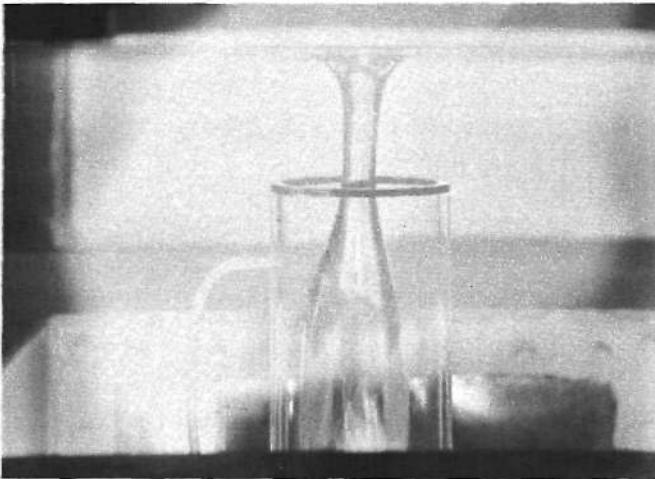$Q/D_R^{5/2}(2g)^{1/2} = 0.379$, $h/D_R = 0.352$

Figure 17. Weir flow, clinging nappe, clockwise iwist in nappe

Drop inlet E, series 3

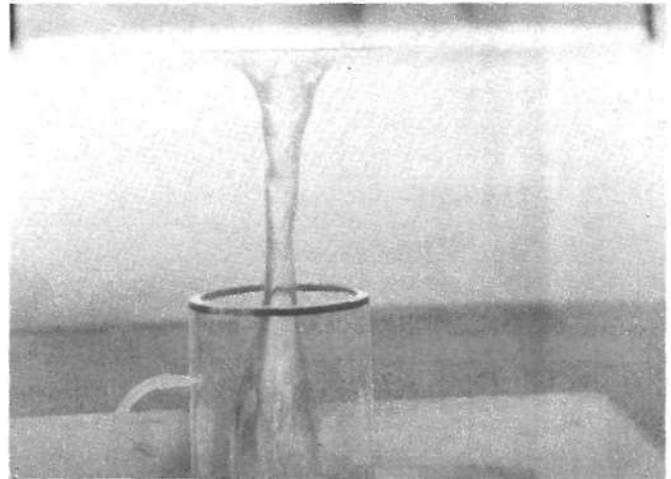$Q/D_R^{5/2}(2g)^{1/2} = 0.460$, $h/D_R = 0.427$

Figure 18. Beginning of a vortex

Drop inlet E, series 3

$Q/D_R^{5/2}(2g)^{1/2} = 0.560$, $h/D_R = 0.851$

Figure 19. Well-developed vortex affecting spillway performance

Drop inlet E, series 3

$Q/D_R^{5/2}(2g)^{1/2} = 0.692$, $h/D_R = 1.538$

Figure 20. Differing form of well-developed vortex affecting spillway performance

Series 2. The head-discharge curve for this test is unique and reversible with only weir- and full-flow controls being exhibited. This type of head-discharge curve is desirable for drop-inlet spillways.

Series 3. For the initial small discharges the drop-inlet crest exhibited weir control. As the inflow to the reservoir increased, a small circulation of the flow developed slowly around the drop-inlet entrance. However, the discharge through the spillway continued to be weir controlled and looked similar to the weir flow shown in figure 14. For larger discharges the circulation strength increased and developed a twist in the weirflow nappe as shown in figure 17. Further increases in discharge would increase circulation strength until a vortex would form. The time of this change from weir flow to vortex flow at the drop-inlet entrance was unpredictable. The change was usually

accompanied by a rapid rise in the reservoir water level, indicating a decreasing discharge through the spillway. The beginning of a vortex is shown in figure 18. Shortly afterward, the vortex that developed was similar to the one shown in figure 19. This well-defined vortex profile is similar to the profile corresponding to the irrotational vortex analysis. The diameter of the air core decreases from a maximum at the reservoir water surface to a minimum near the elevation of the drop-inlet crest. Inside the drop inlet the air core expands rapidly between the inlet crest and a point approximately 0.5D below the crest. Below this point, the diameter of the air core increases slowly in the downstream direction. This vortex caused the discharge through the spillway and the reservoir level to be unsteady.

Another form of the vortex is illustrated in figure 20. The

surface of this vortex was rough, although the general overall shape is similar to the one shown in figure 19. The spillway discharge and reservoir level were unsteady.

The effect of the vortex on the spillway performance and capacity becomes less and less as the reservoir level is raised. The vortex air core lengthens and becomes smaller. As the air core becomes smaller its entrance at the reservoir surface does not remain directly above the drop-inlet entrance but begins to move laterally. The direction of this lateral motion is slow and unpredictable. Figure 21 shows this type of long slender or finger vortex. This vortex had no measurable effect on the spillway full-flow capacity or performance. Also, the vortex was intermittent in that it would dissipate, disappear, and reform in an unpredictable manner. Sometimes the air core would form but it would not extend to the drop inlet.

The scatter of the instantaneous head-discharge points in figure 16 indicates the random effect of the vortex on the head-discharge relationship. The data show the vortex may reduce the discharge as much as 50 percent of the full-flow discharge for this model. The vortex for a particular discharge may also result in a head increase of about 300 percent larger than the head required if the vortex is not present. The vortex effect at a head of $2.28D_R$ and greater was negligible.

Series 15. The initial flow control was, as in series 3, the weir at the drop-inlet crest. Also, as in series 3, at an unpredictable discharge the weir flow changed to a vortex with a random scattering of the instantaneous head-discharge points shown in figure 16. The vortex that formed was similar to that formed for series 3, figure 19. The effect of the vortex on the spillway performance became less and less as the reservoir level was raised and was negligible for all heads above $1.05D_R$. This head for no effect is smaller than the one for series 3 because the spillway full-flow capacity was reduced by partially closing the tailgate at the barrel outlet. The vortex shown in figure 22 is for a head of $1.25D_R$. The vortex air core was large and appeared to be strong when viewed from above. Air entrainment at the bottom of the air core is a milky white color because of the mixture of air in the water. For this vortex the reservoir level was steady, indicating no effect on the spillway discharge.

Comparing the sizes of the vortices affecting spillway discharge (figures 19 and 20) with the size of the vortex not affecting the spillway discharge (figure 22) shows that the size of a vortex does not always indicate its effect on the spillway performance or discharge.

The scatter of instantaneous head-discharge points in figure 16 (series 15) indicates the random effect of the vortex on the head-discharge relationship. The data show the vortex may have reduced the discharge as much as 30 percent of the full flow for this test. The vortex for a particular discharge may also result in a head increase of about 150 percent larger than the head required if the vortex is not present. These potential vortex effects on capacity and head are less than the corresponding values for series 3 because the full-flow capacity for series 15 was less than that for series 3.

The rating curve for all heads higher than $1.05 D_R$ was stable and reversible. Long narrow vortices that formed sucked
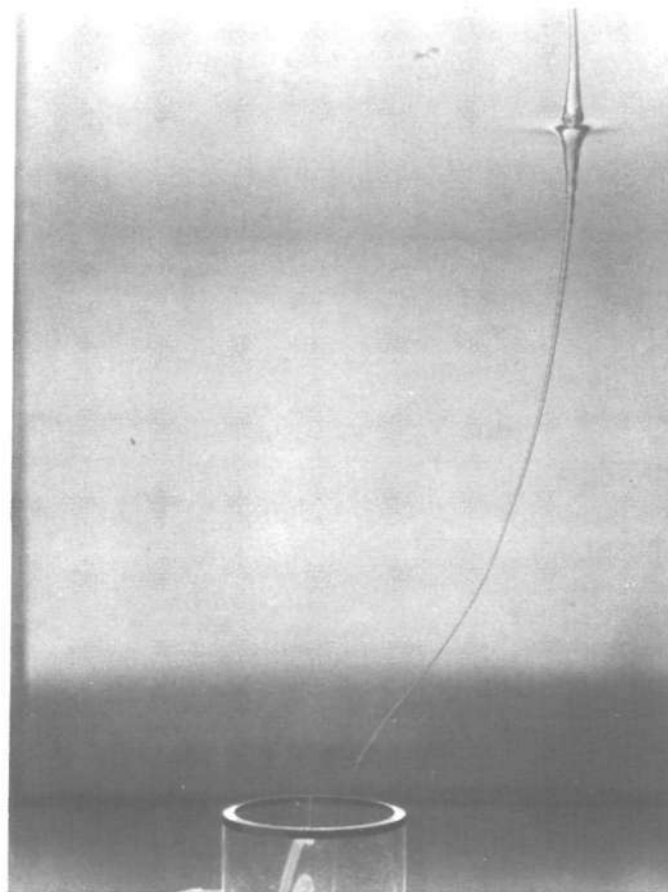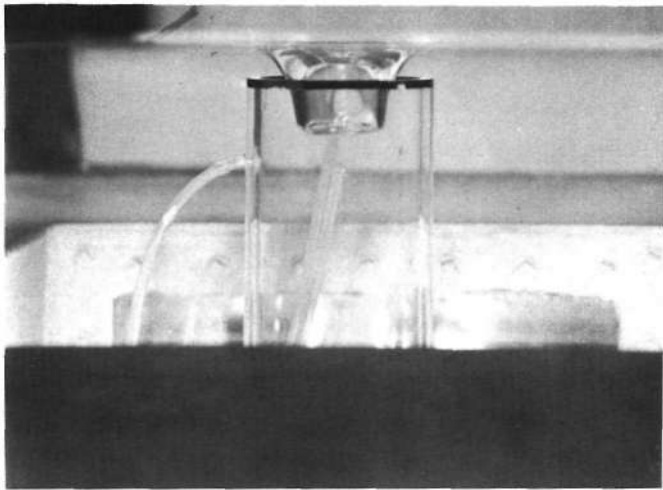

Drop inlet E, series 3

$$Q/D_R{}^{5/2}(2g)^{1/2} = 0.871, \quad h/D_R = 4.345$$

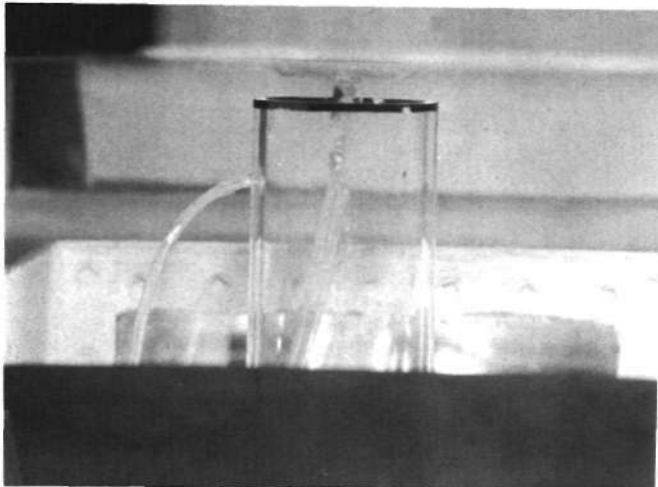**Figure 21.** Long slender finger-type vortex, no effect on spillway performance
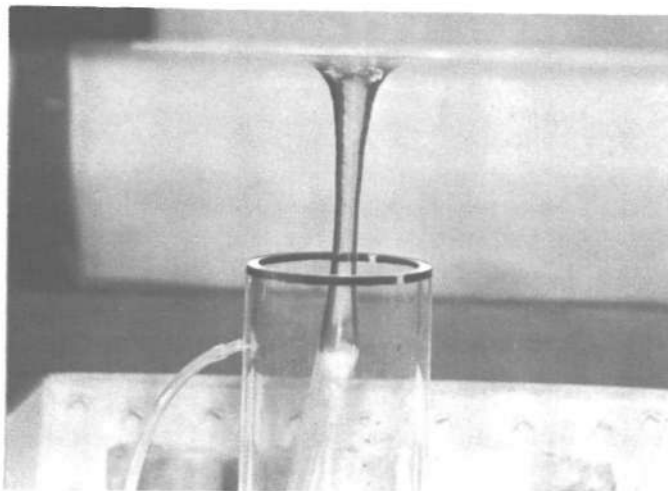
Drop inlet E, series 15

$$Q/D_R{}^{5/2}(2g)^{1/2} = 0.569, \quad h/D_R = 1.25$$

Figure 22. Well-developed vortex, no effect on spillway performance

Drop inlet E, series 16

$$Q/D_R^{5/2}(2g)^{1/2} = 0.166, \ h/D_R = 0.219$$

Figure 23. Flow conditions in drop inlet at intersection of weir- and full-flow curves

Drop inlet E, series 16

$$Q/D_R^{5/2}(2g)^{1/2} = 0.167, \ h/D_R = 0.241$$

Figure 24. Vortex flow in drop inlet, no effect on spillway performance

in small amounts of air, but these did not affect the rating curve. These vortices would form and dissipate in an unpredictable manner.

Series 16. As in series 3 and 15, the spillway discharge was initially controlled by the weir at the drop-inlet crest. As the discharge increased the gated full-flow capacity was reached. Figure 23 shows the flow condition in the drop inlet at the intersection of the weir- and full-flow curves. At the instant the picture was taken, the inflow into the spillway was controlled by the weir at the drop-inlet entrance and the reservoir level was steady. The barrel was flowing full of water. For the next run at a very slight increase in discharge, the flow at the entrance changed from that shown in figure 23 to a vortex similar to the one shown in figure 24. Although this vortex formed, it did not suck any air into the spillway and it did not affect the spillway performance or discharge.

The lack of scatter of the head-discharge data in figure 16 (series 16) shows the vortex did not affect the head-discharge relationship. There was no effect on either discharge or head. This test shows that the full-flow capacity of this spillway can be a value small enough to eliminate the effect of a vortex on the spillway performance.

The rating curve for all heads higher than the head at the intersection of the weir- and full-flow curves was stable and reversible. The long narrow vortices that formed did not suck any air into the spillway although the circulation appeared strong when viewed from above.

Comments on Vortices

The above descriptions of observed vortices at the entrance to a drop-inlet spillway clearly show that vortices can and will form naturally if an antivortex device is not used. The spillway discharge or head at which a vortex will form is unpredictable. The vortices may be strong and may significantly affect the spillway performance, or they may be weak and not have a significant effect on the spillway performance. The effect of the vortex on the spillway performance cannot be determined by observing the vortex action alone. Characteristics that have been observed in the laboratory for both strong and weak vortices are:

1) The vortex always has circulation.
2) The vortex may rotate clockwise.
3) The vortex may rotate counterclockwise.
4) The air core may be large.
5) The air core may be small.
6) The vortex may be noisy.
7) The vortex may be quiet.

To determine whether an observed vortex is strong or weak requires plotting the head-discharge relationship obtained in the presence of vortices and comparing the plotted point with the curve obtained without vortices.

Vortex Envelope for Circular Drop Inlet

The head-discharge data presented in figure 16 for the four tests on a circular drop-inlet show vortices have varying effects on the performance of circular drop-inlet spillways. For example, depending upon the full-flow capacity of the spillway, a minimum head above the drop-inlet crest was required to make the influence of a vortex on spillway performance insignificant. These minimum heads for series 3 and 15 were $2.28D_R$ and $1.05D_R$, respectively. In addition, if the full-flow discharge is less than about $Q/[D_R^{5/2}(2g)^{1/2}] = 0.32$ then any vortices that formed had an insignificant influence on the spillway performance. The vortex envelope shown in figure 16 indicates the limiting effect of the vortex on the head-discharge relationship. The vortex had little, if any, effect on the spillway capacity for heads above the envelope.

The vortex envelope equation empirically determined for the data in figure 16 is

$$h/D_R = (32/\pi^2) \ [Q/D_R^{5/2}(2g)^{1/2}]^2 \qquad (47)$$

and applies specifically to closed-conduit spillways with a drop-inlet entrance of the same geometric proportions as drop-inlet model E.

Since equation 47 was determined for a circular drop inlet with a diameter of $5D/3$ and a square crest, another nondimensional form of this equation can be obtained by removing the brackets, squaring the quantities in the brackets, and multiplying the right hand side by $[(\pi/4)^2 D_R^4/A_R^2]$. Equation 47 then becomes

$$h/D_R = 2.0 \ (Q^2/2gA_R^2)/D_R \qquad (48)$$

The control section for equation 47 or 48 is near the drop-inlet entrance as evidenced by the vortex air core expanding near the inlet as shown in figures 19, 20, and 22.

Circular drop inlets are not the only geometric shapes used as entrances for closed-conduit spillways. Drop inlets that are square or rectangular in plan are also used. The fact that vortices do not always affect the performance of a circular drop inlet would lead one to believe that vortices may not always affect the performance of square or rectangular drop inlets. Therefore, a relationship that shows the limiting effect of vortices on spillway performance and discharge could be used in examining experimental data to determine the geometric proportions of circular, square, and rectangular drop inlets for which the limiting vortex effect would be predictable. Knowing these geometric proportions and the limiting vortex effect a designer will be able to determine when an antivortex device on the spillway is required for satisfactory hydraulic performance.

Head-Discharge Curve

The complete.'head-discharge curve for the spillway is composed of parts showing weir control, possibly vortex control, and full flow. Each part of the head-discharge curve will be discussed separately.

Weir Control. Equation 2 is used for determining the spillway discharge for weir control at the inlet crest and applies to circular, square, and rectangular drop inlets. The head-discharge curve is the same for each of these geometric shapes if L_c and C_w are identical for all three geometries. Therefore equation 2 may be written

$$Q/L_c(2g)^{1/2}=C_w h^{3/2} \qquad (49)$$

Equation 49 can be made nondimensional by dividing through by a length, A, to the 3/2 power to yield

$$Q/\lambda^{3/2}L_c(2g)^{1/2} = C_w(h/\lambda)^{3/2} \qquad (50)$$

The quantities $Q/\lambda^{3/2}L_c(2g)^{1/2}$ and h/λ are used to plot the weir-controlled section of the head-discharge curve. For a constant value of C_w, equation 50 will be a single curve for any value of Q or A. Therefore, all drop inlets that have the same value of C_w can be represented by a single curve for the weir-controlled section of the head-discharge curve.

Vortex Control. The vortex envelope, equation 47, shown in figure 16, intersects the weir flow head-discharge curve at a head and discharge which are dependent upon the position of the weir-flow curve. For discharges smaller than this discharge value, the vortices that formed did not have any effect on the

spillway performance. For heads larger than the head value at the intersection of the vortex envelope and weir curves, the vortex envelope represents the minimum head above the drop-inlet crest to make the influence of a vortex on spillway performance insignificant. The specific value of this minimum head is determined by the intersection of the spillway full-flow curve and the vortex envelope.

In order to plot the vortex envelope for the circular drop inlet on the same graph with equation 50 for weir control, a rearrangement of equation 47 or equation 48 is required so that the nondimensional head and discharge parameters are the same for weir control and the vortex envelope. Equation 50 has the quantities L_c and λ which do not appear in equation 47 or its alternate form, equation 48. Equation 48 contains the horizontal area A_R of the drop inlet. Dimensionally the quantities A_R and L_c can be related by

$$A_R= \lambda L_C \qquad (51)$$

where A is the ratio of the drop-inlet horizontal area to the length of the drop-inlet crest. Substituting equation 51 in equation 48, replacing D_R by A_R/λ for the circular drop inlet, and rearranging, yields

$$h/\lambda = 2.0[Q/\lambda^{3/2}L_c(2g)^{1/2}]^2 \qquad (52)$$

which is a nondimensional relationship for the vortex envelope. Equation 52 can also be obtained from equation 47 by substituting for D_R the quantity $(4\lambda L_c/\pi)^{1/2}$ and dividing both sides of the equation by $\lambda^{1/2}$.

Although equation 52 was determined experimentally for one size circular drop inlet, from series 2, 3, 15, and 16 described in this section, it has an advantage over equations 47 and 48 in that the characteristic length D_R identifying the drop-inlet geometry has been eliminated. This is an advantage since A and L_c can also be used to describe the geometry of circular, square, and rectangular drop inlets whereas D_R is characteristic of only the circular drop inlet. Therefore, instead of requiring a different equation expressing the limiting effects of vortices for each drop-inlet geometry, equation 52 is the only one needed. Equation 52 is used to examine experimental data to determine the geometric proportions of circular, square, and rectangular drop inlets for which the limiting effect of vortices are predictable by this equation.

Full Flow. Equation 15 is used in determining the spillway discharge for full flow for circular, square, and rectangular drop inlets. For a particular head the magnitude of the discharge will depend upon the head-loss coefficients for every part of the spillway. The head and computed discharge are then expressed in the nondimensional head-discharge parameters of equations 50 and 52.

Need for Antivortex Device

The complete head-discharge curve using h/X and $Q/\lambda^{3/2}L_c(2g)^{1/2}$ for the head and discharge coordinates shown in figure 25 is composed of a typical weir-control curve (equation 50), the vortex envelope (equation 52), and two typical full-flow curves. The full-flow curves were drawn assuming a vortex is not present. In drawing these curves for a

typical spillway, it is assumed the spillway has the proper proportions so that neither orifice nor short-tube control can occur.

The head-discharge curve for a drop-inlet spillway as shown in figure 25 will at a glance convey to the designer considerable information about the spillway performance. If the full-flow curve shown by the dashed curve intersects the weir curve (equation 50) to the left of the weir curve and vortex envelope intersection, point 'A', the resulting head-discharge curve will be single-valued and predictable for a properly proportioned spillway with or without an antivortex device. If the full-flow curve (solid curve), computed and plotted assuming a vortex is not present, intersects the weir curve to the right of point 'A', an effective antivortex device is needed. The resulting head-discharge curve will be single-valued and predictable with the vortex fully controlled. However, if an antivortex device is not used when the full-flow curve is to the right of point 'A', a single-valued head-discharge curve will not be obtained. The magnitude of the uncertainty in head or discharge depends upon how far to the right of point 'A' the full-flow curve is located. The uncertainty in head or discharge is bounded by the area above the weir curve, to the right of the vortex envelope, and to the left of the full-flow curve.

Horizontal Circular Plate Antivortex Device

These test results describe the effects of a horizontal circular plate antivortex device, positioned above the drop inlet, on the performance of spillways with a circular drop-inlet entrance. The approaching flow well upstream of the drop-inlet entrance utilized the full width of the approach channel. In the vicinity of the drop-inlet entrance the flow approached the drop inlet from all directions and no attempt was made to inhibit normally developed circulation. The deep approach was used in these tests.

Effect of Antivortex Plate without Vanes

Model E-3, series 1, was the first model test made by the State Water Survey using a horizontal circular plate without vanes over the drop inlet as an antivortex device. The plate was suspended by a center support attached to the top of the plate. The plate had an overhang of $L_0/D_R = 0.425$ and was positioned at $d/D_R = 1.00$ above the drop-inlet crest.

The flow condition for the initial small spillway discharge was weir control at the inlet crest. However, as the spillway discharge was increased the weir flow changed into a vortex at an unpredictable discharge. The instantaneous head-discharge points were random and scattered, similar to those shown in figure 16 for series 3. At larger discharges, with a strong vortex present, the water level would fluctuate and sometimes touch the plate. The plate would close the vortex air core and the water level would then drop below the plate. Further increases in the discharge did result in the water level remaining in contact with the plate and the reservoir level being stabilized. The reservoir level increased very slightly for
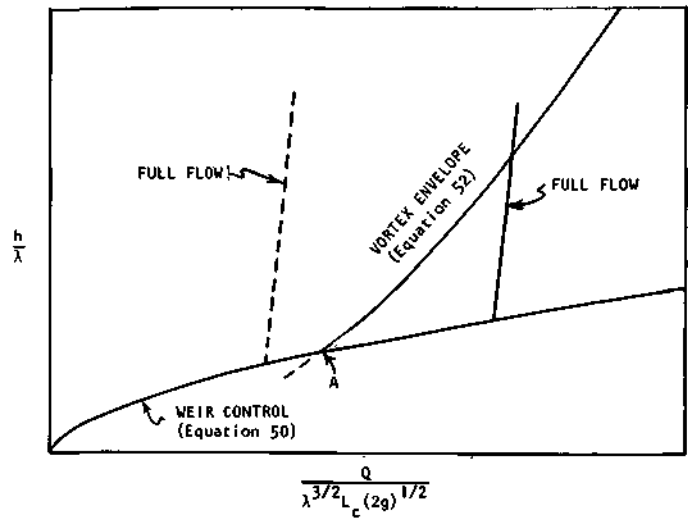

Figure 25. Vortex envelope and typical head-discharge curves for weir control and full flow

larger discharges until the spillway full flow was obtained.

It is apparent from the above description of flow conditions that the antivortex plate positioned at $d/D_R = 1.00$ above the inlet crest was not effective in controlling the vortex. Therefore, the same plate used for series 1 was positioned at $d/D_R = 0.50$. The test results for this plate position were similar to those obtained for $d/D_R = 1.00$.

The model E-3 antivortex plate without vanes was also used for series 4 with the plate positioned at $d/D_R = 0.25$, and for series 5 with the plate at $d/D_B = 0.125$. Each of these series of tests resulted in suppressing the vortex at the inlet; however, strong circulation below the plate existed during the time the reservoir level was stabilized. Therefore, to eliminate the circulation below the plate, three vanes were attached to all plates used for models C-1, C-2, C-3, E-1, E-2, E-4, and E-5.

Flow Conditions for a Properly Positioned Antivortex Plate

Figure 26 shows the head-discharge curve obtained for model E-4 *(see table 4)* when a circular horizontal antivortex plate is positioned above the inlet crest so that it influences the head on the spillway. The solid curve is divided into three parts which are identified in figure 26 as weir flow, plate flow, and full flow. The dashed curve, shown for reference, is the head-discharge curve obtained for drop inlet model E (series 2, no antivortex plate) when sheet metal cross vanes were placed on the drop-inlet crest to control the effects of vortices. The sequence of flow conditions is described as the spillway discharge increased from an initial small quantity until the spillway flowed full of water.

During the very small initial discharges the flow condition at the inlet is weir with a clinging nappe. Weir control exists as the head and discharge are increased, and during this time the weir nappe may be free or clinging. During the weir flow regime the spillway performs as though the horizontal plate were not present.

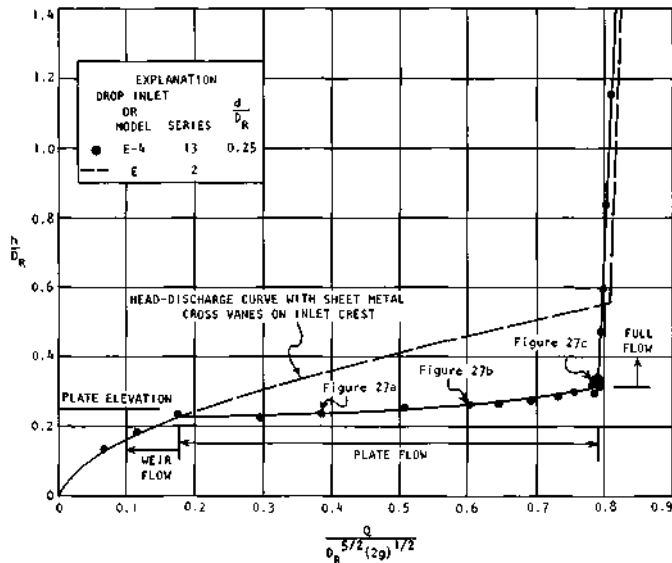By increasing the discharge the head above the inlet crest

**Figure 26. Effect of a horizontal circular antivortex
plate on the spillway performance and discharge**

will rise until the water touches the bottom of the antivortex plate and seals the inlet. After sealing the inlet the water level in the reservoir drops slightly to a level just below the bottom of the plate, as indicated by the solid curve for plate flow in figure 26. Further increases in the spillway discharge cause very small increases in the reservoir level. This is because a partial vacuum is created beneath the plate in the plate-flow range of discharge. The partial vacuum increases the head across the plate so that the increased water discharge is obtained for very small increases in the reservoir level. Because the partial vacuum creates a demand that cannot be satisfied by the available discharge, air is sucked intermittently into the spillway after the inlet seals. In the plate-flow range the air intake was very noisy for intermediate discharges, but the noise decreased noticeably as the spillway began to flow full of the air-water mixture. The sucking in of air momentarily breaks the water seal at the plate. Small surface waves were generated by the breaking and sealing of the inlet. These small waves did not have a significant effect on the discharge for this series.

As the water discharge increases to full flow the air intake decreases until the spillway is full of water. The small scatter of the data near the intersection of the plate-flow and full-flow curves was the result of strong eddy action at the tips of the vanes attached to the plate. For full flow the reservoir level increases rapidly for small increases in the discharge.

Occasional vortex fingers developed for the full-flow runs but these did not have any measurable effect on the spillway full flow.

The flow conditions in the barrel were similar to those described for "Weir Control by Drop-Inlet Crest."

Figure 26 indicates that the horizontal antivortex plate can, when properly positioned, significantly reduce the head necessary for the spillway to prime and flow full of water when compared with the priming head at the usual intersection of the weir- and full-flow curves.
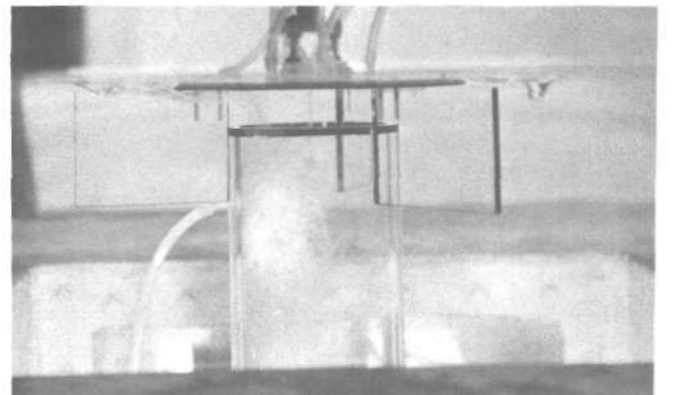
Figure 27 shows photographs of plate control flow condi-
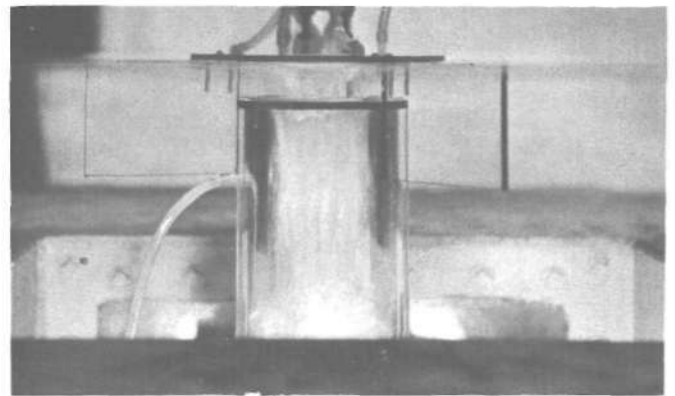
(a) Drop inlet E-4, series 13

$$Q/D_R^{5/2}(2g)^{1/2} = 0.387, \quad h/D_R = 0.236,$$
$$d/D_R = 0.25$$
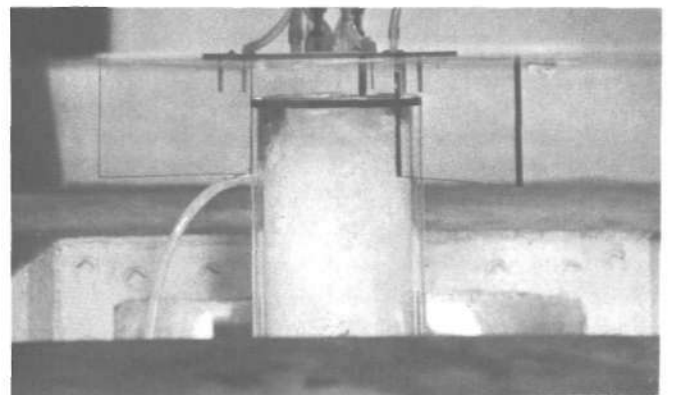
(b) Drop inlet E-4, series 13

$$Q/D_R^{5/2}(2g)^{1/2} = 0.605, \quad h/D_R = 0.263,$$
$$d/D_R = 0.25$$

(c) Drop inlet E-4, series 13

$$Q/D_R^{5/2}(2g)^{1/2} = 0.790, \quad h/D_R = 0.342,$$
$$d/D_R = 0.25$$

**Figure 27. Plate-flow conditions at drop inlet with a horizontal
circular antivortex plate properly positioned above the drop-inlet crest**

29

tions for the series 13 head-discharge curve in figure 26. Figure 27a for a $Q/D_R^{5/2}(2g)^{1/2} = 0.387$ shows the reservoir level is slightly below the bottom of the plate. Also, the flow is springing free from the outer periphery of the drop-inlet crest. The white jet in the drop inlet is a mixture of air and water. Figure 27b shows the flow conditions after the discharge has been increased to $Q/D_R^{5/2}(2g)^{1/2} = 0.605$. The reservoir level is slightly above the bottom of the plate. Eddy action is shown near the outer edge of the vane on the right of the drop inlet. The flow is springing free from the outer periphery of the drop-inlet crest, and the drop inlet is nearly full of an air-water mixture. Figure 27c shows the flow conditions after the discharge has been increased to $Q/D_R^{5/2}(2g)^{1/2} = 0.790$ and the reservoir level is above the top of the plate. Very strong eddy action is taking place at each vane. A small amount of air is being sucked into the drop inlet by eddy action along the near side of the left-hand vane. The spillway is almost full of water.

Effect of Waxed Antivortex Plate

The head-discharge curves in figures 26 and 28, as well as the photograph in figure 27a, show the reservoir level is generally below the elevation of the underside of the antivortex plate for a part or all of the plate-flow range. The initial lowering of the reservoir level occurred immediately after the water touched the plate and sealed the inlet. This sealing of the inlet and lowering of the water level can be attributed to the partial vacuum beneath the plate, to possible surface tension effects, or to a combination of the partial vacuum and surface tension effects.

The possibility that surface tension may affect the head-discharge curve in the plate-flow range was investigated by conducting four series of tests. Two series of tests (series 119 and 120) were made with a clean horizontal plate, and two series of comparison tests (series 121 and 122) were made
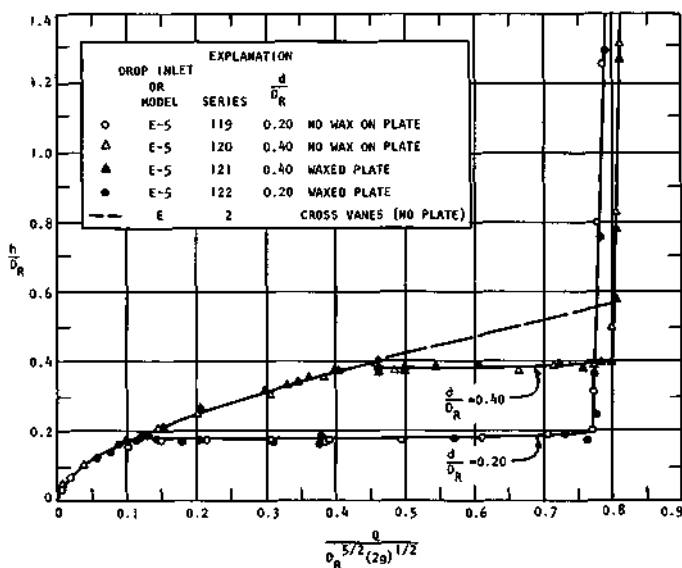
after applying a coat of commercially available liquid wax to the plate used for series 119 and 120. The wax was used to prevent the water from wetting the plate, thereby reducing to a minimum the capillary effect on the plate-flow phenomena. Both the clean and waxed antivortex plates were positioned above the inlet crest at distances d/D_R of 0.20 and 0.40.

The test results are shown in figure 28. The flow conditions for these four tests were weir flow, plate flow, and full flow as described under "Flow Conditions for a Properly Positioned Antivortex Plate." In the plate-flow range a single curve for each plate position well represents the data for the plate waxed or not waxed. Therefore, the lowering of the reservoir level after sealing the inlet with water appears to be a pressure phenomenon and is not the result of surface tension effects.

Effect of Antivortex Plate Positioned
too Close to Drop-Inlet Crest

The head-discharge curves obtained with the antivortex plate positioned at a very small distance $(d/D_R = 0.025)$ above the inlet crest are shown in figure 29. The data are for model E-4 with the plate overhang $L_0/D_R = 0.425$. The curve shown for reference (long dashes) is the head-discharge curve obtained for the circular model drop inlet E when sheet metal cross vanes were placed on the inlet crest to control the formation of vortices.

The sequence of flow conditions which produced the data for figure 29 is different from those observed when the antivortex plate is higher. For the very small initial reservoir inflow the water level rose as weir flow until it touched the antivortex plate and sealed the inlet. After sealing, the reservoir level continued to rise along curve A. This is because the area between the inlet crest and the plate acted as an orifice, and its discharge capacity was considerably smaller than the inflow into the reservoir. Also, after sealing the inlet, no air

Figure 28. Head-discharge curves for horizontal circular antivortex plate with and without wax on the plate
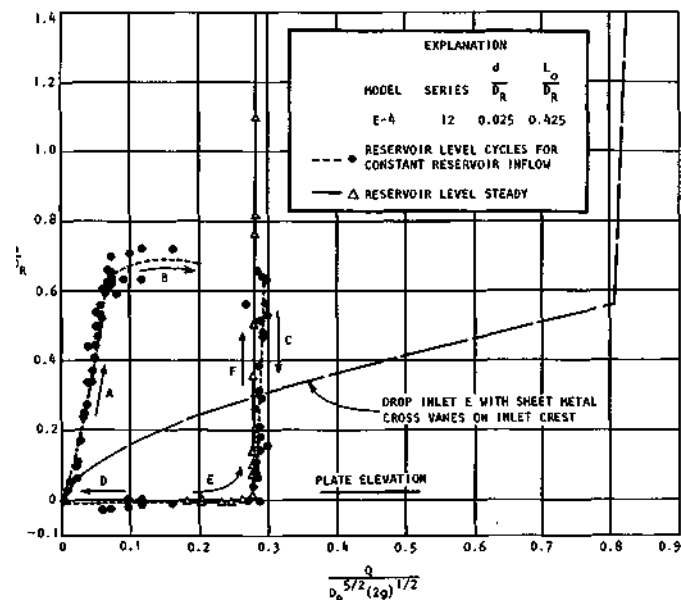

Figure 29. Effect on spillway performance of positioning the antivortex plate too close to the drop-inlet crest

was sucked into the spillway. As the reservoir water level continued to rise, the head between the reservoir level and the inside of the drop inlet slowly increased. Therefore, the spillway discharge gradually increased. During this time the water level in the drop inlet rose to seal the entrance to the barrel, thus trapping air in the drop inlet. The water in the drop inlet gradually became an agitated mixture of air and water. The air-water mixture was discharged through the barrel, and eventually the spillway began to flow full of water only. This flow condition was near the highest reservoir level observed for curve A. The spillway discharge then increased very rapidly along curve B to the full-flow curve C. Because the reservoir inflow was insufficient to meet the spillway full-flow demand, the reservoir storage was depleted until the reservoir water level was slightly below the antivortex plate. Air was then intermittently sucked into the spillway and the spillway discharge decreased very rapidly along curve D back to the beginning of curve A. The discharge continued to cycle along curve A to B to C to D and back to A for several successive runs in which the reservoir inflow was increased from run to run. Eventually a run was made in which the reservoir level did not cycle but remained at the level of the antivortex plate. The reservoir inflow at this level equaled the spillway discharge, and plate flow controlled the spillway discharge.

For further increases in the reservoir inflow the spillway discharge moved to the right along the solid curve E to the full-flow curve F. In the full-flow range the reservoir level moved upward along curve F for increases in the reservoir inflow. The head-discharge relationship represented by the solid curves E and F in figure 29 was single-valued and reversible. The curves A to D were not single-valued nor reversible.

The above discussion is an example of a spillway flow condition that is undesirable and unpredictable; it must and can be avoided by properly positioning the antivortex plate above the inlet crest.

In the initial model tests performed by the State Water Survey, a normally developed circulation around the entrance to the drop inlet was quite evident. The full width of the approach channel was used for the flow approaching the spillway entrance. The flow was permitted to enter the spillway periphery from all directions. No attempt was made to inhibit or to force development of the circulation around the spillway entrance. The crest of the spillway entrance was at a distance of *2D* above the level of the approach channel. The circulation rotated clockwise at times and counterclockwise at other times. In fact, the direction of rotation changed from clockwise to counterclockwise and vice versa during test runs in which no changes were made in model operation. The effect of this normally developed circulation on the drop-inlet spillway performance or capacity was unknown.[8]

Blaisdell[9] reported that normally developed circulation around the spillway entrance when the spillway crest is at the same elevation as the bottom of the approach channel resulted in a serious reduction in spillway capacity. This reduction in capacity was evident in both the weir- and full-flow range.

Specific tests using drop inlet model E *(see table 1)* were conducted by the Water Survey to determine the effect of the normally developed circulation of the flow around a drop-inlet entrance to a closed-conduit spillway on the hydraulic performance of the spillway. This required making tests on the spillway for normally developed circulation, no circulation, and forced circulation for the deep and flush approach depths. Five series of tests with the deep approach were made with the drop-inlet crest at a distance of *2D* above the approach channel floor. For an additional five series of tests a false bottom was installed in the approach channel flush with the drop-inlet crest. The test conditions for each group of test series are summarized in table 5. The head-discharge curves for each of the five series of tests with the deep approach are shown in figure 30. The head-discharge curves for each of the five series of tests with the flush approach are shown in figure 31.

The flow conditions that occurred for the five series of tests with the deep approach and for three of the five series of tests with the flush approach were weir and full flow. In the weir-flow range the nappe was observed to be free at times and clinging at other times. In the full-flow range the vortices that
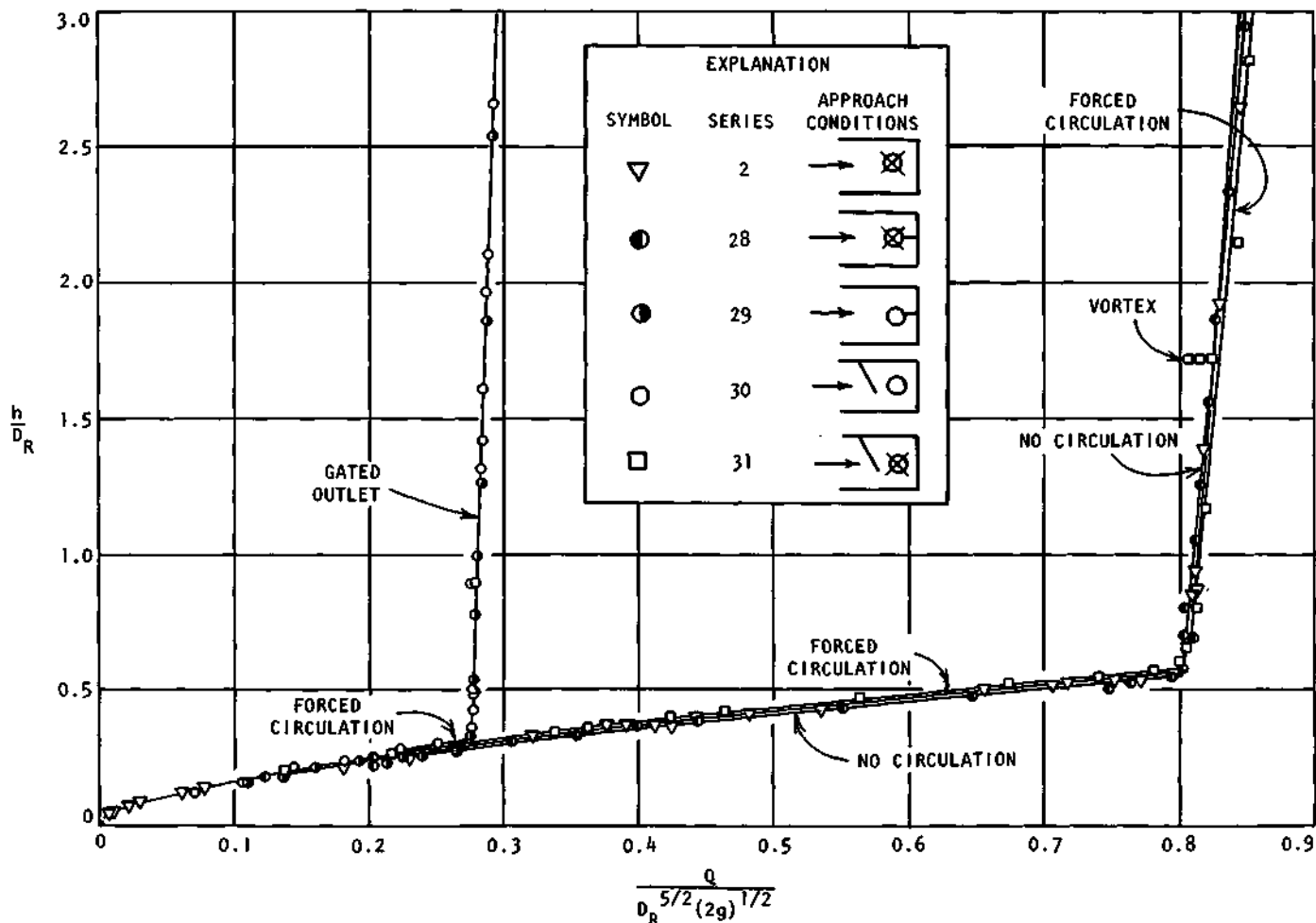

Figure 30. Circulation-effects on performance and capacity of drop-inlet spillway with deep approach

developed had a negligible effect on the head-discharge relationship.

For the other two series of tests with the flush approach the flow conditions were weir flow in combination with a strong twist and full flow. In the weir-flow range the nappe was free at times and clinging at other times. In the full-flow range the vortices that developed had a measurable effect on the head-discharge curve at only one head.

Normally Developed Circulation

Circulation of the flow around the drop-inlet entrance developed normally for series 2 (deep approach) and series 90 (flush approach). In the weir-flow range the nappe was free for some runs and clinging for other runs. Surface circulation was quite evident during the full-flow regime, and although sheet metal cross vanes on the drop inlet were used as an antivortex device, an occasional slender transient vortex core would develop. The vortex extended only a short distance below the reservoir surface and did not have any effect on the spillway discharge. The rating curve was single-valued and reversible for series 2 (figure 30) and series 90 (figure 31).

Circulation Eliminated

Circulation of the flow around the drop-inlet entrance was prevented with a dike *(see figure 13)* for series 28 (deep approach) and series 92 (flush approach).

In the weir-flow range for series 28 the nappe was predominantly clinging but was observed to be free for a few runs. In the full-flow range a short transient vortex was observed at a head $h/D_R = 1.55$. This surface vortex, which developed despite the use of a dike and the cross vane antivortex device, did not suck air into the spillway or have any effect on the spillway discharge. The rating curve shown in figure 30 for series 28 was single-valued and reversible.

In the weir-flow range for series 92 the nappe was free at the lower heads $(h/D_R<0.41)$ and clinging at large heads. In the full-flow range the vortex did not form for this series. The rating curve shown in figure 31 for series 92 was single-valued and reversible.

Circulation Eliminated, Reduced Full-Flow Capacity
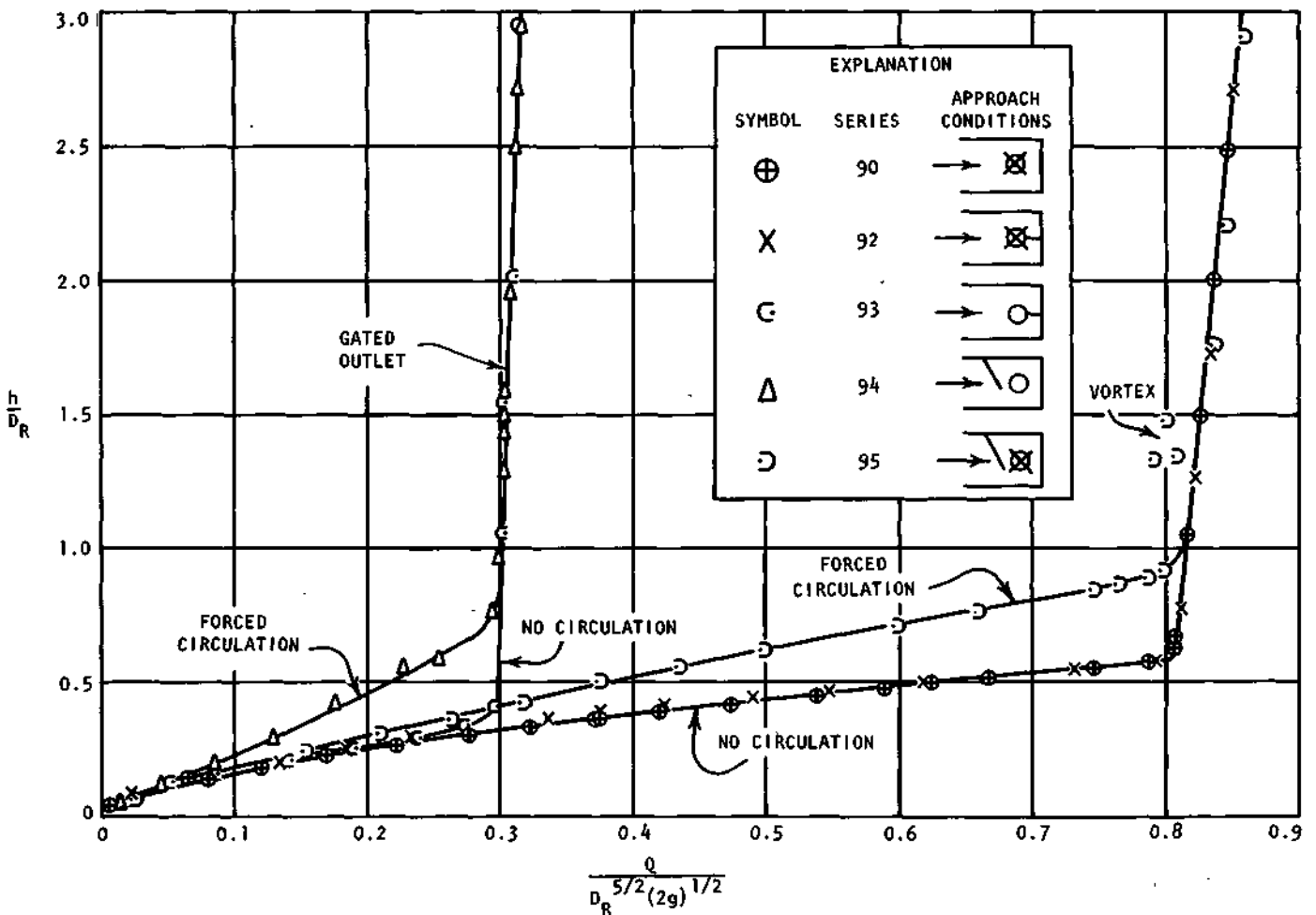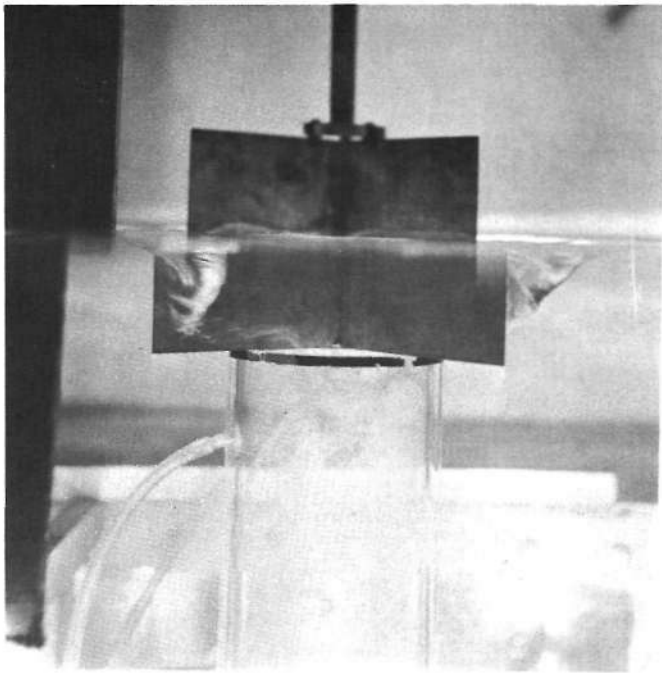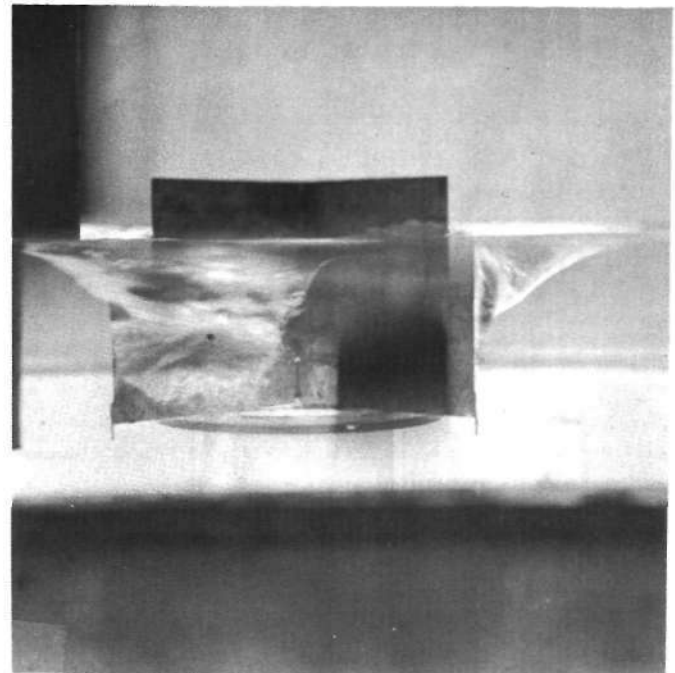
Circulation of the flow around the drop-inlet entrance was

Figure 31. Circulation-effects on performance and capacity of drop-inlet spillway with flush approach

(a) Series 31, deep approach

$Q/D_R^{5/2}(2g)^{1/2} = 0.800$, $h/D_R = 0.61$

(b) Series 95, flush approach

$Q/D_R^{5/2}(2g)^{1/2} = 0.798$, $h/D_R = 0.92$

Figure 32. Flow conditions at drop-inlet entrance for forced circulation. Air is sucked into the drop inlet by vortices at tips of cross vanes. The spillway discharge is very close to full flow. The tailgate at the barrel outlet is fully open

eliminated with a dike *(see figure 13)* and the spillway full-flow capacity was decreased by partially closing the tailgate at the barrel outlet for series 29 (deep approach) and for series 93 (flush approach). In the weir-flow range the nappe may be clinging or free. Both types of nappe were observed. In the full-flow range no vortex formation occurred even though no antivortex device was used. The rating curve was single-valued and reversible for series 29 (figure 30) and for series 93 (figure 31).

Forced Circulation

Forcing circulation of the flow around the drop-inlet entrance by using a guide wall *(see figure 13)* resulted in an extremely strong circulation throughout the entire range of flows for the deep approach (series 31), as well as for the flush approach (series 95).

For series 31 in the weir-flow range the nappe was free at all times. This was true only at low heads for series 95 since at the higher weir flows the nappe was clinging. For both test series, as the discharge was increased very strong eddies developed at the tips of the cross vanes for the higher weir flows, and these eddies persisted into the full-flow range until the vanes were well submerged. Strong eddies that developed at the tips of the cross vanes for nearly full flow before the vanes were submerged are shown in figure 32a (series 31) and in figure 32b (series 95). The air carried through these eddies into and through the spillway did not create any observed unsteadiness for the spillway discharge.

The strong circulation for the deep approach (series 31) slightly increased the head (figure 30) in the normal weir-flow range in comparison with the head obtained for normal circulation (series 2) and for no circulation (series 28). However, for the flush approach (series 95) the shallow approach depth and the very strong circulation combined to greatly increase the head (figure 31) in the normal weir-flow range in comparison with the head obtained for normal circulation (series 90) and for no circulation (series 92).

During full flow for the deep and flush approaches vortices occasionally extended into the drop inlet, but with one exception for each approach depth, these did not seriously affect the spillway discharge. The extreme effects of the deep approach on the spillway discharge for this one run are plotted in figure 30 at an h/D_R of 1.71. A picture of these vortices is shown in figure 33a. For the flush approach the extreme effects on the spillway discharge and head occurred between heads of $h/D_R = 1.33$ to 1.5 as shown in figure 31. A picture of this vortex action at $h/D_R = 1.49$ is shown in figure 33b.

Forced Circulation, Reduced Full-Flow Capacity

For both approach depths, circulation of the flow around the drop-inlet entrance was forced by using a guide wall *(see figure 13)*, and the spillway full-flow capacity was decreased by partially closing the tailgate at the barrel outlet. Also, the cross vane antivortex device used for series 31 and 95 was removed during these reduced capacity tests for series 30 and 94.
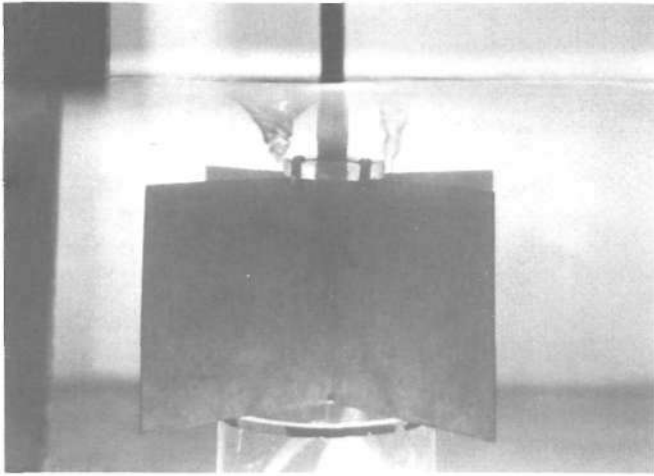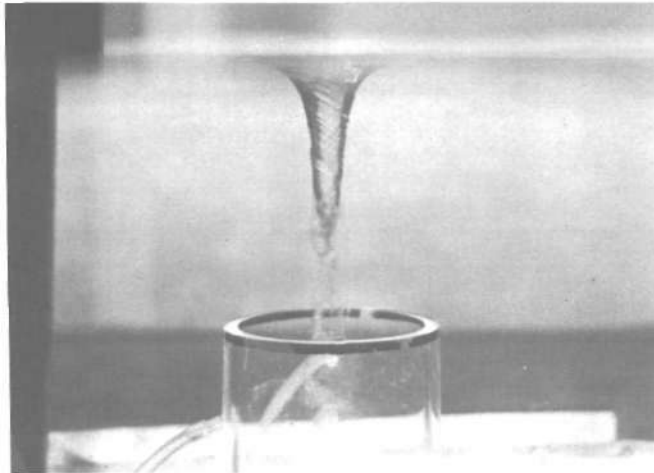
(a) Series 31, deep approach
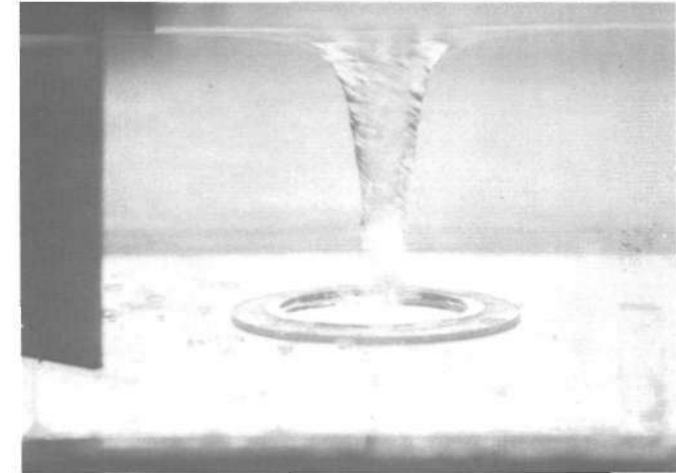$Q/D_R^{5/2}(2g)^{1/2} = 0.816$, $h/D_R = 1.71$
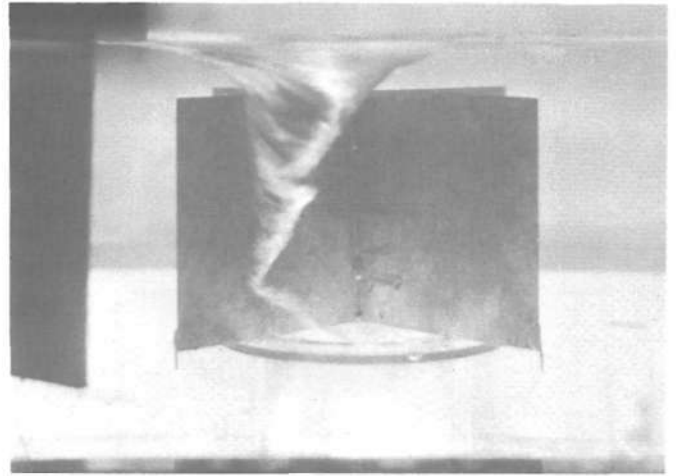
(b) Series 95, flush approach
$Q/D_R^{5/2}(2g)^{1/2} = 0.796$, $h/D_R = 1.49$

Cross vanes, tailgate open, vortices noisely sucking air into drop inlet

(c) Series 30, deep approach
$Q/D_R^{5/2}(2g)^{1/2} = 0.283$, $h/D_R = 1.42$

(d) Series 94, flush approach
$Q/D_R^{5/2}(2g)^{1/2} = 0.304$, $h/D_R = 1.44$

Tailgate partially closed, vortex quiet, very small air intake

Figure 33. Flow conditions at the drop-inlet entrance for forced circulation

For series 30 (deep approach) the forced circulation resulted in a strong circulation in the weir-flow range and in the full-flow range for heads below about $h/D_R = 2.0$. In the weir-flow range the nappe was clinging for the lower heads $(h/D_R < 0.23)$ and free at higher heads as shown by the water drops on the inside of the drop-inlet wall in figure 34a. The free nappe for this weir flow had a slight twist. A vortex developed as soon as the weir was submerged and the spillway flowed full. Although this vortex appeared to be vigorous and the air core was large, very little air was drawn into the spillway and the spillway discharge was steady. Figure 35a shows the vortex at the inlet for $h/D_R = 0.35$. This vortex is combined with a free nappe at the drop-inlet crest. The air trapped under the free nappe was gradually evacuated, and when the next run was made at $h/D_R = 0.50$, the nappe was clinging although the vortex core remained as can be seen in figure 35b. The spillway discharge was steady for the flow conditions shown in figure 35. Figure 33c shows a vortex at a head $h/D_R = 1.42$. This vortex with a relatively large core and strong circulation appears to be serious, but it did not affect the spillway discharge.

For series 94 (flush approach) there was strong circulation in both the weir- and full-flow ranges. In the weir-flow range the nappe was clinging for all runs. A typical clinging nappe with a strong twist is shown in figure 34b. As soon as the weir control was submerged and the spillway flowed full, a vortex
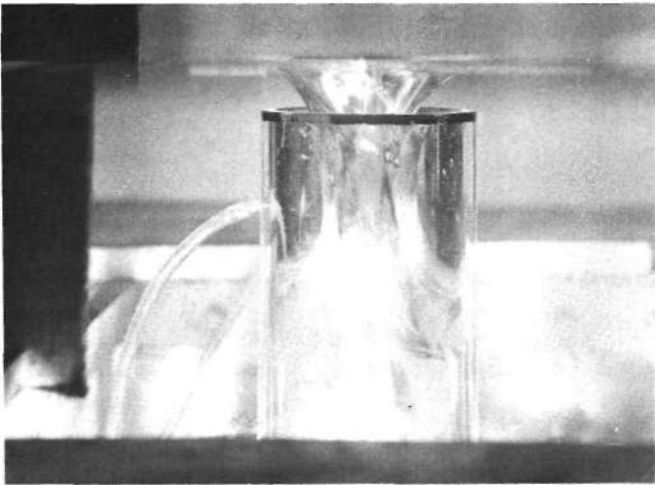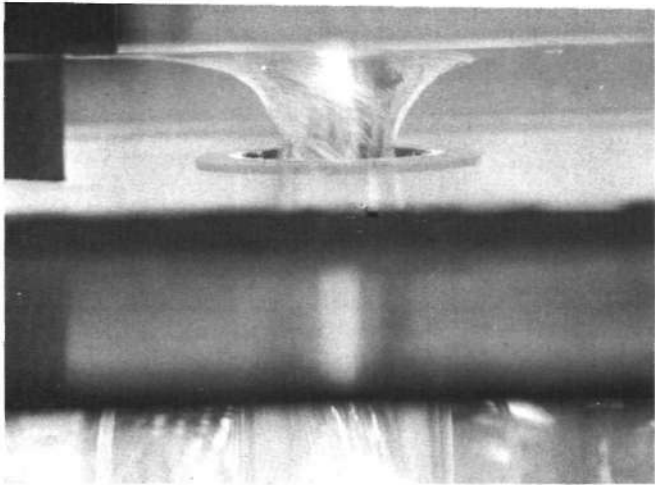
(a) Series 30, deep approach

$Q/D_R^{5/2}(2g)^{1/2} = 0.221$, $h/D_R = 0.28$

Free nappe

(b) Series 94, flush approach

$Q/D_R^{5/2}(2g)^{1/2} = 0.226$, $h/D_R = 0.56$

Clinging nappe, twist in nappe

Figure 34. Weir-flow conditions at the drop-inlet entrance for forced circulation

developed. This vortex appeared to be vigorous and the air core was large, however, the spillway discharge was steady. Figure 33d shows a vortex at a relative head h/D_R of 1.44. This vortex with a relatively large core and strong circulation appears to be serious, but it did not affect the spillway discharge.

The rating curves for series 30 (figure 30) and for series 94 (figure 31) were single-valued and reversible.

Comments on Circulation Effects

Examination of the rating curves in figure 30 for the deep approach and in figure 31 for the flush approach shows that when vortex formation at the inlet is controlled:

1) Normally developed circulation has an insignificant effect on the spillway capacity in the weir- and full-flow ranges.
2) Eliminating circulation around the drop-inlet entrance yields essentially the same results as normally developed circulation.
3) Forced circulation has an insignificant effect on the spillway full-flow capacity.
4) Forced circulation has a significant effect in the weir-flow range for the flush approach, but a very small effect for the deep approach.

The head-discharge rating curves in figures 30 and 31 indicate that the location in a reservoir of a closed-conduit spillway with a drop-inlet entrance should not affect the spillway performance.
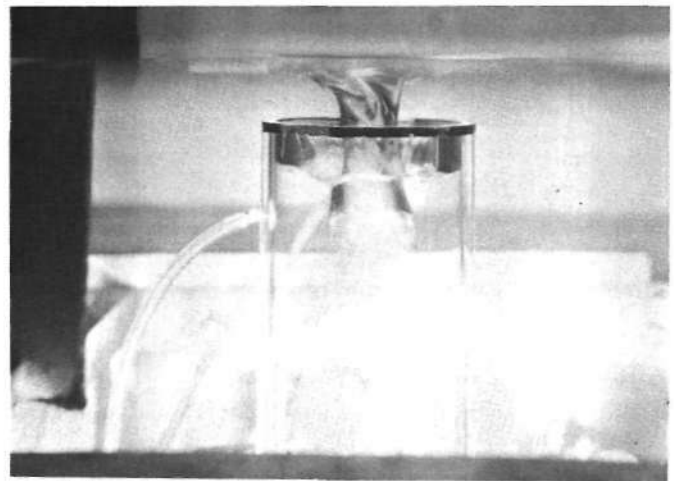
(a) Air pocket under nappe at crest

$Q/D_R^{5/2}(2g)^{1/2} = 0.277$, $h/D_R = 0.35$
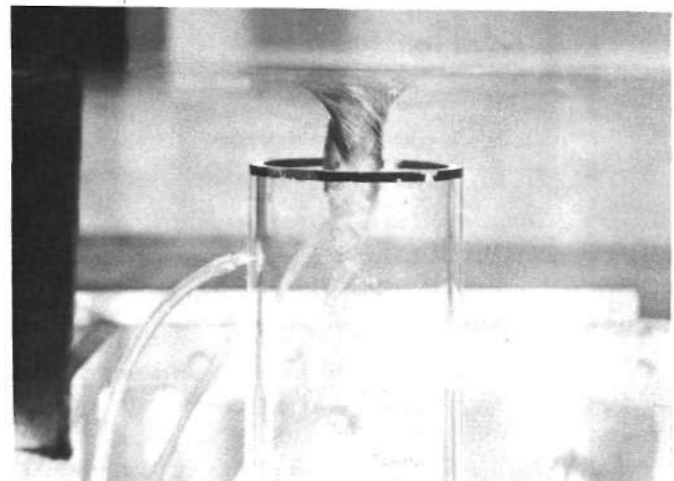
(b) No air pocket at crest

$Q/D_R^{5/2}(2g)^{1/2} = 0.277$, $h/D_R = 0.50$

Figure 35. Flow conditions at the drop-inlet entrance for two successive runs of series 30 for forced circulation, deep approach, tailgate partially closed, counterclockwise vortex, and very small air intake. The barrel is flowing full

A designer must have specific information to properly design a closed-conduit spillway with a drop-inlet entrance for a specified performance and capacity. The information presented here will enable the designer to determine the spillway capacity for weir control, the minimum capacity when a vortex is free to form, and the capacity for plate flow.

Weir Coefficient of Discharge

The coefficient of discharge C_w for equation 2 was determined for the model spillway drop inlets shown in table 1. All the drop inlets were tested with a deep approach to the inlet crest and those selected for testing with the channel approach flush with the inlet crest are marked with an asterisk. All drop inlets were tested with and without sheet metal cross vanes.

The weir coefficient of discharge C_w for the pircular drop inlets A—G for the deep approach is given by the solid curve in figure 36. The dashed curves are drawn for a ± 5 percent variation of C_w from the solid curve to indicate the precision of the data. The method used to determine the equations for C_w was similar to that used by Blaisdell.[9] The equations for C_w were determined after plotting $[Q/D_R^{5/2}(2g)^{1/2}]^{2/3}$ against h/D_R as shown in figure 37. It is evident that two straight lines, which were determined by the method of least squares, well represent the data for drop inlets A—G. The equation for the upper straight line is

$$[Q/D_R^{5/2}(2g)^{1/2}]^{2/3} = 2.3128(h/D_R) - 0.386 \quad (53)$$

or

$$Q/D_R^{5/2}(2g)^{1/2} = [2.3128(h/D_R) - 0.386]^{3/2} \quad (54)$$

Also, equation 3 for the head-discharge curve in the weir-control range is

$$Q/D_R^{5/2}(2g)^{1/2} = C_w(h/D_R)^{3/2}$$

Equating the right hand quantities of equations 54 and 3 leads to

$$C_w(h/D_R)^{3/2} = [2.3128(h/D_R) - 0.386]^{3/2} \quad (55)$$

from which

$$C_w = 1.12[1 - 0.17/(h/D_R)]^{3/2} \quad (56)$$

when h/D_R is equal to or greater than 0.475.

When $0.05 < h/D_R \quad 0.475$ the equation for C_w in figure 36 is

$$C_w = 0.638[1 - 0.027/(h/D_B)]^{3/2} \quad (57)$$

The weir coefficient of discharge C_w for the square drop inlets H and J with a deep approach is given by the solid curve in figure 38. The dashed curves are drawn for a ± 10 percent variation of C_w from the solid curve to indicate the precision of the data. It is unknown why the scatter of these data is so much larger than that of the data of figure 36. The determination of the equation

$$C_w = 0.554[1 - 0.018/(h/B)]^{3/2} \quad (58)$$

for the curve in figure 38 was made in the same manner as for the circular drop inlets.

Equations for the weir coefficients of discharge for the other drop inlets were computed in the same way as for these examples. Table 7 lists a summary of the equations for the weir coefficient of discharge C_w for all the drop inlets tested along with the head range for which each equation is applicable or for the head range covered by the tests. The geometrically similar drop inlets are grouped together in table 7 when the
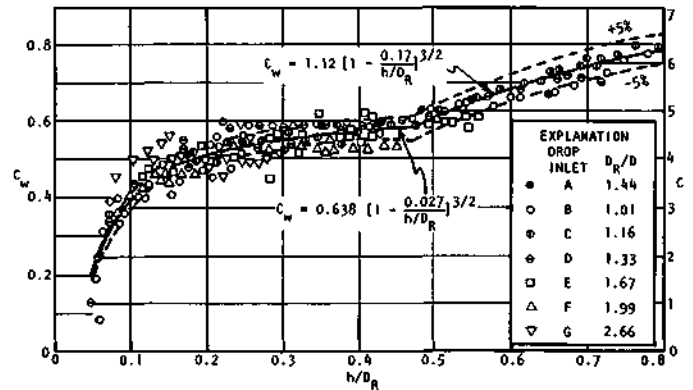

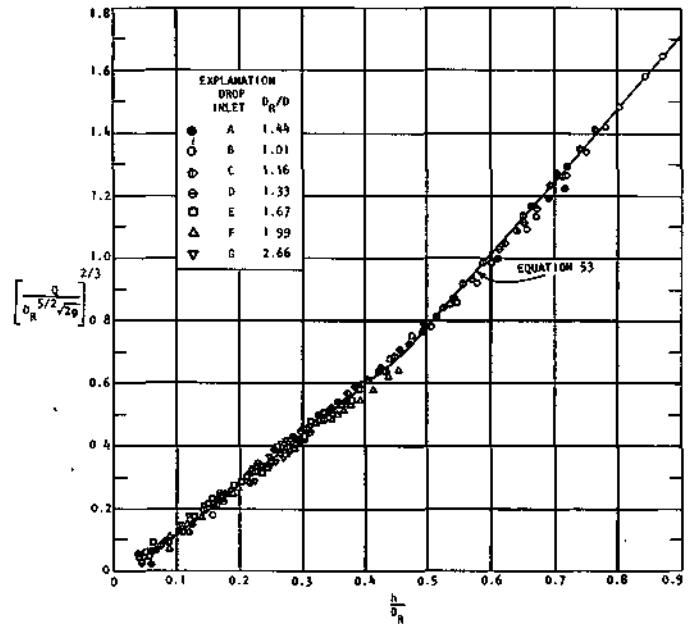Figure 36. Weir coefficient for circular drop inlets with a deep approach

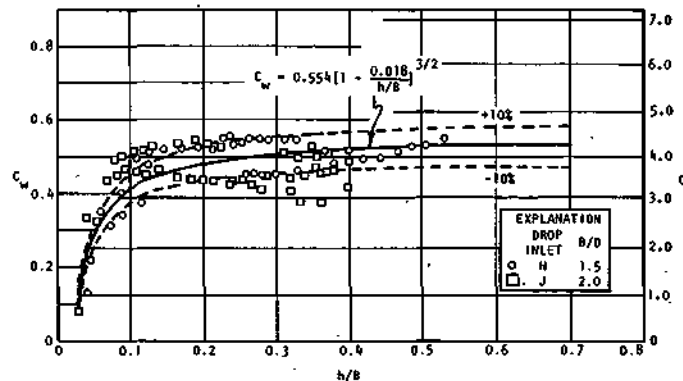Figure 37. Head-discharge curve for weir flow, circular drop inlets, and a deep approach

Figure 38. Weir coefficient for square drop inlet with a deep approach

Table 7. Experimental Equations for Weir Coefficient C_w

| Drop inlet	C_w	Experimental head range
	Deep approach (depth = 2D)*	
A,B,C,D,E,F,G	$C_w = 0.638[1 - 0.027/(h/D_R)]^{3/2}$	$0.05 < h/D_R < 0.475$
A,B,C,D,E	$C_w = 1.12[1 - 0.17/(h/D_R)]^{3/2}$	$0.475 < h/D_R < 0.80$
H,J	$C_w = 0.554[1 - 0.018/(h/B)]^{3/2}$	$0.03 < h/B < 0.53$
I	$C_w = 0.514[1 - 0.012/(h/B)]^{3/2}$	$0.05 < h/B < 0.45$
K	$C_w = 0.527[1 - 0.012/(h/B)]^{3/2}$	$0.05 < h/B < 0.275$
L,M	$C_w = 0.461[1 - 0.026/(h/B)]^{3/2}$	$0.05 < h/B < 1.0$
N	$C_w = 0.544[1 - 0.044/(h/B)]^{3/2}$	$0.1 < h/B < 0.65$
O	$C_w = 0.416[1 - 0.035/(h/B)]^{3/2}$	$0.08 < h/B < 0.42$
O	$C_w = 0.511[1 - 0.084/(h/B)]^{3/2}$	$0.42 < h/B < 1.0$
	Flush approach	
C,D,E	$C_w = 0.596[1 - 0.028/(h/D_R)]^{3/2}$	$0.05 < h/D_R < 0.53$
C	$C_w = 1.02[1 - 0.18/(h/D_R)]^{3/2}$	$0.53 < h/D_R < 0.85$
I	$C_w = 0.475[1 - 0.022/(h/B)]^{3/2}$	$0.05 < h/B < 0.45$
H	$C_w = 0.531[1 - 0.021/(h/B)]^{3/2}$	$0.045 < h/B < 0.55$

Drop inlet G approach depth = 5D

data indicate this is desirable. The scatter of the data for all the drop inlets, except those shown in figure 38, was quite similar to or less than the scatter shown for circular drop inlets in figure 36.

The scatter of the data in figures 36 and 38 is the result of the unpredictability of the nappe conditions. Since no effort was made to insure obtaining a particular nappe, the nappe was at times clinging and at other times free. Also, the unknown varying pressure underneath the nappe influences the weir coefficient. The use of cross vanes to extend the weir-control range and to control the formation of vortices would not insure either a free or clinging nappe. The scatter of the data with and without the vanes did not indicate any systematic effect of the vanes on the weir coefficient.

Circulation Effect on Weir Coefficient

The weir discharge coefficient C_w determinations discussed above were calculated from test data taken when normally developed circulation around the drop-inlet entrance was present. The effect of this circulation on the weir coefficient was unknown. Therefore, the weir coefficient was calculated for, the five deep approach tests and three of the flush approach tests described in "Circulation Effects." The weir coefficient was not calculated for two flush approach tests (series 94 and 95) for forced circulation because the strong twist in the flow at the inlet resulting from the forced circulation caused the head to be greatly increased in the normal weir-flow range. The head-discharge curves in figure 31 for series 94 and 95 indicate the magnitude of the head increase.

The weir coefficient C_w for each of the five series of tests for the deep approach is plotted in figure 39. With the circulation prevented, series 28 and 29, the single curve of figure 39a well represents the data. For the forced circulation tests, series 30 and 31, the single curve of figure 39b well represents the data. These two curves are also shown in figure 39c, and it is
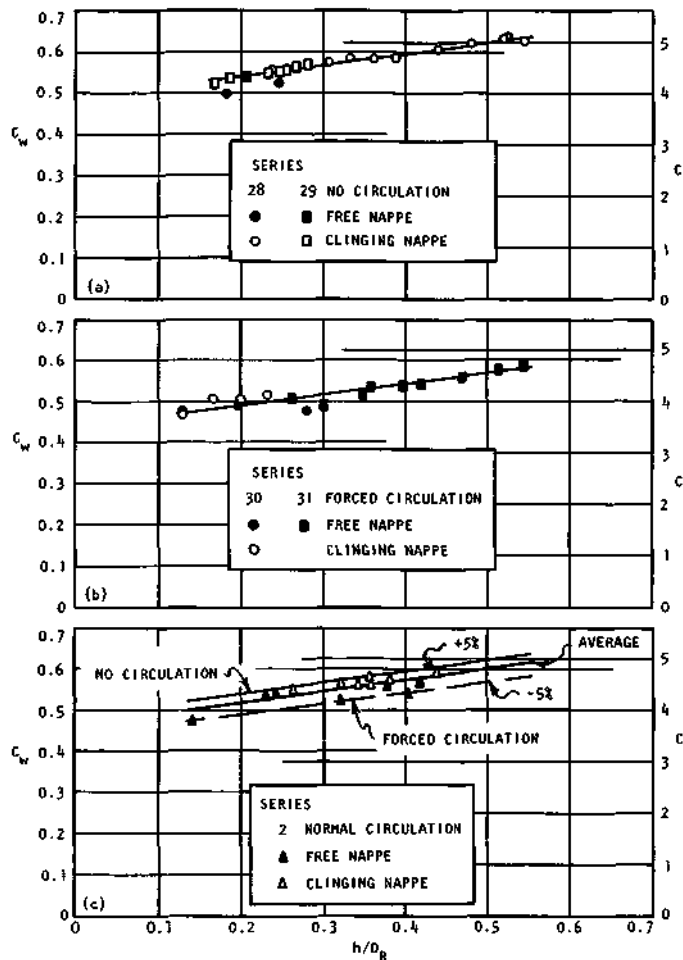
Figure 39. Weir coefficient for no circulation, forced circulation, and normal circulation for deep approach

apparent that no circulation yields a higher weir coefficient than the forced circulation. For the normally developed circulation, series 2, the weir-coefficient data are scattered between these two curves. This scatter is not excessive when it is recognized the data are for different intensities of circulation and that no attempt was made to insure that the weir nappe would be either clinging or free.

For the flush approach the weir coefficient C_w for series 90, 92, and 93 is plotted in figure 40. The solid curve depicts the average curve and the ±5 percent dashed curves indicate the precision of the data. The scatter of the data about the average curve is small compared with the scatter for other series and the various intensities of circulation. No attempt was made to insure either a clinging or free nappe.

It can be concluded that normally developed circulation has an insignificant effect on the weir coefficient for both the deep and flush approaches.

Orifice Control by Drop-Inlet Crest

The discharge through the drop inlets listed in table 1 was not observed at any time as being controlled by the drop-inlet crest acting as an orifice. Therefore, orifice control does not

exist for the drop inlets tested, and the orifice coefficient of discharge C_0 could not be determined.

Short-Tube Control by Drop Inlet

The discharge through the drop inlets listed in table 1 was not observed at any time as being controlled by the drop inlet acting as a short tube. Therefore, short-tube control does not exist for the drop inlets tested, and the short-tube coefficient of discharge C_8 could not be determined.

Vortex Effect

The general effect of vortices on the performance of spillways with a circular drop inlet was discussed in "Vortex Effect and Flow Descriptions." It was shown that vortices may or may not influence the head-discharge relationship. Equation 52 was used to examine experimental data obtained for the tests reported in this section to determine the geometric proportions of drop inlets for which the limiting effect of vortices on spillway capacity can be predicted. The formation of vortices at the drop inlet was a naturally developed flow phenomenon.

For each test series the approaching flow well upstream of the drop inlet utilized the full width of the approach channel. In the vicinity of the drop inlet the flow approached the inlet from all directions and no attempt was made to inhibit normally developed circulation. The tests were conducted with a deep approach for all the drop-inlet models listed in table 1, and the flush approach was used for the selected drop inlets indicated by an asterisk. The tailgate at the barrel outlet was used for several series of tests to reduce the spillway full-flow capacity to values below the ungated capacity.

Figure 40. Weir coefficient for no circulation and normal circulation for flush approach

Maximum   Spillway   Capacity

The vortex effects on spillway capacity for the deep approach are shown in figures 41 and 43. Figure 44 shows the test results for the flush approach. The data in each figure are plotted in accordance with the head and discharge parameters of equation 52. The solid curves, shown for reference, were obtained by placing sheet metal cross vanes on the drop-inlet crest to control the effect of vortices on the spillway capacity. The vortex envelope, equation 52, is also shown for reference. The tailgate at the barrel outlet was not used for any of the test series shown. In each of the three figures the vortex was present at some time during the test series for each drop inlet. The influence of the vortex on spillway capacity for each series is indicated by the scatter of the instantaneous head-discharge data. In general the predominant influence of the vortex on the spillway capacity is in the area to the right of the vortex envelope; however, the vortex at times did have an influence on the normal full-flow spillway discharge to the left of the vortex envelope.

It is apparent in figures 41, 43, and 44 that the vortex effect on the spillway discharge or head can be large or it can be insignificant. For example, the vortex did not have a measurable effect on the head-discharge curve for drop inlet G (series 67) in figure 41 or for drop inlet K (series 77) in figure 43. However for drop inlet E (series 3) in figure 41 the vortex reduced the discharge by as much as 46 percent less than the obtainable discharge if the vortex is controlled. Other large
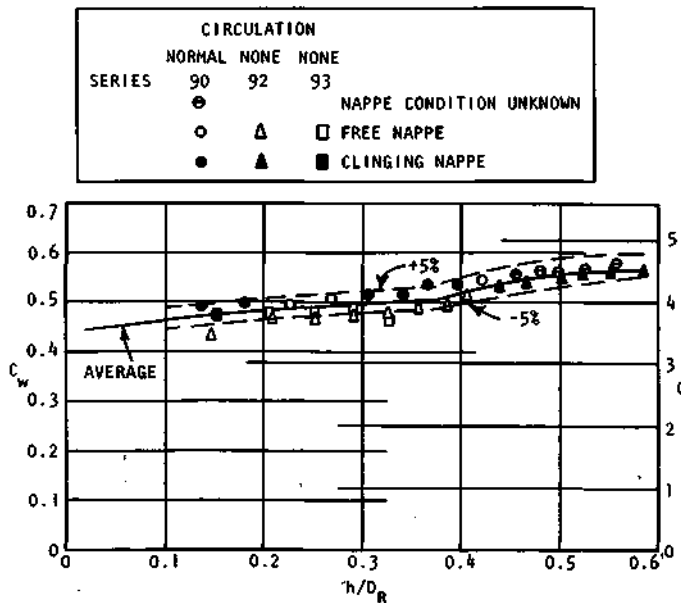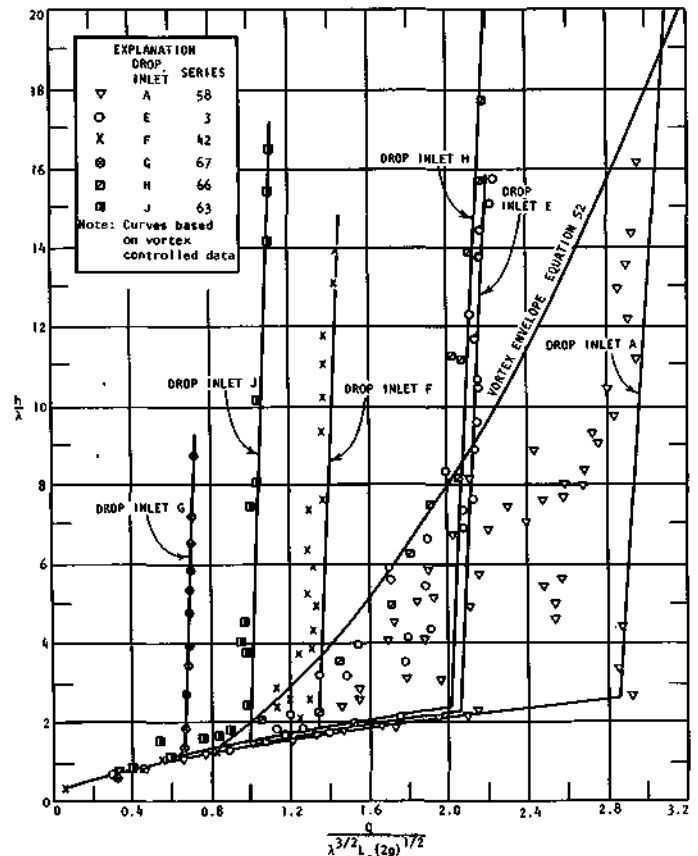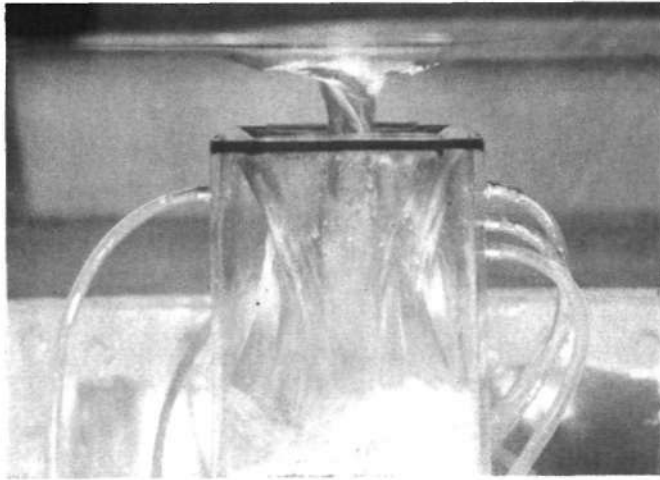

Figure 41. Vortex effect on spillway capacity for deep approach

reductions in spillway capacity are also apparent in figures 43 and 44. These reductions in spillway capacity occurred in the area to the right of the vortex envelope. The vortex influence on the normal full-flow discharge to the left of the vortex envelope for the data presented varied from 0 to 11 percent in figure 41, from 0 to 14 percent in figure 43, and from 0 to 6 percent in figure 44.

The vortex control section for figure 41 was the drop-inlet

Drop inlet J, series 63

$$Q/\lambda^{3/2}L_c(2g)^{1/2} = 0.657, \quad h/\lambda = 1.45$$

Figure 42. Vortex combined with a free nappe at the drop-inlet crest
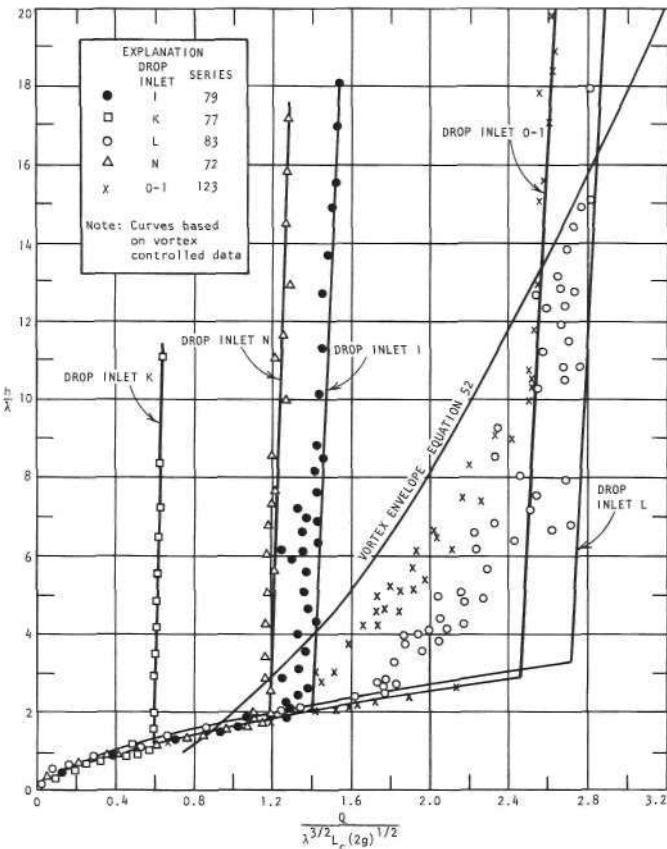

Figure 43. Vortex effect on spillway capacity for deep approach

entrance for all the data to the right of the vortex envelope and for the data to the left of the vortex envelope for drop inlets A, E, G, and H. The large variation in discharge to the left of the envelope in the normal full-flow range for drop inlets F and J occurred during runs in which the minimum area of the vortex air core shifted from the drop-inlet entrance to the barrel entrance. That is, the expansion of the air core took place in the barrel rather than at the entrance to the drop inlet. The deviations in the instantaneous head-discharge data in the normal weir-flow range for drop inlets F and J were the result of a combination of a vortex at the inlet entrance and a free nappe. Figure 42 shows this flow condition for drop inlet J. Because vortices for drop inlets F and J had a serious effect on their head and discharge to the left of the vortex envelope in the normal weir-flow range, an antivortex device would be recommended.

In figure 43 the rather large variation in the instantaneous head-discharge data for drop inlet I to the left of the vortex envelope occurred when the vortex air core expanded in the barrel near its entrance indicating a shift in the vortex control section from the drop-inlet entrance to the barrel transition. The vortex control section was the drop-inlet entrance for the remaining data shown.

Series of tests for the deep approach were also performed for circular drop inlets C and D, and rectangular drop inlet M to determine the influence of vortices on spillway capacity. The test results for drop inlets C and D were similar to those obtained for drop inlets A and E shown in figure 41. The test results for drop inlet M were similar to those obtained for drop inlet L shown in figure 43.

In figure 44 the large variation in the head-discharge data for drop inlet H occurred near the intersection of the normal full-flow curve and vortex envelope during runs in which the vortex air core expanded in the barrel entrance. Also, the slight vortex effect on discharge for drop inlet H for $h/\lambda = 8$ to 9.5 occurred when the vortex air core expanded in the barrel entrance. The vortex control section was the drop-inlet entrance for the data to the right and left of the vortex envelope except as noted above for drop inlet H.

Series of tests were also performed for drop inlet D and the test results were similar to those obtained for drop inlet E shown in figure 44.

Reduced Spillway Capacity

The head-discharge data shown in figures 41 and 43 for the deep approach and in figure 44 for the flush approach were obtained by utilizing the maximum obtainable spillway capacity in the test apparatus for each drop inlet. Therefore, a logical question is, would the vortex seriously affect the spillway discharge for a drop inlet such as drop inlet I (figure 43) for the deep approach or for drop inlet H (figure 44) for the flush approach if the spillway full-flow capacity were reduced to the discharge value at the intersection of the weir and vortex-envelope curves? To answer this question, the tailgate at the barrel outlet was partially closed to reduce the spillway full-flow capacity to the discharge value near the intersection of
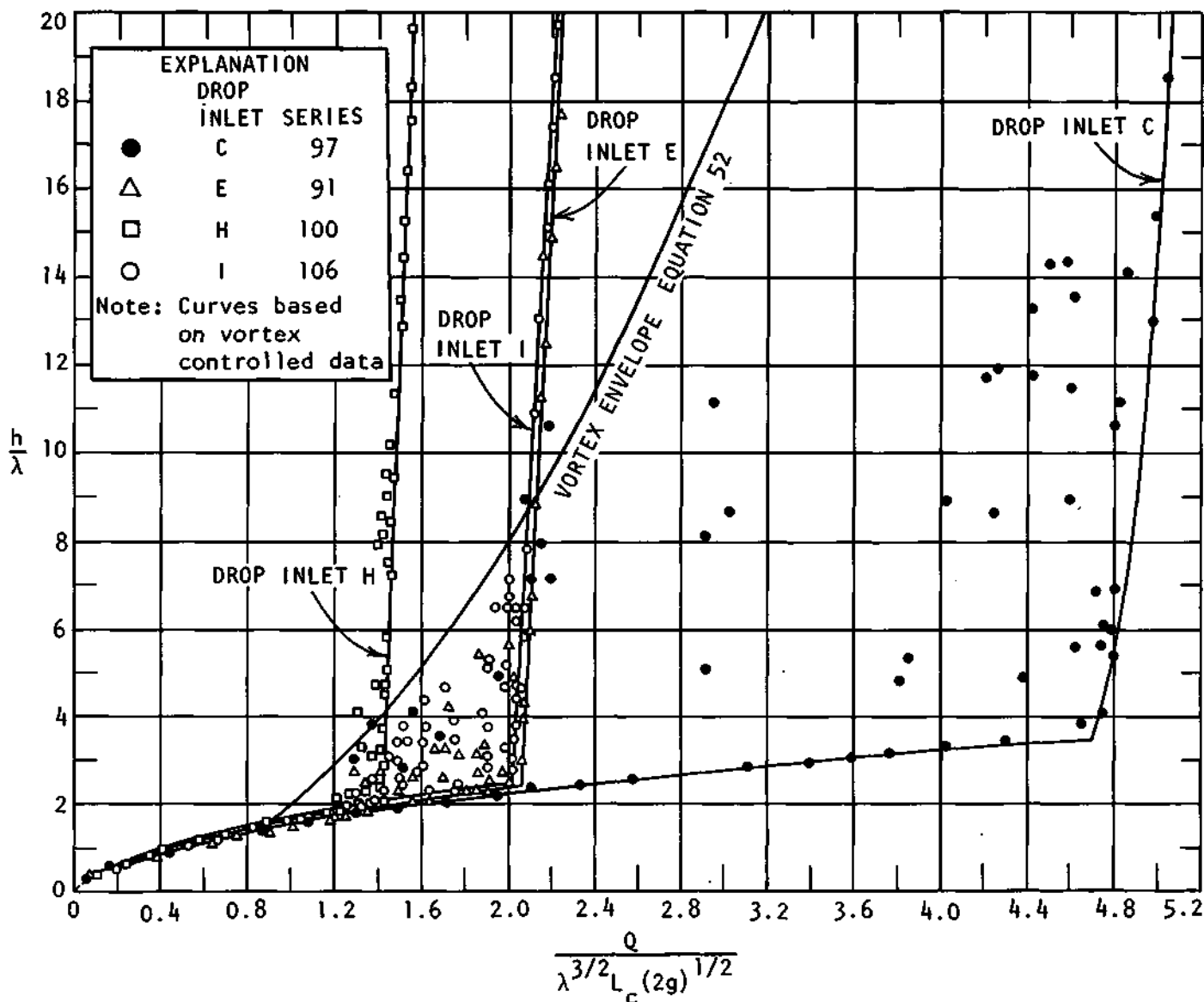
Figure 44. Vortex effect on spillway capacity for flush approach

the weir and vortex-envelope curves as shown in figure 45. The spillway performed as expected for the deep and flush approach; that is, the initial discharges were controlled by the weir at the inlet, and the full-flow discharges were controlled by the spillway head losses. Vortices did form in the full-flow range. Their maximum effect on the discharge was only 4.5 percent as shown in figure 45 for drop inlet I with the deep approach, and only 1.5 percent for drop inlet H with the flush approach. These small effects on the discharge are not considered serious.

For the deep approach similar reduced spillway capacity tests were also performed on circular drop inlets C, D, E, and F, square drop inlets H and J, and rectangular drop inlets L, M, and N. Reduced spillway capacity tests were not performed on drop inlets G and K since their maximum attainable full-flow capacities were to the left of the vortex envelope, and the formation of vortices did not affect spillway capacity *(see figures 41 and 43).* During these reduced spillway capacity

tests vortices did not affect the weir flow head-discharge curves for drop inlets C, D, E, H, L, M, and N. The vortices that formed in the full-flow range for these drop inlets had a small (2 percent) measurable effect on the spillway discharge for only one series of tests. This small reduction in capacity was transient and is considered to be insignificant. During the tests for drop inlets F and J vortices did form in the normal weir-flow range and they had an effect on the spillway discharge. The variations in discharge were similar to those obtained for the ungated tests conducted on these two drop inlets *(see figure 41).* The vortices that formed after full flow was attained did not have a measurable effect on the discharge.

For the flush approach reduced spillway capacity tests were also performed on circular drop inlets C, D, and E, and square drop inlet I. During these tests vortices did not affect the weir flow head-discharge curves for drop inlets C, D, E, and I. The vortices that formed in the full-flow range for these drop inlets did not have a measurable effect on the discharge.
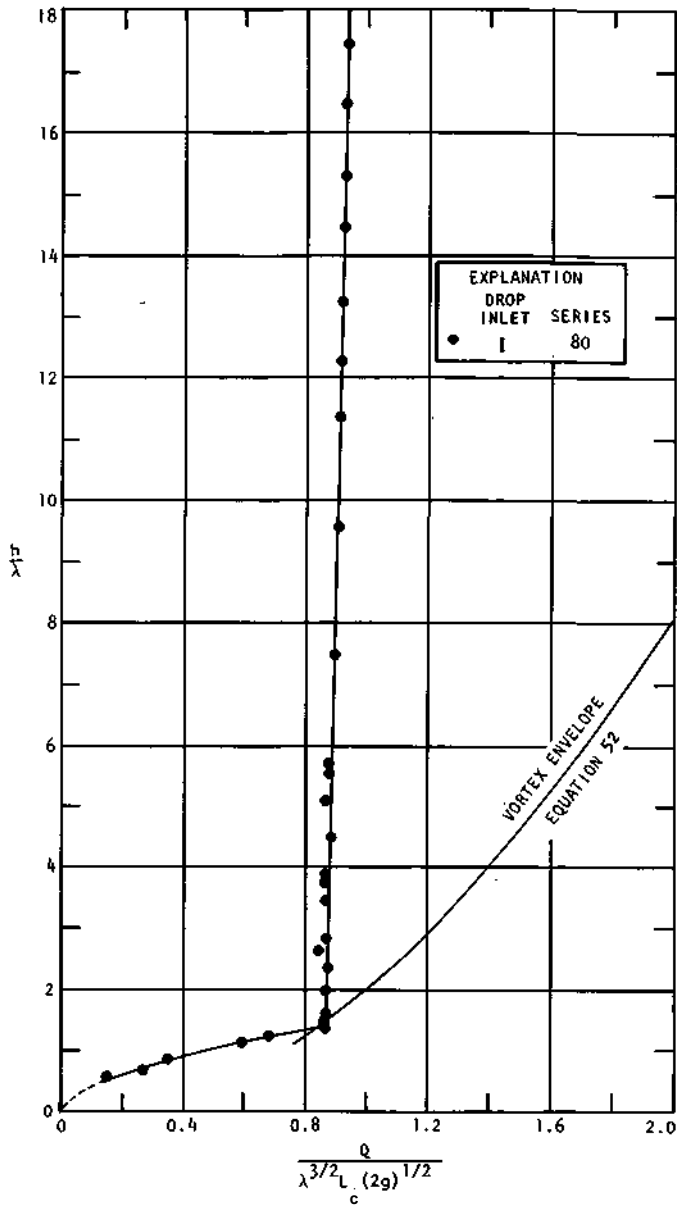
41

Figure 45. Vortex effect for reduced spillway capacity and deep approach

Minimum Drop-Inlet Height with Vortices

The vortex-envelope curve (equation 52) was developed with the vortex control section near the entrance of a relatively tall drop inlet. For a decrease in the drop-inlet height, absolute and relative, it was observed during the tests that the vortex control section gradually shifts to the area of the transition between the drop inlet and the barrel. During this shift of control section the effect of the vortex on the limiting head-discharge curves varies from no effect to a very large one *(see figure 25)*. That is, for a relatively tall drop inlet the effect of the vortex activity would be to the right of point 'A' and would be enclosed between the weir curve, the vortex envelope, and the solid full-flow curve. The vortex would have only a minimal effect on the full-flow curve above the vortex-envelope curve. The data presented in figure 46 exemplify the vortex effect on the spillway head and discharge for a relatively tall drop inlet.

The height of the drop inlet can be reduced so that the adverse effect of the vortex activity can extend to the left of the envelope as shown in figure 25. The data presented in figure 47 are representative of this effect. Also the vortex activity can reduce the full-flow capacity as shown in figure 47 by the data at the left of the full-flow curve and above the vortex-envelope curve.

There is no clear line of demarcation to indicate when the reduction in spillway capacity due to vortex activity can be considered serious. Therefore, in determining the minimum height of drop inlets arbitrary criteria were established for the allowable adverse effect of the vortex on the spillway capacity. The criterion used to establish the recommended minimum drop-inlet height was that the discharge with a vortex could not be more than 6 percent less than the discharge read from the vortex-envelope curve or from the full-flow curve above the vortex-envelope curve.

Model tests were conducted to determine the minimum drop-inlet height for which the anticipated effect of vortex activity would not cause more than 6 percent reduction in the spillway capacity. Each model was operated without an antivortex device, with a deep approach to the drop inlet, and through the full range of flow from weir to vortex to full flow.

The drop inlets were reduced in height by cutting from the midsection and replacing the original crest on the shortened base. The drop inlet was tested and the procedure repeated until the head-discharge data frequently plotted to the left of the vortex envelope or the full-flow curve.

The model test results with the recommended minimum drop-inlet heights are presented in table 8. Also given are the
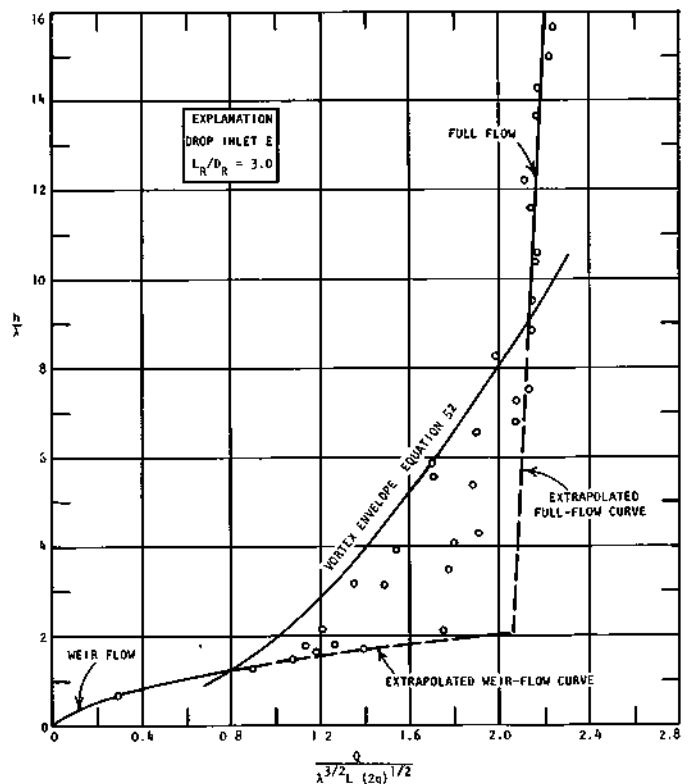

Figure 46. Vortex effect on the spillway head and discharge for a relatively tall drop inlet

42

head-loss coefficients for the drop-inlet entrance, for the transition between the drop inlet and barrel, and for the combined entrance and transition. The maximum percentage of model discharge deviation to the left of the vortex-envelope curve and full-flow curve above the envelope are shown. It is apparent that all models met the 6 percent criterion for discharge deviation from the vortex-envelope curve and the full-flow curve above the vortex-envelope curve.

The test data for the recommended minimum drop-inlet height for model E are shown in figure 48. The head-discharge data below the solid full-flow curve are bounded by the vortex envelope on the left, the extrapolated weir-flow curve on the bottom, and the extrapolated full-flow curve on the right. The data plotted to the left of the solid full-flow curve show the deviation of the discharge that may be expected due to vortex effect.

The full-flow curve in figure 48 is relatively far to the right of the intersection of the weir and vortex-envelope curves. The position of the full-flow curve obviously depends upon the capacity of the spillway. Therefore, for smaller capacities this curve moves to the left. As the full-flow curve moves to the left for smaller spillway capacities the vortex effect is reduced to values less than the percentages given in table 8. When the full-flow curve is at or to the left of the intersection of the weir and vortex-envelope curves, the vortex activity has an insignificant effect on the head-discharge relationship. This was described and documented earlier in "Reduced Spillway Capacity."

The solid head-discharge curves shown in figure 48 repre-

Figure 48. Typical vortex effect on the spillway head and discharge for a recommended minimum drop-inlet height

sent the minimum expected performance of the spillway when an antivortex device is not used.

Therefore, to determine the minimum expected performance of prototypes having a drop-inlet height equal to or greater than the relative heights shown in table 8 requires computing and plotting the weir curve, the vortex envelope, and the full-flow curve. The full-flow curve is computed with the assumption that no vortex is present. The computed nondimensional head and discharge parameters are those in equation 52.

The plotted minimum performance curves for a closed-conduit spillway with a properly proportioned drop-inlet entrance will show at a glance if the head-discharge curve will be affected by vortices. A single-valued head-discharge curve is obtained when the spillway full-flow curve is to the left of the intersection of the weir curve and the vortex-envelope curve. An antivortex device is not needed for this predictable hydraulic performance of the spillway.

When the spillway full-flow curve is to the right of the intersection of the weir curve and the vortex-envelope curve, uncontrolled vortices can and do affect the spillway's hydraulic performance. The magnitude of the effect depends upon how far to the right the full-flow curve is located. To obtain single-valued predictable head-discharge curves an antivortex device

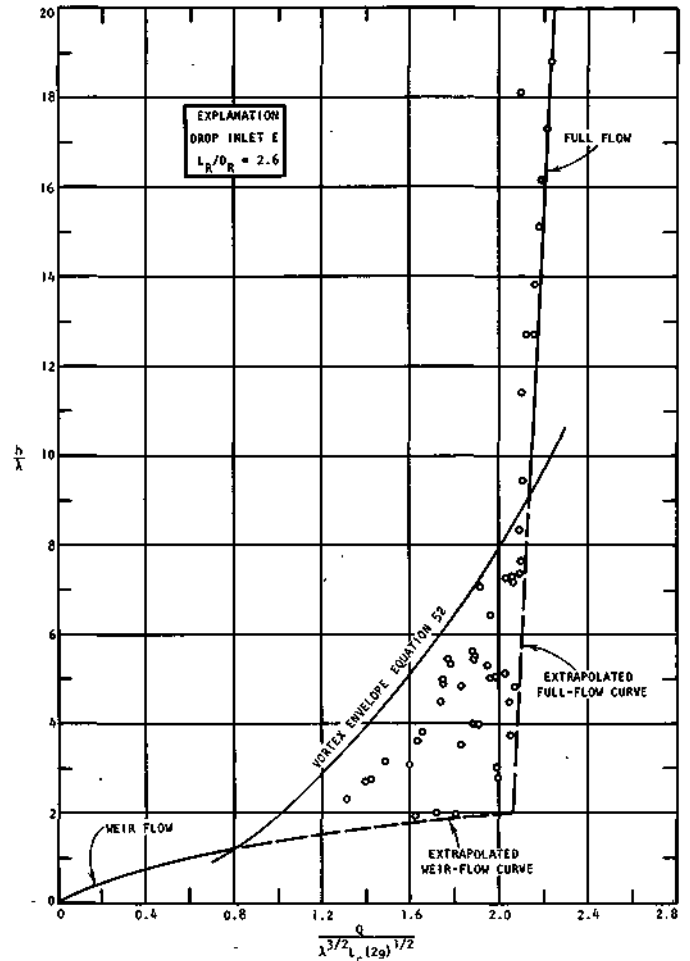Figure 47. Vortex effect on the spillway head and discharge for a relatively short drop inlet

Table 8. Recommended Minimum Drop-Inlet Heights for Predicting Vortex Effect on Spillway Performance

Drop inlet*	L_R/D_R	L_R/B	Percentage of discharge to the left of Vortex-envelope curve	Full-flow curve	K_E	K_T	K_R	$R_B \times 10^{-5}$	Barrel crown pressure minimum observed $h_n/(V_B^2/2g)$	Barrel station
Circular										
B	4.99		0	<1	0.64	0.46	1.15	3.17	-0.23	0.53D
C	3.5		0	3.2	0.52	0.27	0.56	3.62	-0.12	0.49D
D	3.78		0	<1	0.50	0.23	0.39	3.72	-0.10	0.46D
E	2.6		0	4.5	0.63	0.11	0.20	3.94	0.14	0.43D
G	2.5		0	<1	0.66	0.10	0.12	3.87	0.10	0.39D
Square										
H		2.7	0	2.3	0.65	0.17	0.25	3.85	0.13	0.46D
I		3.3	0	6.0	0.35	0.41	0.43	3.54	-0.45	0.42D
K		2.6	0	<1	0.46	0.42	0.44	3.59	0.19	0.43D
Rectangular										
L		4.89	0	2.1	0.06	0.24	0.26	3.94	-0.79	0.40D
N		5.05	0	3.3	0.18	0.24	0.25	3.85	-0.86	0.46D
O-1		4.04	0	5.5	0.68	0.17	0.28	3.88	-0.10	0.41D

*See table 1 for drop-inlet dimensions. (Test conditions similar to those in table 2, except no antivortex device was used.)

must be used. Otherwise, only the minimum hydraulic performance can be expected.

The results of the vortex tests in this report do not enable a designer to predict when a vortex will occur or the magnitude of its adverse effect on the discharge. The results, however, do enable him to predict the maximum effect vortices may have on the spillway capacity and hydraulic performance. The designer must then decide if an antivortex device is necessary for satisfactory hydraulic performance or if he can tolerate the demonstrated nonunique effects of vortices on the head-discharge relationship.

Test Results by Other Investigators

The following test results on closed-conduit spillways with a drop-inlet entrance were obtained by other investigators. Permission to present these data is gratefully acknowledged to the following individuals and organizations:

1) To Mr. Fred W. Blaisdell, Hydraulic Engineer, Soil and Water Conservation Research Division, Agricultural Research Service, U.S. Department of Agriculture, St. Anthony Falls Hydraulic Laboratory, Minneapolis, Minnesota, for permission to report the head-discharge data he obtained from four model tests. These tests were made by him at the St. Anthony Falls Hydraulic Laboratory (SAF).

2) To Mr. M. M. Culp, Chief, Design Branch, Soil Conservation Service, U.S. Department of Agriculture, Washington, D.C., for permission to report the head-discharge data obtained from a model study for the Grave Creek Project performed for the Soil Conservation Service by the Civil Engineering Department of Swarthmore College. The data are taken from the unpublished report of this model study entitled "Report on Hydraulic Testing of Scale Model of Drop Spillway for Grave Creek Project," by M. Joseph Willis and Charles W. Newlin, Civil Engineering Department, Swarthmore College, Swarthmore, Pennsylvania, July 9, 1958.

3) To Mr. W. O. Ree, Hydraulic Engineer, Agricultural Research Service, U.S. Department of Agriculture, Stillwater, Oklahoma, for permission to report the head-discharge data from a prototype study at the Stillwater Outdoor Hydraulic Laboratory. The data are taken from an unpublished report entitled "Tests of Steel Deck Grating for Vortex Suppression on Closed Conduit Spillways," by W. R. Gwinn, Hydraulic Engineer, Stillwater Outdoor Hydraulic Laboratory, Agricultural Research Service, USDA, Stillwater, Oklahoma, December 1958.

St. Anthony Falls Model Tests. The following test results of vortex effects on spillway capacity were obtained by the St. Anthony Falls Hydraulic Laboratory. Four model tests were conducted on closed-conduit spillways with rectangular drop-

Table 9. St. Anthony Falls Hydraulic Laboratory Model Spillway Proportions

Series	Model plan dimensions Width B/D	Side length	Crest Thickness t/B	Shape	Radius	L_R/B	Z/D	L_B/D	Remarks
W-304	1.0	10B	0.444	Quarter round	t/2	5.0	27	110	Nominal barrel diameter = 2 1/4 inches Barrel on a steep slope
W-305	1.0	2B	0.111	Quarter round	t/2	5.0	27	110	
W-401	1.0	5B	0.444	Quarter round	t/2	5.0	27	110	
W-403	1.0	3B	0.444	Quarter round	t/2	5.0	27	110	

inlet entrances. These rectangular drop inlets were normally operated as two-way drop inlets with the flow entering the spillway over the two long sides of the drop inlet. Flow was prevented from entering the shorter sides (ends) of the drop inlet by end walls which were part of an antivortex device. However, for the test results reported here the antivortex device and supporting end walls were removed.

Each model test series was performed with a deep approach which utilized the full width of the approach channel for the flow approaching the spillway entrance. The flow was permitted to enter the spillway periphery from all directions, and no attempt was made to inhibit or to force development of circulation around the spillway entrance. Therefore, the vortex was free to form naturally.

The test procedure for each series was similar to the State Water Survey procedure described in this report. A complete description of the test apparatus has been reported by Blaisdell and Donnelly.[5]

The pertinent dimensions for each model are given in table 9. The models were constructed from clear polished lucite.

The head and discharge data obtained for each of the four SAF rectangular drop inlets were computed with nondimensional parameters, and are plotted in figure 49. The dashed curves are the estimated full-flow curves that would have been obtained if sheet metal cross vanes had been placed on the inlet crest to control the effect of vortices on the spillway capacity. The vortex envelope, equation 52, is also shown for reference. Each drop inlet was operated through its entire flow range from weir flow to vortex flow or full flow. The largest head shown for each series was the maximum attainable without running the risk of overflowing the test apparatus.

A vortex did not form for series W-304, figure 49, and a single-valued head-discharge curve was obtained. The vortex was present sometime during the test series W-305, W-401, and W-403 as indicated by the scatter of the instantaneous head-discharge data for these drop inlets. The maximum variation in discharge for series W-401 is about 4 percent and this small effect is not believed to be serious.

For series W-403 the maximum deviation of the discharge to the left of the estimated full-flow curve above the vortex envelope is about 6.5 percent. This deviation can probably be considered to seriously affect the head-discharge relationship in the normal full-flow range.

For series W-305 the scatter in the instantaneous head-discharge data is entirely to the right of the vortex-envelope curve. Although the data are limited, it is believed that for higher heads and larger discharges the vortex effect would be confined to the right of the vortex envelope in a manner similar to that for drop inlet L shown in figure 43.

Although no tests were made with reduced spillway full-flow capacity, it is the authors' opinion that if the full-flow capacity for series W-305 and W-403 were reduced to a value equal to or less than the discharge value at the intersection of the weir and vortex-envelope curves the effect of vortex formation on the spillway capacity would be negligible. This opinion is based upon the reduced spillway capacity tests already described.
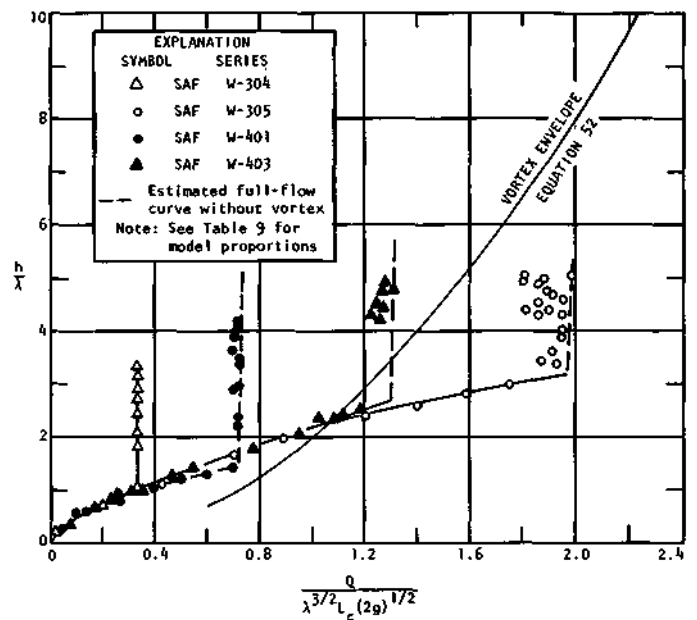

Figure 49. Vortex effect on spillway capacity for St. Anthony Falls rectangular drop inlets with deep approach

Grave Creek Project Model Test. The test results of vortex effects on spillway capacity and performance presented here were obtained from a model test of the Grave Creek Project drop inlet in Pennsylvania. The spillway with a rectangular drop inlet was a 1/15 scale model of the spillway prototype. The spillway, equipped with a horizontal antivortex plate, normally operated as a two-way drop inlet with the flow entering the spillway over the two long sides of the drop inlet. Flow was prevented from entering over the shorter sides (ends) of the drop inlet by end walls which supported the horizontal antivortex plate. The test results presented here are for the horizontal antivortex plate in place and for the plate removed.

The model tests were performed with a deep approach which utilized the full width (8 feet) of the approach channel. No attempt was made to inhibit or force the development of circulation around the spillway entrance. The end walls on the drop inlet did, however, have a guiding effect on the flow in the immediate vicinity of the spillway entrance and probably inhibited vortex formation.

The proportions for the lucite rectangular drop-inlet model were: horizontal width of $6 = D$, horizontal length of 36, drop-inlet height of $L_R/B = 28.17$, and a crest thickness of t/B — 0.416. The outer edge of the crest was square and the crest inner edge was quarter round with a radius of $t/2$. The total drop through the spillway was $Z/D = 30.6$. The barrel had a length of $188D$ and was laid on a 1.56 percent slope. The prototype barrel had an inside diameter of 2 feet. The antivortex plate when in place was positioned at a distance of $56/6$ above the drop-inlet crest. The plate was 36 wide and had an overhang L_0 of 2.5 6.

The head-discharge data obtained from the model tests with the horizontal antivortex plate in place and with the plate removed were computed with nondimensional parameters. These data are shown in figure 50. The vortex-envelope curve, equation 52, is shown for reference. The solid triangle symbols
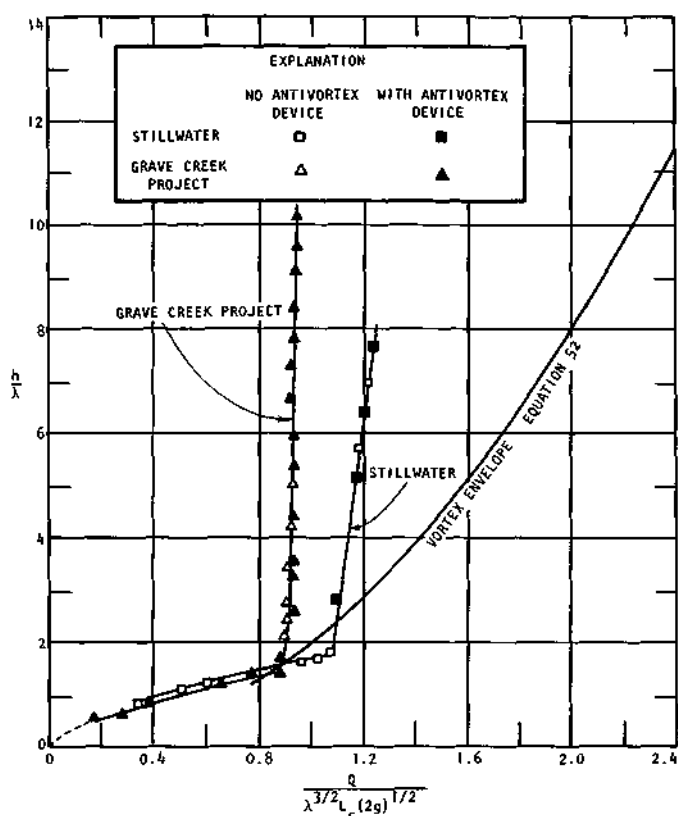
Figure 50. Vortex effect on spillway capacity for Grave Creek Model and Stillwater prototype

are for the instantaneous head-discharge data obtained with the antivortex plate in place. The scatter of these data is small (± 1 percent) and the vortex did not form for any run. The open triangular symbols are for the instantaneous head-discharge data obtained after removing the antivortex plate. Two vortices formed for each of the lowest two heads, and a single vortex was present for the remaining four larger heads. The vortex reduced by a maximum of 2 percent the discharge obtained for these same heads with the antivortex plate in place. This small effect of the vortex on the head-discharge data obtained in these tests is not considered to be serious.

Stillwater Prototype Test. The following test results of vortex effects on spillway capacity and performance were obtained at the Stillwater Outdoor Hydraulic Laboratory in Oklahoma from tests conducted on a prototype closed-conduit spillway with a square drop-inlet entrance. The spillway was equipped with a removable horizontal antivortex plate which was square in plan. The plate was mounted on a steel framework which was supported by four corner posts located at the corners of the drop-inlet side walls. The test results presented are for the antivortex plate in place and for the plate removed.

The prototype drop inlet was located at the toe of the dam which formed the reservoir. The approach to the spillway entrance was deep, and the flow had ample access to all four sides of the drop inlet. No attempt was made to prevent circulation of the flow around the drop-inlet entrance. The flow entered the reservoir directly across the reservoir from the spillway. A complete description of the testing facility and test procedure has been reported by Blaisdell.[10]

The drop inlet, corner posts, and barrel were concrete. The square drop inlet had a horizontal width B of 1.250, height of $L_R/B = 3.33$, and a crest thickness of $t/B = 0.267$. The outer edge of the crest was square and the crest inner edge was quarter round with a radius of $t/2$. The square corner posts with 0.75-inch chamfered edges had a width of 0.2676 and a height of 0.40B. The square antivortex plate constructed of $5/8$-inch thick plywood was centered over the drop inlet at a distance above the inlet crest of 0.40B. The plate had an overhang L_0/B of 5/6 on each side of the drop inlet. The total drop through the spillway Z/D was 9.14. The 24-inch diameter barrel was laid on a 1.85 percent slope and had a length of 54.2D.

The head-discharge data obtained from the prototype tests with the horizontal antivortex plate in place and with the plate removed were computed with nondimensional parameters. These data are shown in figure 50. The vortex-envelope curve, equation 52, is shown for reference. The solid square symbols are for the instantaneous head-discharge data obtained with the antivortex plate in place. The scatter of these data is very small and a vortex did not form for any run. The open square symbols are for the instantaneous head-discharge data obtained after removing the antivortex plate. The scatter of these data is small although a vortex was present for each run in the full-flow range. The single curve in the full-flow range well represents the data with and without the antivortex plate, with and without vortices.

Harspraanget Diversion Tunnel

Rahm[11] presented head-discharge data and a description of the flow through the diversion tunnel at Harspraanget Hydro-Electric Power Plant that can be used to verify the results of the Water Survey study since this diversion tunnel was quite similar to a closed-conduit spillway with a drop-inlet entrance.

The vertical inlet with a circular horizontal cross section and the nearly horizontal tunnel described by Rahm corresponds to the drop inlet and barrel, respectively, as defined in this report. The crest of the vertical inlet was at ground level, so that the approach to the inlet was essentially flush.

The dimensions of the diversion tunnel as given by Rahm were used to compute the nondimensional proportions of the diversion tunnel in the terminology used in this report. The vertical inlet (drop inlet) with a diameter D_R of 11 meters (m) and a length L_R of 25m from the inlet crest to the tunnel (barrel) invert gives an L_R/D_R of 2.27. The inlet crest was gently curved from a diameter of 17m to the uniform drop inlet (vertical inlet) diameter in a vertical distance of 1m, so the weir crest length $L_C/D_R = 4.85$. The bottom of the drop inlet joined the nearly horizontal excavated tunnel with a good approximation of a well-rounded transition. The average barrel (tunnel) diameter $D = 11.8$m was computed from the average cross-sectional area of 110m^2. Therefore the relative drop inlet diameter D_R/D is 0.93. The tunnel length L_B of 280m gives an L_B/D of 23.7. The drop Z through the spillway, measured from the small scale drawings in Rahm's report, of about 7m gives a Z/D of about 0.59. The outlet was "an

oblique upward mouth" about 50m long and this resulted in the invert of the outlet being about 5.7m above the tunnel crown. Approximately 50m downstream from the drop inlet a vertical gate shaft was excavated from ground level to the tunnel. Also, about 100m downstream from the drop inlet a transport tunnel connected to the diversion tunnel was used to remove excavated rock. The transport tunnel was inclined upward to the ground surface and its exit was below the dam.

The head-discharge data presented by Rahm were recomputed using nondimensional parameters, and plotted in figure 51. The vortex envelope, equation 52, is shown for reference. The open symbols are for data obtained when the gate shaft was open, and the solid symbols are for data obtained when the gate shaft was closed. When the gate shaft was open the water entered this shaft at heads h/k larger than 3.65. The values used for the head-discharge curve are "mean values for approximately stable flow conditions over a period of at least 8 hours." During this period the variation in storage in the reservoir was about 0.5 percent; therefore the difference between inflow to the reservoir and outflow through the diversion tunnel was disregarded.

In figure 51 the flow condition at the inlet entrance is weir with a clinging nappe for heads $h/k < 1.17$. When the flow range was between 500m^3/sec [17,650 cfs, $Q/\lambda^{3/2}L_c(2g)^{1/2}$ = 0.885] and 850m^3/sec [30,000 cfs, $Q/\lambda^{3/2}L_c(2g)^{1/2}$ = 1.50] the flow at the inlet described by Rahm was an air core and clinging nappe with the minimum diameter of the air core located near the top of the drop inlet. This type of flow is similar to the vortex flow observed by the authors and shown in figure 52.

During the rates of flow discussed in the preceding paragraph air was carried through the diversion tunnel. Mr. Rahm describes the phenomena at the tunnel outlet:

"At some rates of flow, water spouts could be observed at the tunnel outlet, . . . water being thrown up 5 to 10m [16.4 to 32.8 ft] above the water level. These water spouts had no clear periodicity but came at intervals of 1 to 3 seconds. They did not occur at discharges lower than about 200m^3/s [7060 cfs, $Q/\lambda^{3/2}L_c(2g)^{1/2}$ = 0.35], but above this value they became stronger and more powerful as the discharge increased. When a discharge of 800 to 850m^3/s [28,250 to 30,000 cfs, $Q/\lambda^{3/2}L_c(2g)^{1/2}$ = 1.42 to 1.50] was reached, the spouts disappeared.

"These spouts were produced at the outlet by the expanding of large air bubbles formed within the tunnel by air sucked down at the tunnel inlet. . . there was no air, or only a small volume, at low discharges, but as the flow increased and the control section moved downwards in the tunnel inlet, the volume of air increased. At maximum discharge through the tunnel practically no air was entrained."

Mr. Rahm's comments on flow conditions at the tunnel inlet are:

"As long as the flow did not exceed 850m^3/s [30,000 cfs], the water level above the tunnel inlet varied continuously and regularly with the fluctuations in discharge. On July 6th [1949], however, the rate of flow increased rapidly from 850m^3/s, which rate had been maintained
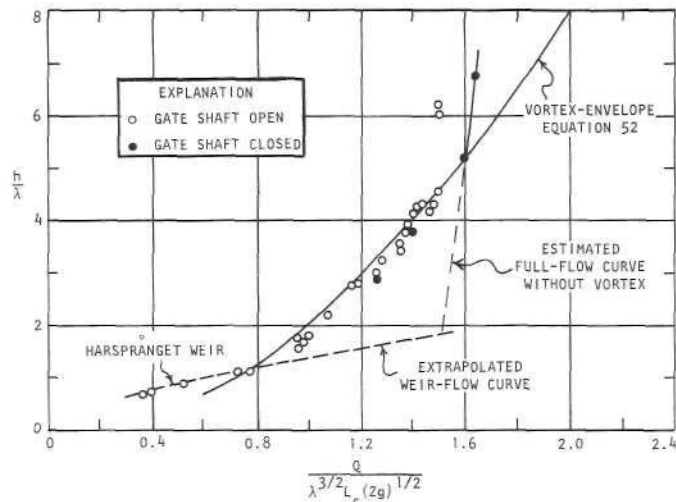
Figure 51. Harspraanget diversion tunnel head-discharge curve
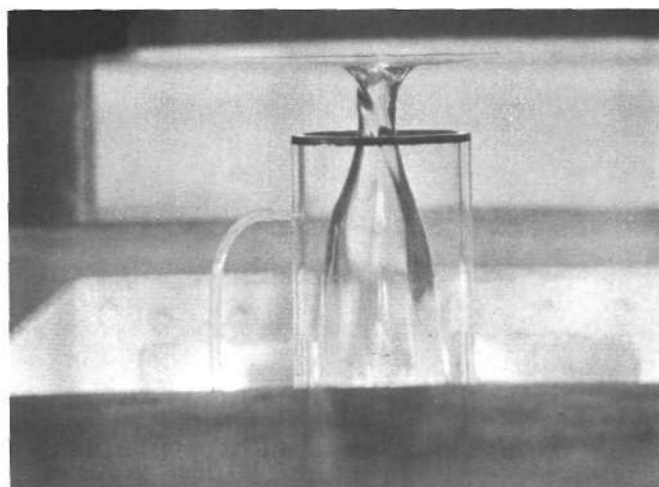
Drop inlet E, series 3

$Q/\lambda^{3/2}L_c(2g)^{1/2} = 1.18$, $h/\lambda = 1.96$

Figure 52. Vortex with minimum air core diameter near entrance to drop inlet

constant for about 24 hours, to slightly above 870m^3/s [30,700 cfs]. This caused a rise in the water level of no less than 2.5m from $[h/\lambda = 4.68]$ to $[h/k = 6.06]$, in 2 hours. ... In order to prevent the site from being flooded, the flow was reduced ... to its initial value of 850m^3/s. Even so, the water level did not fall to its previous position of equilibrium corresponding to this rate of flow, i.e., $[h/\lambda = 4.68]$, as had been expected. Instead, a stable level was reached at a considerably higher value, $[h/\lambda = 6.24]$.

"When the water level was higher than about $[h/\lambda = 3.65]$, the water was discharged both through the tunnel inlet and through the gate shaft. ... At higher water levels, this caused the formation of whirlpools at both inlets, a strong one at the tunnel inlet and a weaker one at the gate shaft. The water rotated clockwise above the tunnel inlet and counter-clockwise above the gate shaft. It was therefore justifiable to assume that the water flowing through the gate shaft contributed to the reduction in the total discharge

47

through the diversion tunnel by increasing the energy loss at its inflow into the diversion tunnel or by disturbing the inflow towards the tunnel inlet."

Since the flow through the gate shaft was thought to influence the discharge through the diversion tunnel, the reservoir level was lowered and the gate shaft closed. With the gate shaft closed the discharge through the tunnel was determined for four reservoir levels. These data are the solid symbols in figure 51. The data show that for the same head the discharge through the tunnel with the gate shaft closed was larger than the discharge obtained with the gate shaft open. This is also true for the head $h/$ = 2.94 at which there was no flow into the gate shaft when the shaft was open. It is evident from these data that the open gate shaft did reduce the discharge through the diversion tunnel.

The data presented in figure 51 do not exhibit the randomness of the data obtained by the State Water Survey model tests. This is largely due to the differences in development of the circulation and vortex formation at the inlet in the model tests and for the diversion tunnel. In the model tests the strength of the circulation and vortices developed varied widely since the circulation was free to develop in either the clockwise or counterclockwise directions. Also, for a constant inflow into the model test apparatus, the circulation could and did change directions. However, Rahm's data indicate a constant effect of circulation and vortex formation that approximates the vortex-envelope head-discharge relationship given by equation 52.

The inlet for Rahm's diversion tunnel was located on a river bank, therefore the flow had a strong tangential component of velocity. This resulted in the circulation around the inlet always being in the clockwise direction. Mr. Rahm states:

"The high water level observed on July 6th remained unchanged even after the rate of inflow had been reduced to a value that formerly corresponded to a water level 2.7m [$h/$ = 4.27] lower. This fact is probably due to the topographical configuration of the ground surface around the tunnel inlet. The increase in the rate of flow from 850 m^3/s [30,000 cfs] to 870 m^3/s [30,700 cfs] caused a rise in water level and an intensification of the vortical motion above the inlet, especially when a vortex was also formed above the gate shaft. Since the inlet is located on the river bank, this rise in water level increased the extent of the body of water between the inlet and the river bank, and hence afforded more favourable conditions for intense vortical motion at the inlet. The vortex strength was therefore maintained at a high value even after the reduction in the rate of flow. This state of flow with strong vortical motion at high water levels was then as stable as the former weak rotation at low water levels."

Energy was required to maintain the strong circulation which resulted in the intense vortex motion at the tunnel inlet. The energy, which served no useful purpose, was in addition to that required to discharge the flow through the diversion tunnel. This is evident in figure 51 in which the weir curve has been extrapolated for larger discharges, assuming the vortex is not present. For a particular discharge, the difference in heads between the extrapolated weir curve and the discharge data indicate that the circulation and vortex effect can require a large excess of energy. This required excess in energy can result in the head above the inlet crest being as much as two to two and one-half times the head needed for the diversion tunnel discharge if the circulation and vortex were eliminated.

The advantages of fully controlling the vortex formations at the entrance to drop inlets for closed-conduit diversion tunnels are:

1) A single-valued head-discharge curve is obtainable.
2) The uncertainties of forced circulation and vortex effects on the head-discharge curve are eliminated.
3) Considerable savings by the construction of lower cofferdams should be possible.

Horizontal Circular Plate Antivortex Device

The effect of a horizontal circular plate antivortex device on the performance of closed-conduit spillways with a circular drop inlet was described in the section on "Spillway Performance." This plate, properly positioned above the drop-inlet entrance, did suppress the reservoir level and caused very small increases in reservoir level for large increases in discharge until the spillway flowed full *(see figure 26)*. The initial full-flow head was considerably lower than the full-flow head obtained without the antivortex plate.

The test results presented below show the effect on spillway capacity of the antivortex plate elevation and size in the plate-flow range. Also presented is an equation for determining the spillway head-discharge curve in the plate-flow range.

Effect of Antivortex Plate Elevation

The head-discharge curves obtained for various elevations above the inlet crest of an antivortex plate are shown in figure 53. The plate overhang L_0/D_R for models C-2 and E-4 are very close to the same value so the test results are presented together. The dashed curve, shown for reference, is the head-discharge curve obtained for circular drop inlets when sheet metal cross vanes were placed on the drop-inlet crest to control the formation of vortices. The flow conditions for each series were similar to those described in "Flow Conditions for a Properly Positioned Antivortex Plate."

The curves in figure 53 show that as the elevation d/D_R of the antivortex plate is lowered, the reservoir level at which the discharge control changes from weir flow to plate flow and the priming head for full flow are also lowered. However, as the antivortex plate elevation is lowered, the full-flow capacity also becomes smaller indicating an increase in the entrance head-loss coefficient K_E.

In the plate-flow range for model C-2 small surface wavelets formed as the seal of the spillway by water touching the antivortex plate was broken and reestablished. The breaking and sealing action, which noisily sucked in air on breaking of the seal at the inlet, was associated with slug flow (moving

hydraulic jump) in the barrel. As a slug traveled down the barrel, air would be sucked into the spillway and form the trough of the wavelet. While a new slug was forming at the barrel entrance, the inlet would seal and the crest of the wavelet would form. The amplitude of the wavelet was about $0.010 \, D_R$ to $0.015 \, D_R$ and is shown as double points for the particular discharge. Although the above action was measurable it was not believed to seriously affect the plate flow head-discharge curve.

A transient vortex formed during the test on model C-2, series 52, which had a small effect (about 2 percent) on the discharge as indicated at $h/D_R = 0.55$. This slight vortex effect is not believed to be serious and should be tolerable.

Effect of Antivortex Plate Size

The head-discharge curves obtained for various amounts of plate overhang L_0/D_R for a plate elevation above the drop-inlet crest of $d/D_R = 0.25$ are shown in figure 54. The data

are for models C-l, C-2, C-3, E-2, and E-4. The dashed curve, shown for reference, is the head-discharge curve obtained for circular drop inlets when sheet metal cross vanes were placed on the drop-inlet crest to control the formation of vortices. The flow conditions for each series were similar to those described in the section "Flow Conditions for a Properly Positioned Antivortex Plate." The flow conditions for the double points shown for models C-l, C-2, and C-3 were similar to those described in the section "Effect of Antivortex Plate Elevation."

The curves in figure 54 show that as the antivortex plate overhang L_0/D_R decreases, the reservoir level at which the discharge control changes from weir flow to plate flow is raised a small amount. Also, the priming head for full flow is raised by substantial amounts. Changing the plate overhang did not affect the spillway full-flow capacity for the models tested.

A vortex formed for model C-3, series 55, in the full-flow range. The effect was to reduce the spillway capacity about 8 percent for the head range indicated in figure 54. This appears to be more variation in heads and discharges than
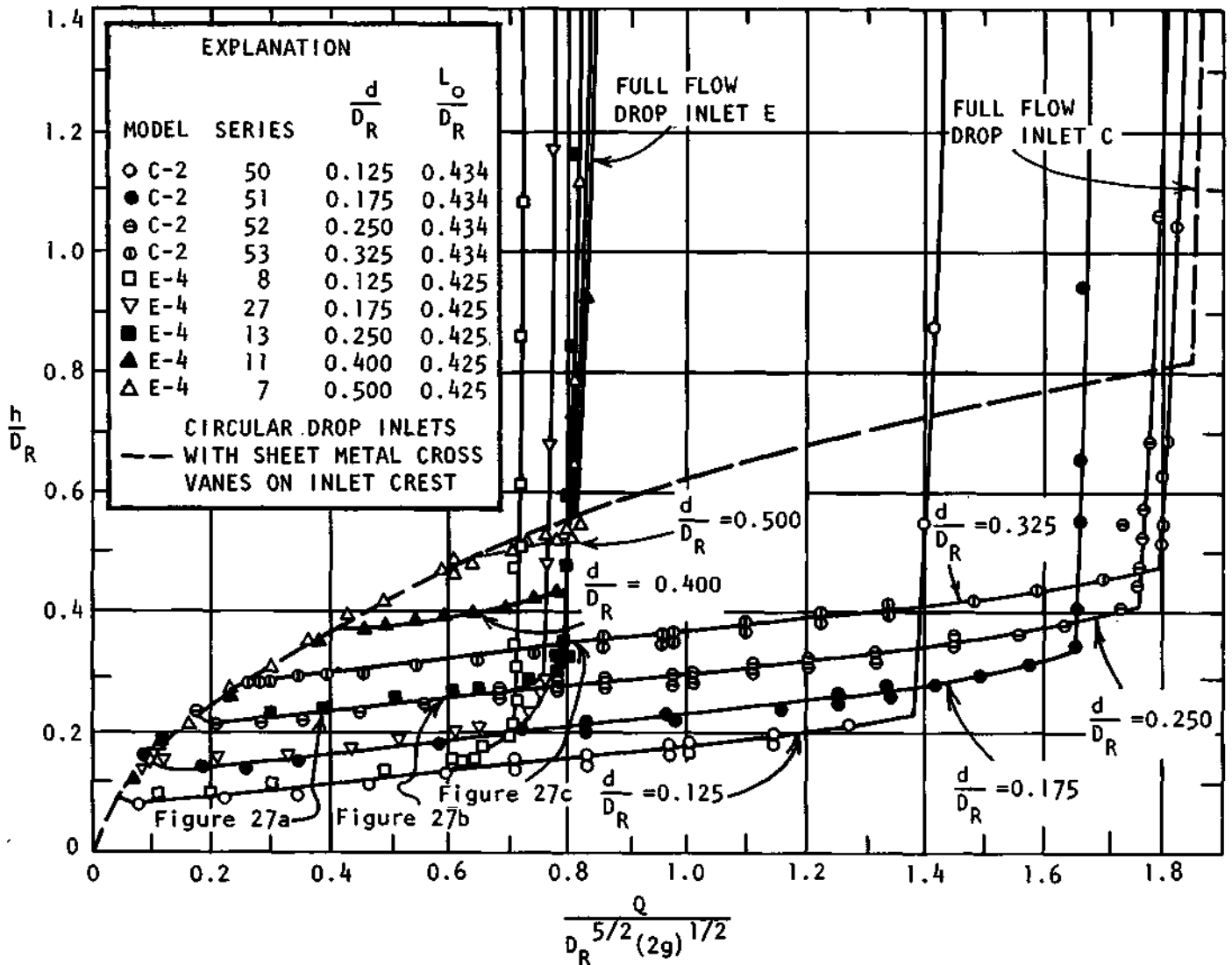

Figure 53. Effect of antivortex plate elevation on the spillway head and discharge for one plate size
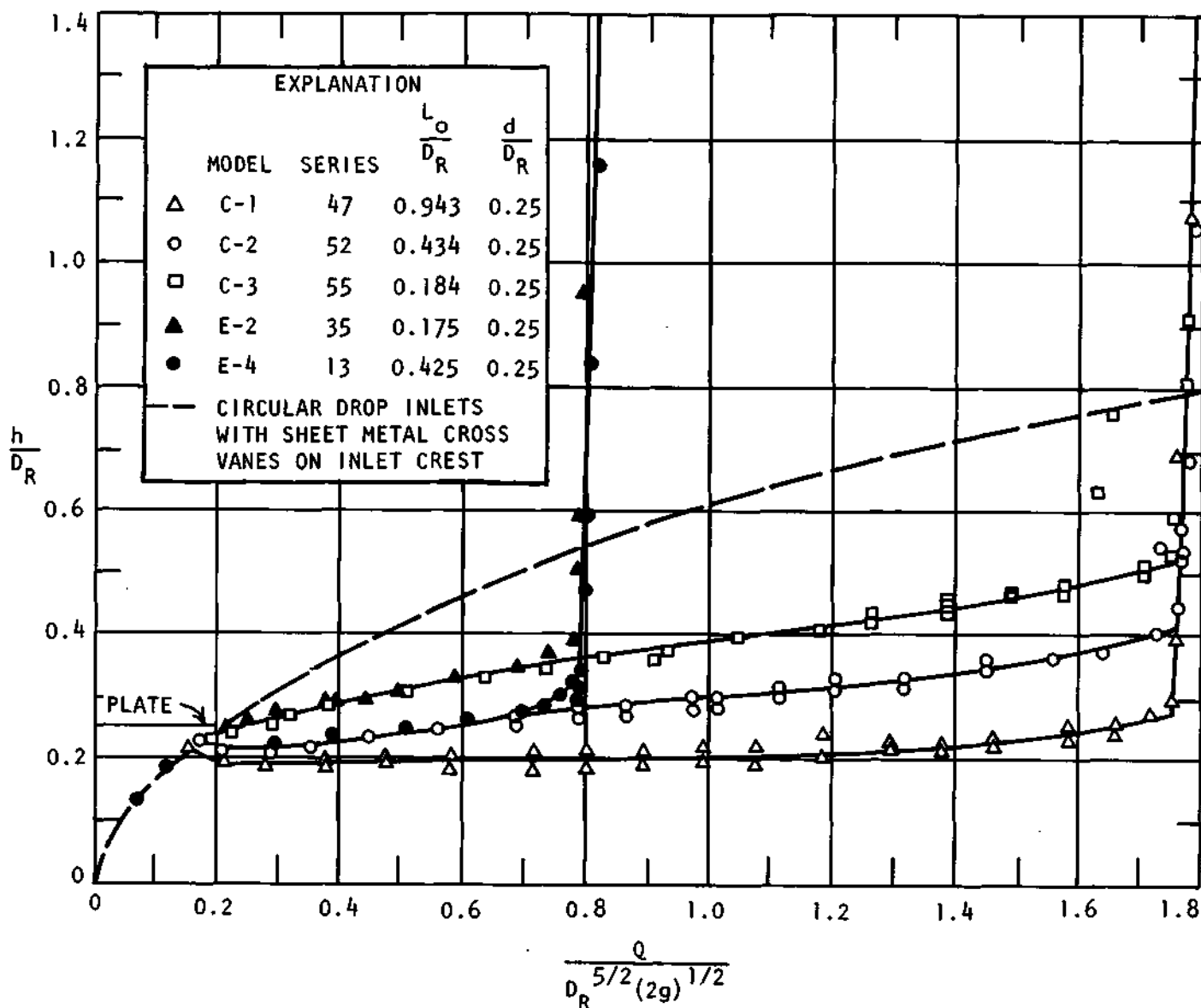
Figure 54. Effect of antivortex plate size on the spillway head and discharge for one plate elevation

can be tolerated. However, a vortex having this much effect on the discharge should not occur if $Q/D_R^{5/2}(2g)^{1/2}$ is less than about 1.6.

Plate Flow Head-Discharge Equation

The head-discharge curve for a closed-conduit spillway with a drop-inlet entrance which has a circular horizontal antivortex plate positioned above the inlet crest so that the plate influences the head on the spillway is composed of three parts *(see figure 26):* 1) weir flow, 2) plate flow, and 3) full flow. Therefore, three equations are required to fully define the entire head-discharge curve. The weir-flow and full-flow parts of the curve are computed by standard hydraulic procedures using the proper weir coefficient and head-loss coefficients. For the plate-flow range, equation 40 indicates the head-discharge curve in

functional form. This clearly shows that the actual equation is not a simple one. Therefore, an empirical equation has been developed for the plate-flow range of the head-discharge curve.

The empirical head-discharge equation for the plate-flow range was developed graphically from test results of model studies. Experimentally determined plate-flow head-discharge curves such as those shown in figures 53 and 54 were used. As a first approximation, the experimental plate-flow curves were idealized by drawing a straight line for each curve obtained for each plate overhang L_0/D_R and plate elevation d/D_R. Therefore, the equation for each idealized head-discharge curve has the form:

$$h/D_R = b + m \ [Q/D_R^{5/2}(2g)^{-1/2}] \qquad (59)$$

where m is the slope of the line and b is the ordinate intercept. The influence of the slope and intercept on the head-discharge curve was obtained separately.

The slope, $m,$ of each straight line versus L_0/D_R was plotted

50

on semilog paper with L_0/D_R along the log scale. This semilog plot yielded

$$m = 0.036 - 0.20 \quad log(L_0/D_R) \tag{60}$$

Figures 53 and 54 show that the ordinate intercept, *b*, is influenced by the plate elevation d/D_R. Therefore, in order to include the effect of d/D_R, the quantity $b — (d/D_R)$ for each straight line versus L_0/D_R was plotted on semilog paper with L_0/D_R along the log scale. This semilog plot yielded

$$b = d/D_R - 0.07 - 0.05 \, log(L_0/D_R) \tag{61}$$

Equations 60 and 61 were substituted in equation 59 to yield the plate-flow head-discharge equation

$$h/D_R = d/D_R - 0.07 - 0.05 \ log \ (L_0/D_R)$$
$$+ [0.036 - 0.20 \ log(L_0/D_R)] \ [Q/D_R^{5/2}(2g)^{1/2}] \tag{62}$$

Because equation 62 was empirically determined, the following limitations must be observed:

plate elevation, $d/D_R = 0.125$ to 0.40
plate overhang, $L_0/D_R = 0.175$ to 1.50

SPILLWAY CAPACITY, FULL FLOW

The test results reported in this section are for the spillway flowing full of water.

The approaching flow, well upstream of the drop inlet, used the full width of the approach channel. Near the drop inlet the flow approached the inlet crest from all directions. Circulation around the drop inlet was permitted to form naturally. The effect of this natural circulation on the performance of the spillway was negligible and is discussed in detail in "Circulation Effects" *(see page 32).*

Tests were conducted without an antivortex device on the drop-inlet crest and with sheet metal cross vanes on the drop-inlet crest to eliminate the effect of vortices on the spillway performance. The effects of vortices on the spillway performance are discussed in the section on "Vortex Effect and Flow Descriptions" *(see page 23).*

Tests were also conducted using a circular antivortex plate. The effect of the antivortex plate on spillway performance is discussed in "Horizontal Circular Plate Antivortex Device" *(see page 28).*

The tailgate at the barrel outlet was used for some tests to reduce the spillway full-flow capacity to values less than the ungated capacity.

Head-Discharge Curves

Head-discharge curves obtained for drop inlets with the sheet metal cross vane antivortex device on the inlet crest are shown: 1) for circular drop inlets with a deep approach in figure 55, and for a flush approach in figure 56; 2) for square drop inlets with a deep approach and a square inlet crest in figure 57, and for a quarter-round inlet crest in figure 58; 3) for square drop inlets with a flush approach in figure 59; and 4) for rectangular drop inlets with a deep approach in figure 60. Each curve shown in these figures is for the maximum spillway discharge obtainable in the test apparatus.

The flow conditions for each series in figures 55—60 were weir flow and full flow. The small scatter in the data for the weir-flow range is caused by the weir nappe being free part of the time and clinging at other times. Intermittent vortices developed in the full-flow range for all the drop inlets except for drop inlet G in figure 55. These vortices did not have any effect on the spillway capacity. Each rating curve was single-valued and reversible.

The head-discharge curves in figure 60 for the weir-flow range of the rectangular drop inlets show that the head required for weir flow for drop inlet N (series 75) is considerably smaller than the head required for drop inlets L and M (series 82 and 86). This difference is primarily because the weir-crest length for drop inlet N is considerably longer than those for drop inlets L and M *(see table 1).*
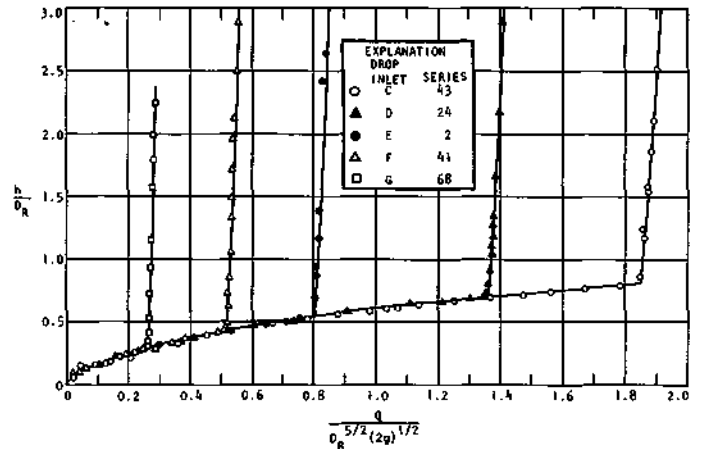

Figure 55. Typical head-discharge curves for circular drop inlets with cross vane antivortex device on inlet crest and deep approach
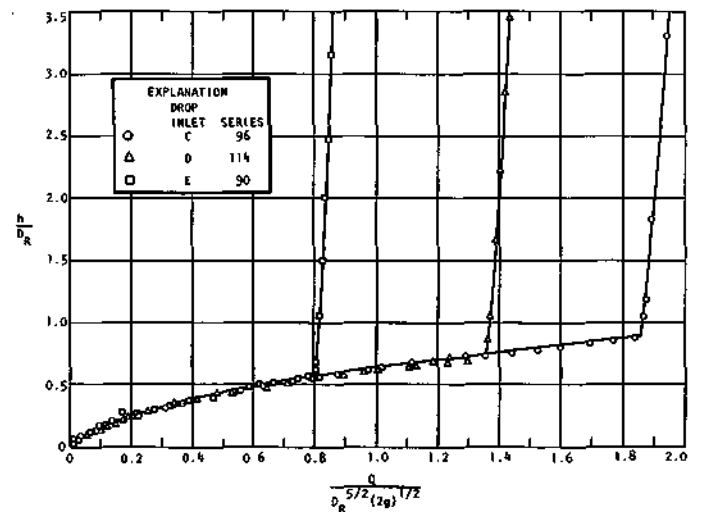

Figure 56. Typical head-discharge curves for circular drop inlets with cross vane antivortex device on inlet crest and flush approach
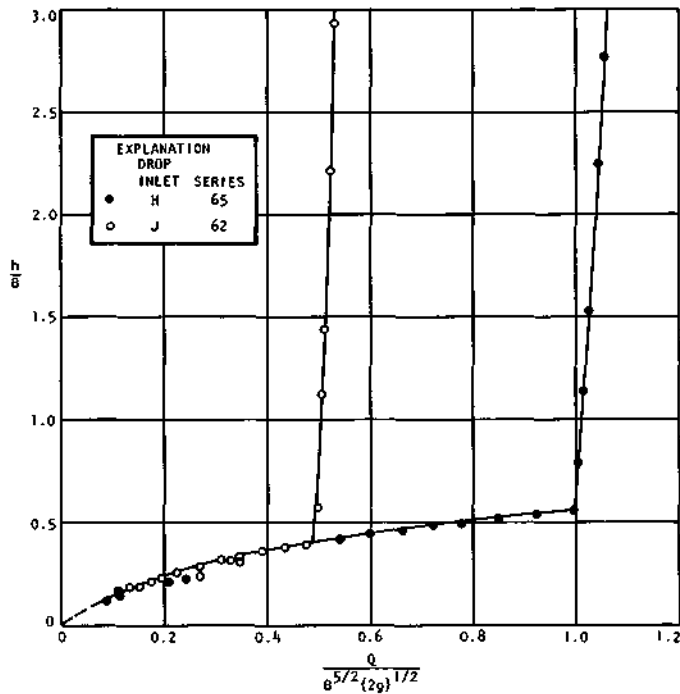
51

Figure 57. Head-discharge curves for square drop inlets with cross vane antivortex device on square inlet crest and deep approach

Figure 58. Head-discharge curves for square drop inlets with cross vane antivortex device on quarter-round inlet crest and deep approach

Head-Loss Coefficients

The test results for the drop inlet head-loss coefficients K_E, K_T, and K_B are given in table 2 for the deep approach, table 3 for the flush approach, table 4 for the antivortex plate, table 6 for circulation, and table 8 for the recommended minimum drop inlet heights.

Entrance Head-Loss Coefficient K_E

Circular Drop Inlets. A comparison of the entrance head-loss coefficients, K_E in table 2 for the deep approach, for the ungated spillway shows that placing sheet metal cross vanes on the drop-inlet crest increased K_E an appreciable amount when compared with the value obtained when the vanes were omitted from the crest. The only exception to this increase was for drop inlet G which had a smaller K_E when the vanes were used. The reversal in this trend can be partially explained by the fact that an air pocket existed beneath the full-flow nappe at the entrance to the drop inlet for series 67 and this probably influenced the head loss. Series 67 was the only full-flow test in which air was trapped within the spillway.

A comparison of the entrance head-loss coefficients, K_E in table 3 for the flush approach, for the ungated spillway shows that placing sheet metal cross vanes on the drop-inlet crest increased K_E in the same manner as for the deep approach. Also, the magnitude of the increase was about the same for the deep and flush approaches.

Square Drop Inlets. A comparison of the head-loss coefficients, K_E in table 2 for the deep approach, for the ungated spillway shows that placing sheet metal cross vanes on the

Figure 59. Head-discharge curves for square drop inlets with cross vane antivortex device on inlet crest and flush approach

drop-inlet crest increased K_E an appreciable amount as compared with the value obtained when the vanes were omitted from the crest. The increase in K_E was larger for drop inlets H and J than for drop inlets I and K. This difference was due to the rounding of the inside edge of the drop inlet crest for drop inlets I and K *(see table 1).* Also, the values of K_E in table 2 show that rounding the inside edge of the drop-inlet
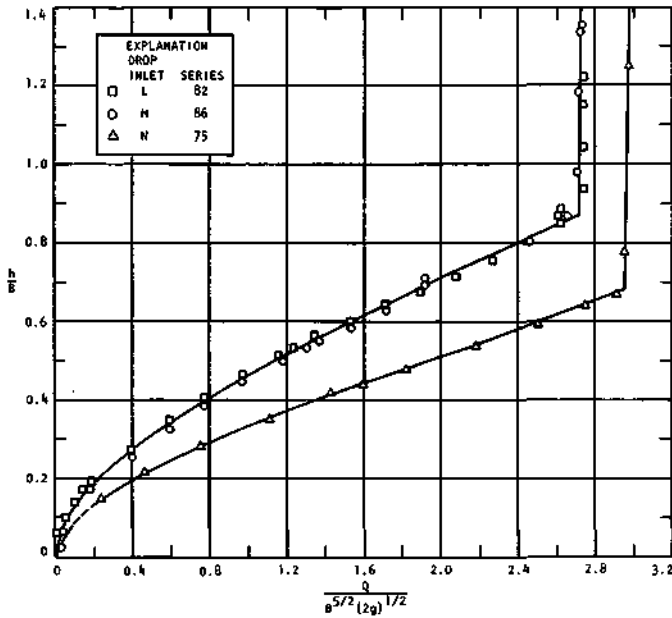
Figure 60. Head-discharge curves for rectangular drop inlets with cross vane antivortex device on quarter-round inlet crest and deep approach

Figure 61. Antivortex plate position versus the drop-inlet entrance head-loss coefficient

crest as was done for drop inlets I and K will reduce K_E to a value considerably less than the K_E obtained for square crests.

A comparison of the head-loss coefficients, K_E in table 3 for the flush approach, for the ungated spillway shows that placing sheet metal cross vanes on the drop-inlet crest increased K_E in the same manner as for the deep approach. Also, the magnitude of the increase was about the same for the deep and flush approaches. The effect of rounding the inside edge of the drop-inlet crest (drop inlet I) when compared with a square drop-inlet crest on the value of K_E is similar to that obtained for the deep approach.

Rectangular Drop Inlets. A comparison of the entrance head-loss coefficients, K_E in table 2 for the deep approach, for the ungated spillway shows that placing sheet metal cross vanes on the drop-inlet crest increased K_E when compared with the values obtained when the vanes were omitted from the crest.
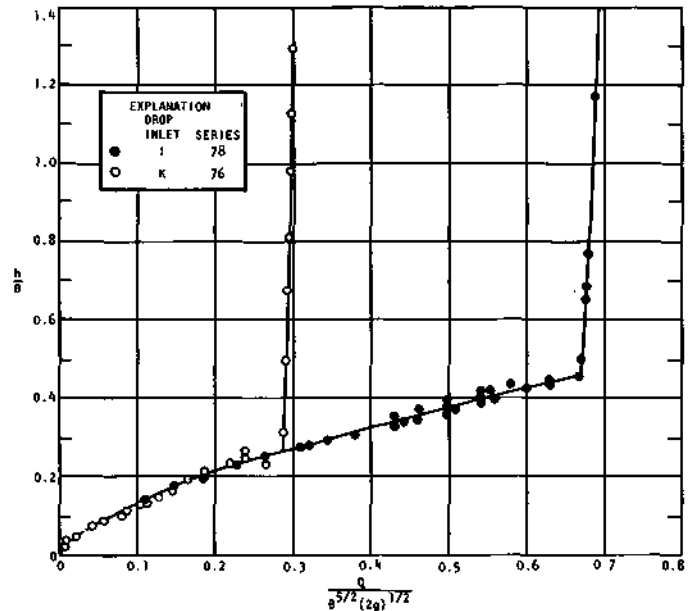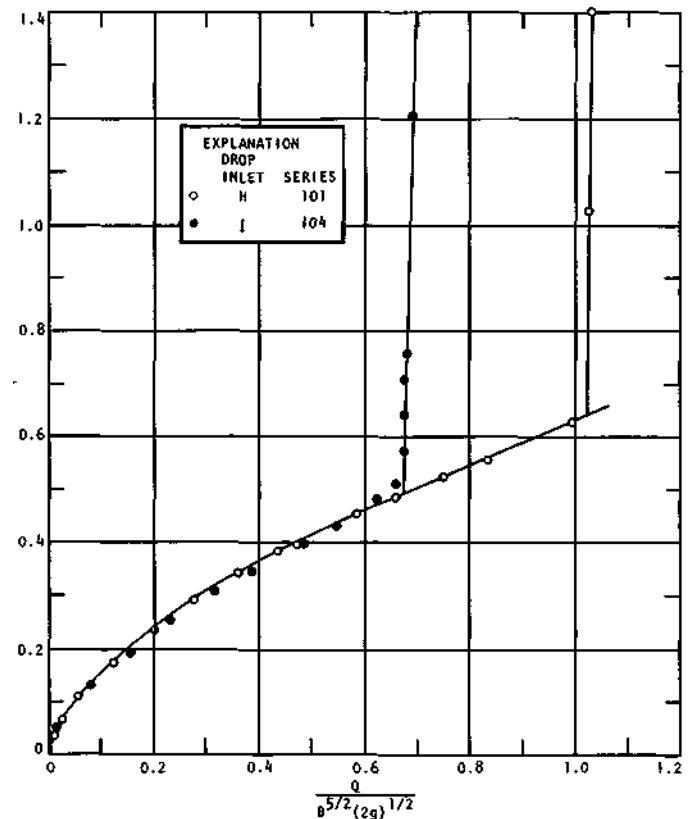
Circulation Effects. Maximum capacity tests (tailgate fully open) for the average entrance head-loss coefficients K_E are shown in table 6 for the deep approach. Examination of K_E for no circulation (series 28) and forced circulation (series 31) shows that K_E decreased a small amount when the circulation of the flow was increased. However, this value (0.56) is the same as that obtained for normal circulation (series 2). Therefore, the effect of forced circulation on K_E is insignificant when compared with K_E for normal circulation.

For the reduced capacity tests for the deep approach there appears to be a rather large increase in K_E when the circulation is changed from no circulation, series 29 (K_E — 0.55), to forced circulation, series 30 (K_E = 0.70). The difference of 0.15 in K_E is, however, within the limits of experimental error for these two tests.

The drop-inlet piezometric head used in equation 20 to compute K_E was read to the nearest 0.01 foot. An error of
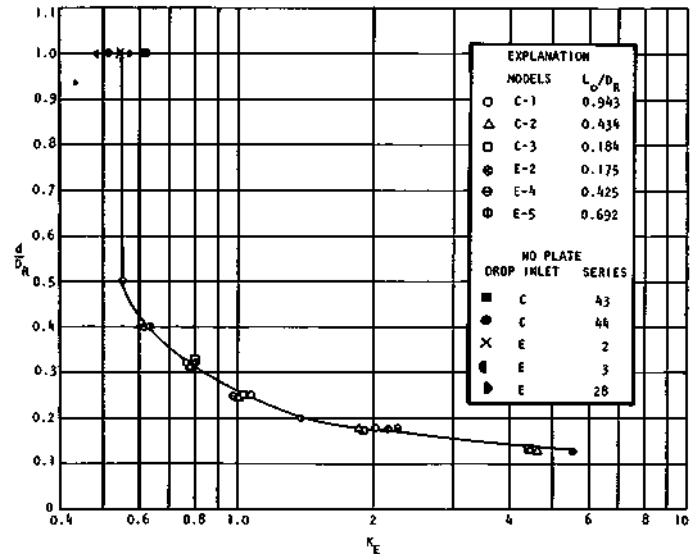
0.01 foot in this piezometric head would result in an error of 0.17 in K_E for the reduced capacity tests of series 29 and 30. Therefore, the difference of 0.15 in K_E is not surprising and it can be attributed to this possible error of 0.01 foot in the piezometric head.

For the maximum capacity tests, series 2, 28, and 31, the potential error of 0.01 foot in piezometric head would result in an error of 0.02 in K_E. Therefore, the difference in K_E values for these tests is insignificant.

For the flush approach maximum capacity tests the average head-loss coefficient K_E is shown in table 6. Examination of K_E for normal circulation (series 90), for no circulation (series 92), and forced circulation (series 95) shows that K_E decreased a small amount for each successive test. These differences are small and are not considered significant for the three degrees of circulation, since the experimental error in K_E is 0.02.

For the reduced capacity tests for the flush approach changing from no circulation (series 93) to forced circulation (series 94) resulted in a small increase in K_E of 0.04. This increase is not considered significant since it happens to be much smaller than the possible error that could result from the 0.01 foot accuracy of the piezometric head used to compute K_E.

Horizontal Plate Antivortex Device. A comparison of the entrance head-loss coefficients, K_E in table 4, shows that the position of the antivortex plate above the drop-inlet crest has an important influence on the value of K_E. Figure 61 shows the variation of K_E with plate position for various values of the plate overhang L_0/D_R. When the plate is relatively close (d/D_B = 0.125) to the inlet crest K_E is large. As the plate clearance is increased K_E decreases to a minimum at d/D_R = 0.50. The plate clearance d/D_R = 0.50 is larger than the maximum value of 0.40 recommended for the plate flow head-discharge curve (equation 62). Therefore, the curve in figure 61 should be used for obtaining K_E for the antivortex plate when the plate clearance d/D_R is between 0.125 and 0.40.

53

Circular Drop Inlets. A comparison of the transition head-loss coefficients, K_T in table 2 for the deep approach and in table 3 for the flush approach, for the ungated spillway shows that placing the sheet metal cross vanes on the drop-inlet crest did have a small effect on K_T. However, the vane effect was not always the same when compared with the K_T values obtained without the vanes being placed on the drop-inlet crest. For some drop inlets the vanes caused a small increase in K_T and for others a small decrease in K_T. Therefore, the effect of the vanes on the value of K_T can be considered insignificant for both the deep and flush approach depths. However, the data in tables 2 and 3 clearly show that increasing D_R/D ratios resulted in a decrease for K_T.

Square Drop Inlets. The transition head-loss coefficient, K_T in table 2 for the deep approach and in table 3 for the flush approach, for the ungated spillway was influenced slightly, or not at all, by placing the sheet metal cross vanes on the drop-inlet crest. These small differences in K_T are not considered significant. Of more importance is the effect of rounding the transition between the drop inlet and barrel on K_T. Drop inlets I and K had a square or sharp-edged transition while drop inlets H and J had rounded transitions *(see table 1)*. The data show that rounding the transition can materially reduce the value of K_T as compared with the value of K_T obtained for sharp-edged transitions.

Rectangular Drop Inlets. The transition head-loss coefficient, K_T in table 2 for the deep approach, for the ungated spillway was influenced slightly or not at all by placing sheet metal cross vanes on the drop-inlet crest. These small differences in K_T are not considered significant. The relatively large value of K_T for drop inlet H, when compared with the K_T for drop inlets L and N, was probably because of the influence of the drop inlet's sloping bottom *(see table 1)*. The bottoms for drop inlets L and N were horizontal. The transition for all three drop inlets was square edged.

Circulation Effects. For the deep approach maximum capacity tests (tailgate fully open) the average transition head-loss coefficients K_T are shown in table 6. Examination of K_T for no circulation (series 28) and normal circulation (series 2) shows that K_T increased a small amount compared with the value of K_T for normal circulation when the circulation was prevented. Forcing the circulation (series 31) resulted in a K_T that was well under the value obtained for series 2 or 28. These differences appear to be relatively large; however, the effect on the spillway full-flow discharge was small. This is apparent in the closeness of the head-discharge curves shown in figure 30.

For the reduced capacity tests for the deep approach, forcing the circulation (series 30) caused K_T to be slightly less than the K_T obtained for no circulation (series 29). This difference of 0.01 is considered insignificant. However, the K_T for each of these two tests is considerably larger than the K_T obtained for each of the maximum capacity tests. This large increase in K_T cannot be attributed to experimental error, since an error of 0.01 foot in the piezometric head used to calculate K_T would result in an error of 0.03 for K_T for series 29 and

30. The Reynolds number for these two tests is about one-third of the Reynolds number obtained for the maximum capacity tests. Therefore, it appears that K_T is dependent upon the Reynolds number.

For the flush approach maximum capacity tests (tailgate fully open) the average transition head-loss coefficients K_T are shown in table 6. Examination of K_T for the three degrees of circulation shows that forcing the circulation (series 95) resulted in a small reduction in K_T as compared with the value obtained for normal circulation (series 90) and for no circulation (series 92). This small reduction is not considered significant.

For the reduced capacity tests for the flush approach there is a definite increase in K_T when the circulation is changed from no circulation (series 93) to forced circulation (series 94). This increase in K_T of 0.04 is two times the experimental error, since an error of 0.01 foot in the piezometric head used to calculate K_T would result in an error of 0.02 for K_T. However, this increase in K_T is not evident in the full flow head-discharge curves shown in figure 31. A comparison of the values of K_T shows that K_T for the reduced capacity tests (series 93 and 94) is considerably larger than the values obtained during the maximum capacity tests (series 90, 92, and 95). Also, the Reynolds number for the reduced capacity tests was about 37 percent of the Reynolds number obtained for the maximum capacity tests. Therefore, it appears that K_T is dependent upon the Reynolds number.

Horizontal Plate Antivortex Device. The transition head-loss coefficient K_T is given in table 4 for each model test series in which K_T was determined.

A comparison of the K_T values for models C-l, C-2, and C-3 shows the plate clearance d/D_R and the plate size D_P/D_R influenced K_T. In general, the trend was for K_T to decrease for a particular plate size as the plate clearance decreased, the smallest value of K_T being for the smallest plate clearance. For a particular plate clearance, the trend was for K_T to decrease as the plate size decreased with the smallest value of K_T being for the smallest plate size.

A comparison of the K_T values for models E-l, E-2, E-4, and E-5 does not show any consistent change in K_T attributable to either the plate size or the plate clearance above the drop-inlet crest.

Drop-Inlet Head-Loss Coefficient K_R

Circular Drop Inlets. For the deep approach a comparison of the drop-inlet head-loss coefficients, K_R in table 2, for the ungated spillway shows that placing sheet metal cross vanes on the drop-inlet crest had the same effect as discussed for K_E. Also, K_R decreased in value as the drop-inlet diameter increased when compared with the barrel diameter (table 1). This decrease is similar to that found for K_T.

For the flush approach a comparison of the drop-inlet head-loss coefficients, K_R in table 3, for the ungated spillway shows that placing sheet metal cross vanes on the drop-inlet crest increased K_R in the same manner as for the deep approach.

Also, the magnitude of the increase was about the same for the deep and flush approaches. In addition, the values of K_R for a particular drop inlet, such as drop inlet D with cross vanes on the inlet crest, were essentially the same for the deep and flush approaches. Similar results were obtained when the cross vanes were omitted from the inlet crest. Therefore, changing the approach depth from deep to flush had an insignificant effect on K_R. However, a significant decrease in K_R occurred as D_R/D increased. This decrease was similar to that obtained for the deep approach.

Square Drop Inlets. The drop-inlet head-loss coefficient, K_R in table 2 for the deep approach and table 3 for the flush approach, for the ungated spillway was influenced slightly or not at all by placing the sheet metal cross vanes on the inlet crest. These small changes are not considered significant. Also, K_R is essentially the same for both approach depths for a particular drop inlet such as drop inlet H. Therefore, changing the approach depth is not significant.

A comparison of the head-loss coefficients K_R for drop inlet H with drop inlet I in table 2 or 3 shows that K_R for I is considerably larger than for H. At first glance this increase in K_R does not seem reasonable since B/D for drop inlet I is larger than B/D for H *(see table I),* and one would normally expect a decrease in K_R. It will also be noted in table 1 that drop inlet H has a square-inlet crest and a rounded transition between the drop inlet and barrel, whereas drop inlet I has a rounded inlet crest and a sharp-edged transition. The influence of these differences in inlet crest and transition geometries on K_R should give an indication of the relative importance of rounding the drop-inlet crest as compared with rounding the transition between the drop inlet and the barrel.

The head-loss coefficient K_R is determined from a combination of the entrance head loss H_E and the transition head loss H_T as given by equation 23. However, equation 23 in this form does not readily indicate whether K_E or K_T is the greater part of K_R. Equation 23 can be written as a function of K_E and K_T by replacing H_E and H_T in terms of K_E and K_T from equations 20 and 22, respectively, substituting for V_R in terms of V_B $[V_R = V_B(A_B/A_R)]$, and solving to obtain

$$K_R = K_T + K_E(A_B/A_R)^2 \qquad (63)$$

Equation 63 shows that K_R is the sum of K_T and a proportional part of K_E. The maximum proportional part of K_E is obtained when the square drop inlet width B equals the barrel diameter D. For this size drop inlet the proportional part of K_E is $(A_B/A_R)2$ $(\ /4)^2 = 0.617$. That is, only $0.617K_E$ is added to K_T to obtain K_R. As the width of the drop inlet relative to the barrel diameter increases, the ratio of $(A_B/A_R)^2$ rapidly decreases which in turn decreases the effect of K_E on K_R.

Drop inlet I (series 78 in table 2) can be used to illustrate the advantage of rounding the transition. The width of this drop inlet is 1.756D (table 1) and $(A_B/A_R)z$ is 0.0648. That is, only 6.48 percent of K_E (0.29) or 0.02 contributes to the value of K_R while the full value of K_T (0.43) is included in K_R to give a value of 0.45. No tests were made on drop inlet I with a rounded transition, therefore K_T for this condition is not known. However, drop inlets H and J (series 65 and 62, respectively, in table 2) did have a rounded transition. The

K_T results for these two drop inlets indicate that drop inlet I with a rounded transition would probably have a K_T of about 0.19. If this were true, then K_R would have been 0.19 + 0.02 = 0.21 which is less than half the K_R of 0.45 obtained for the sharp-edged transition. This is a rather large reduction in K_R, demonstrating that changes in the transition geometry that reduce K_T are desirable.

Rectangular Drop Inlets. The drop-inlet head-loss coefficient, K_R in table 2 for the deep approach, for the ungated spillway was influenced slightly by placing the sheet metal cross vanes on the inlet crest. These small changes, the 0.01 increase in K_R for drop inlets L and M and the 0.01 decrease for drop inlet N, are not considered significant.

Circulation Effects. For the deep approach maximum capacity tests (tailgate fully open) the average head-loss coefficients K_R are shown in table 6. Examination of K_R for no circulation (series 28) and normal circulation (series 2) shows that K_R for no circulation increased a small amount compared with the value of K_R for normal circulation. Forced circulation (series 31) resulted in a K_R less than the value obtained for series 2. These differences are not significant since effect on the spillway full-flow discharge was small. This is apparent in the closeness of the head-discharge curves shown in figure 30.

For the reduced capacity tests for the deep approach, forced circulation (series 30) caused K_R to be slightly larger than the K_R obtained for no circulation (series 29). This difference of 0.01 is considered insignificant. However, the K_R for each of these two tests is considerably larger than the K_R obtained for each of the maximum capacity tests. Since the Reynolds number for the two reduced capacity tests is about one-third of the Reynolds number obtained for the maximum capacity tests, it appears that K_R is dependent upon the Reynolds number.

For the flush approach maximum capacity tests (tailgate fully open) the average head-loss coefficients K_R are shown in table 6. Examination of K_R for the three degrees of circulation shows slight differences for no circulation (series 92) and forced circulation (series 95) when compared with K_R for normal circulation (series 90). These small differences are not considered significant and they are not evident for the full flow head-discharge curves shown in figure 31.

Changing the depth of approach from deep to flush yielded the same K_R for the two normal circulation tests (series 2 and 90) as well as for the two no circulation tests (series 28 and 92). The two forced circulation tests (series 31 and 95) resulted in a K_R difference of 0.01 which is insignificant. Therefore, the depth of approach did not affect the head-loss coefficient K_R for the maximum capacity tests.

For the reduced capacity tests for the flush approach there is an increase in K_R when the circulation is changed from no circulation (series 93) to forced circulation (series 94). This increase of 0.05, although relatively large, is not evident on the full flow head-discharge curves in figure 31 for these two tests. However, the K_R for each of these two tests is considerably larger than the K_R obtained for each of the maximum capacity tests. Since the Reynolds number for the two reduced

capacity tests is considerably smaller than the Reynolds number obtained for the maximum capacity tests, it appears that K_R is dependent upon the Reynolds number.

Horizontal Plate Antivortex Device. The head-loss coefficients K_R given in table 4 for each model test series in which K_R was determined show that K_R decreases as the plate elevation d/D_R above the drop-inlet crest increases. This decrease in K_R for increasing values of d/D_R does not continue indefinitely since a plate elevation will be reached at which the plate has a minimum effect on K_R. This plate elevation is attained when K_R for the drop inlet with the plate is the same as K_R without the plate. The limit of the plate elevation is at d/D_R = 0.50 which is the same as that for K_E. This value of d/D_R is larger than the maximum value of 0.40 recommended for the plate flow head-discharge curve (equation 62). Therefore, the values of K_R in table 4 should be used for geometrically similar spillways when the antivortex plate elevation d/D_R is between 0.125 and 0.40.

Barrel Head-Loss Coefficient f

The test results for the barrel or Darcy-Weisbach head-loss coefficient / are given in table 2 for the deep approach, table 3 for the flush approach, table 4 for the antivortex plate tests, and table 6 for the circulation tests. The test results are presented as the percentage difference between the / computed from the experimental measurements and the / computed from the equation for smooth pipes. Also given is the average barrel Reynolds number R_B. The barrel Reynolds number for a test series varied from a minimum of 5 percent less to a maximum of 7 percent larger than the average value.

The relatively small percentage deviation of the barrel resistance coefficient / from the smooth pipe values of / for most of the test series in tables 2, 3, 4, and 6 indicates that polished lucite may be considered smooth in design calculation.

The high / percentage values for drop inlet E (series 2 and 3 in table 2), for model E-3 (series 4, 5, and 6 in table 4), and for model E-4 (series 8 in table 4) were obtained before the barrel piezometers were deburred on the inside of the barrel. (It should be noted that series 1-8 in this report were made before the barrel piezometers were deburred; all other series listed were made after the barrel piezometers were deburred.) Other high / percentage values shown in tables 2 and 3 were obtained for rather flat barrel energy grade lines that resulted from using the tailgate at the barrel exit to reduce the spillway full-flow capacity. Similarly, the high / percentage value for model E-4 (series 10 in table 4) was obtained for a very flat energy grade line that resulted from placing the antivortex plate very close to the drop-inlet crest, which greatly reduced the spillway full-flow capacity. The value of / obtained in these tests was independent of the drop-inlet geometry, the transition geometry, the antivortex plate size, the plate position above the drop-inlet crest, and the circulation of the flow around the drop-inlet entrance.

SPILLWAY PRESSURE DISTRIBUTION, FULL FLOW

The test results for the pressure distributions in drop-inlet spillways are presented for: 1) circular, square, and rectangular drop inlets with and without the sheet metal cross vane antivortex device on the drop-inlet crest; 2) circular drop inlets with a horizontal circular antivortex plate positioned above the drop-inlet crest; and 3) the local pressure deviations in the barrel.

The data for the pressure distributions in the drop inlets and on the antivortex plate are shown in figures 62-71. In each figure the quantity $(P/w)/(V_R^2/2g)$ is a nondimensional

Table 10. Typical Average Values of Local Pressure Deviation
from the Established Barrel Hydraulic Grade Line for Deep Approach

Drop inlet	B		C	D	E	F	G	H	I	J	K	L	M	N
Series	64		43	24	38	41	68	65	78	62	76	82	86	75
Piezometer station along barrel from barrel entrance							$h_n/(v_B^2/2g)$							
Crown*	-0.152		-0.237	-0.144	+0.120	+0.166	+0.111	+0.177	-0.346	+0.110	+0.231	-0.782	-1.016	-0.852
5.02D	+0.035		+0.055	+0.059	+0.076	+0.076	+0.048	+0.081	+0.040	+0.076	+0.026	+0.045	+0.026	+0.042
15.07D	+0.011		+0.026	+0.024	+0.038	+0.037	+0.027	+0.037	+0.031	+0.039	+0.031	+0.029	+0.025	+0.024
25.1 ID	+0.009		+0.006	+0.005	+0.015	+0.015	+0.005	+0.012	+0.005	+0.015	+0.007	+0.009	+0.006	+0.004
35.150	+0.003		-0.004	-0.002	+0.001	+0.001	+0.004	+0.005	+0.011	+0.007	+0.001	+0.006	+0.000	+0.000
45.20D	+0.002		+0.001	+0.001	+0.002	+0.003	+0.002	+0.002	+0.000	+0.003	+0.001	+0.001	+0.000	+0.001
55.240	-0.003		-0.001	+0.000	-0.002	-0.001	-0.003	-0.003	-0.002	-0.003	-0.002	-0.001	-0.002	-0.001
65.290	-0.002		-0.001	-0.002	-0.001	-0.002	-0.002	-0.002	+0.000	-0.003	+0.000	-0.001	-0.001	-0.001
75.330	+0.002		-0.002	-0.001	-0.001	-0.002	+0.003	+0.003	+0.003	+0.005	+0.003	0.000	+0.003	+0.001
85.370	+0.002		+0.004	+0.004	+0.004	+0.003	+0.001	+0.001	+0.000	+0.001	+0.001	+0.001	+0.002	+0.001
95.420	-0.002		-0.000	-0.002	-0.001	+0.000	-0.001	-0.001	-0.002	-0.002	-0.002	-0.001	-0.002	-0.001

*See table 2 for crown piezometer station location.

Table 11. Typical Values of Local Pressure Deviation from the Established Barrel Hydraulic Grade Line for Flush Approach

Drop inlet	C	D	E	H	I
Series	96	114	90	101	104
Piezometer along barrel from barrel entrance	station	$h_n/(V_B^2/2g)$			
Crown*	-0.128	-0.095	+0.130	+0.172	-0.387
5.02D	+0.055	+0.068	+0.072	+0.078	+0.0l|l)
15.07D	+0.033	+0.012	+0.039	+0.039	+0.040
25.110	+0.008	+0.011	+0.014	+0.015	+0.012
35.150	+0.002	+0.005	+0.004	+0.004	-0.001
1)5.200	0.000	-0.001	+0.001	0.000	-0.001
55.24D	-0.001	+0.003	-0.002	-0.001	0.000
65.29D	-0.001	-0.006	0.000	-0.001	0.000
75.33D	+0.002	+0.002	+0.001	+0.002	+0.003
85.37D	+0.002	+0.008	+0.002	+0.001	+0.003
95.42D	-0.003	-0.006	-0.002	-0.002	-0.003

*See table 3 for crown piezometer station location.

pressure coefficient that is always positive because of the definition of AP. This quantity was defined in Part 1 as $AP = P_1 - P$ *(see page 7)*. In this equation P_1 is the reference pressure in the reservoir at the same elevation as the pressure P in the drop inlet or on the antivortex plate. The reference pressure P_1 is larger than P because part of the energy in the reservoir is converted to the kinetic energy of the flow in the drop inlet or along the bottom of the antivortex plate.

The data for typical local pressure deviations in the barrel are given in tables 10 and 11, in terms of a nondimensional pressure coefficient $h_n/(V_B^2/2g)$. In addition the minimum observed values of this pressure coefficient are given in tables 2, 3, 4, 6, and 8 for a barrel crown piezometer located near the barrel entrance.

Circular Drop Inlets

The nondimensional pressure distribution in the circular drop inlets and the pressure on their crests are shown in figure 62 for the deep approach and in figure 63 for the flush approach. The drop-inlet crest pressure values in figures 62a and 63a are plotted according to equation 32. The nondimensional pressure distributions in the upper part of the drop inlet shown in figures 62b and 63b are plotted in accordance with equation 30. The pressure distributions shown in figures 62c and 63c for the lower part of the drop inlet are plotted according to equation 31. The data plotted for each series in figure 62 are the average value for 9 or more full-flow runs. The data shown in figure 63 are the average value of 7 or more full-flow runs except for series 91, 112, and 113 in which 6, 4, and 3 runs, respectively, were averaged.

The pressure $(P/w)/(V_R^2/2g)$ in the center of the crest is shown in figure 62a for the deep approach to be dependent upon the value of t/D_R. The crest pressure data for the flush approach, shown in figure 63a, are too limited to indicate the full effect of t/D_R. However, the data show that changing the depth of approach did reduce the crest pressure for the flush
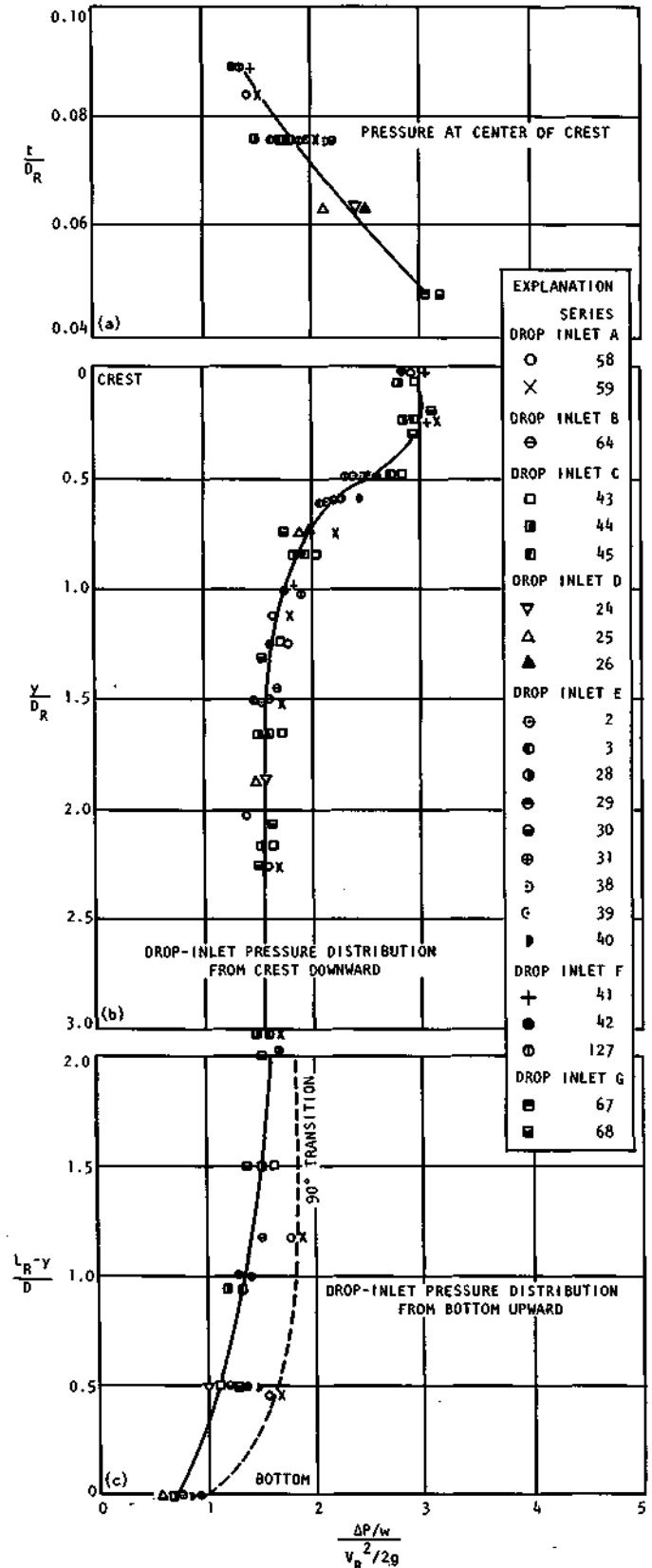

Figure 62. Drop-inlet pressure distribution for circular drop inlets with square crests, deep approach, and the spillway flowing full

approach to a value of $(P/w)/(V_R^2/2g)$ well below that obtained for the deep approach.

The data in figure 62b and 62c for the nondimensional pressure distribution in circular drop inlets (deep approach) exhibit some scatter about each average curve drawn. However, in each case the single solid curve is representative of the pressure distribution in circular drop inlets with square crests. The same comments apply to figures 63b and 63c for the flush approach.

A comparison of the pressure distribution curves in figures 62b and 63b for the upper part of the drop inlet shows these curves are similar in shape, and except for values of y/D_R less than 0.4, the two curves are essentially identical. For y/D_R less than 0.4 the maximum difference between the two curves is 6 percent. Therefore, changing the depth of approach from deep to flush has a measurable decrease in $(P/w)/(V_R^2/2g)$ near the top of the drop inlet. However, this decrease is not considered serious for drop-inlet spillways.

Comparing the solid pressure distribution curves in figures 62c and 63c for the lower part of the drop inlet shows these two curves to be identical. Therefore, changing the depth of approach from deep to flush did not influence the pressure distribution in the lower part of the drop inlet. The solid curves were obtained for models which had the barrel intersecting the drop inlet at an angle of 107.5 degrees. Reducing this angle to 90 degrees did have an appreciable effect on the pressure distribution as shown for drop inlet A in figure 62c. However, this effect was not evident in the pressure distribution for the upper part of the drop inlet (figure 62b).

The pressure distributions shown in figures 62 and 63 can be used to determine the pressure in geometrically similar prototype spillways. The procedure to be used is described later in "Hydraulic Loading on Spillway."

Square Drop Inlets

The nondimensional pressure distribution in square drop inlets with square crests and the pressure on their crests are shown in figure 64 for the deep approach and figure 65 for the flush approach. Similar pressure distributions for square drop inlets with quarter-round crests are shown in figure 66 for the deep approach and figure 67 for the flush approach. The drop-inlet crest pressure values in figures 64a, 65a, 66a. and 67a are plotted according to equation 34. The nondimensional pressure distributions in the upper part of the drop inlet shown in figures 64b, 65b, 66b, and 67b are plotted in accordance with equation 33. The pressure distributions in the lower part of the drop inlets shown in figures 64c, 65c, 66c, and 67c are plotted according to equation 31. The data plotted for each series in figure 64 are the average value of 9 or more full-flow runs except for series 66 in which 5 runs were averaged. The data plotted for each series in figure 65 are the average value of 7 to 10 full-flow runs. The data plotted for each series in figure 66 are the average value of 9 or more full-flow runs except for series 79 and series 80 in which 6 and 7 runs, respectively, were averaged. The data plotted for each series in figure 67 are the average value of 10 full-flow runs.

The crest pressure $(\Delta P/w)/(V_R^2/2g)$ in the center of the square crest for square drop inlets in figure 64a for the deep approach and in figure 65a for the flush approach are too limited to determine the effect of crest thickness on the crest

Figure 63. Drop-inlet pressure distribution for circular drop inlets with square crests, flush approach, and the spillway flowing full

EXPLANATION

	SERIES
DROP INLET C	
O	96
⊖	97
⊕	98
⊛	99
⊖	110
⊖	111
⊕	112
⊙	113
DROP INLET D	
□	114
⊟	115
⊡	116
⬤	117
DROP INLET E	
△	90
▽	91
X	92
+	93
▲	94
▼	95

PRESSURE AT CENTER OF CREST

DROP-INLET PRESSURE DISTRIBUTION FROM CREST DOWNWARD

DROP-INLET PRESSURE DISTRIBUTION FROM BOTTOM UPWARD

$\dfrac{\Delta P/w}{V_R^2/2g}$

Figure 64 (left):

0.08

0.06

$\frac{t}{B}$

0.04

PRESSURE AT CENTER OF CREST

0.02 (a)

0 CREST

0.5

1.0

$\frac{Y}{B}$ 1.5

2.0

2.5

3.0 (b)

EXPLANATION

SERIES

DROP INLET H	
+	65
△	66
▽	124
DROP INLET J	
○	62
◻	63
●	126

DROP-INLET PRESSURE DISTRIBUTION FROM CREST DOWNWARD

2.0

1.5

$\frac{t_R - y}{D}$ 1.0

DROP-INLET PRESSURE DISTRIBUTION FROM BOTTOM UPWARD

0.5

(c)   BOTTOM

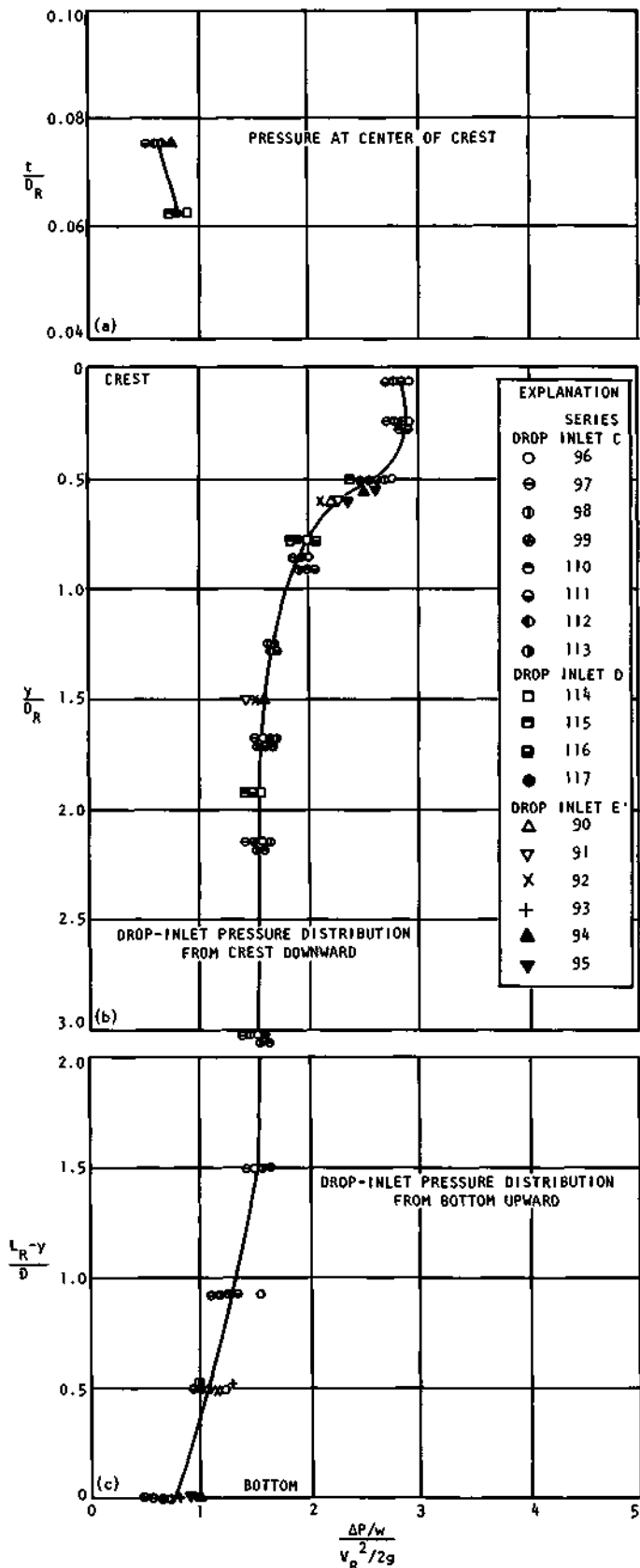0   1   2   3   4   5

$$\frac{\Delta P/w}{V_R^2/2g}$$

Figure 64. Drop-inlet pressure distribution for square drop inlets with square crests, deep approach, and the spillway flowing full

Figure 65 (right):

0.07

0.06

$\frac{t}{B}$

0.05

PRESSURE AT CENTER OF CREST

0.04 (a)

0 CREST

0.5

1.0

$\frac{Y}{B}$ 1.5

2.0

2.5

3.0 (b)

EXPLANATION

SERIES

DROP INLET H	
▲	100
◼	101
⊖	102
⊕	103

DROP-INLET PRESSURE DISTRIBUTION FROM CREST DOWNWARD

2.0

1.5

$\frac{t_R - y}{D}$ 1.0

DROP-INLET PRESSURE DISTRIBUTION FROM BOTTOM UPWARD

0.5

(c)   BOTTOM

0   1   2   3   4   5

$$\frac{\Delta P/w}{V_R^2/2g}$$

Figure 65. Drop-inlet pressure distribution for drop inlet H with square crest, flush approach, and the spillway flowing full
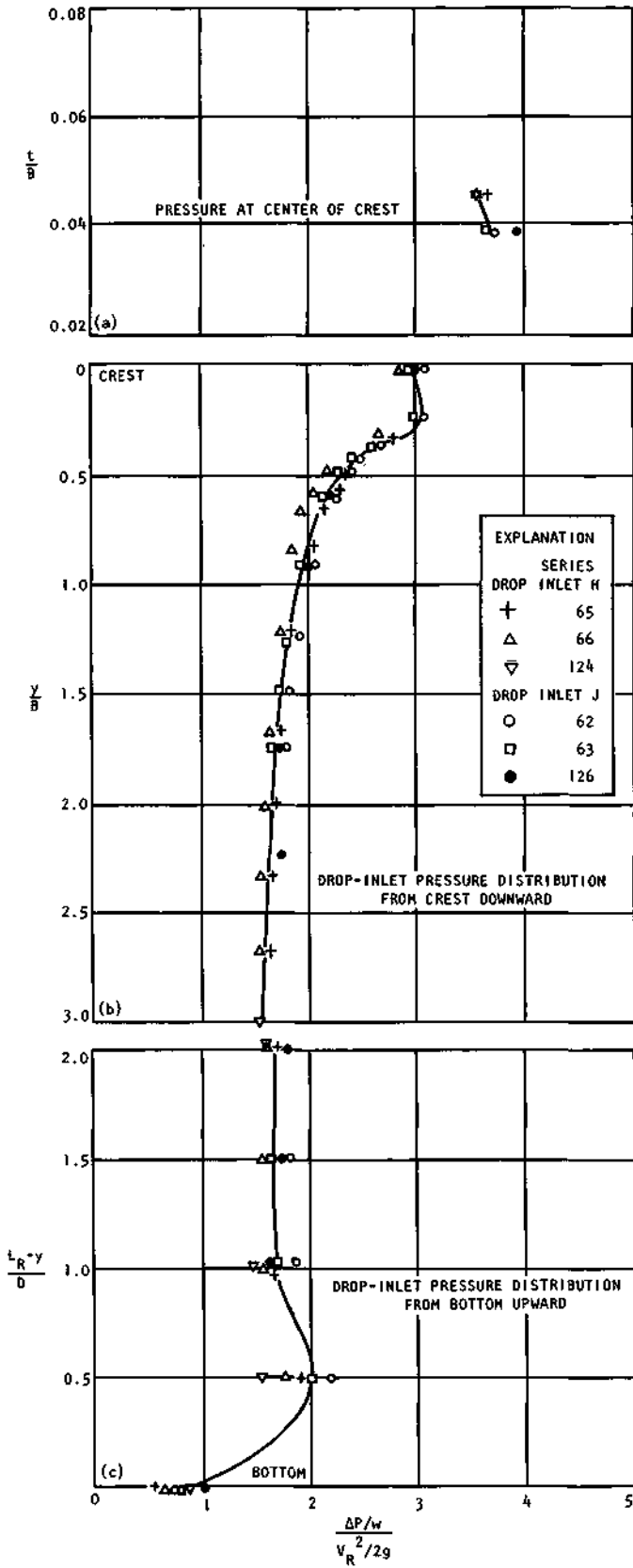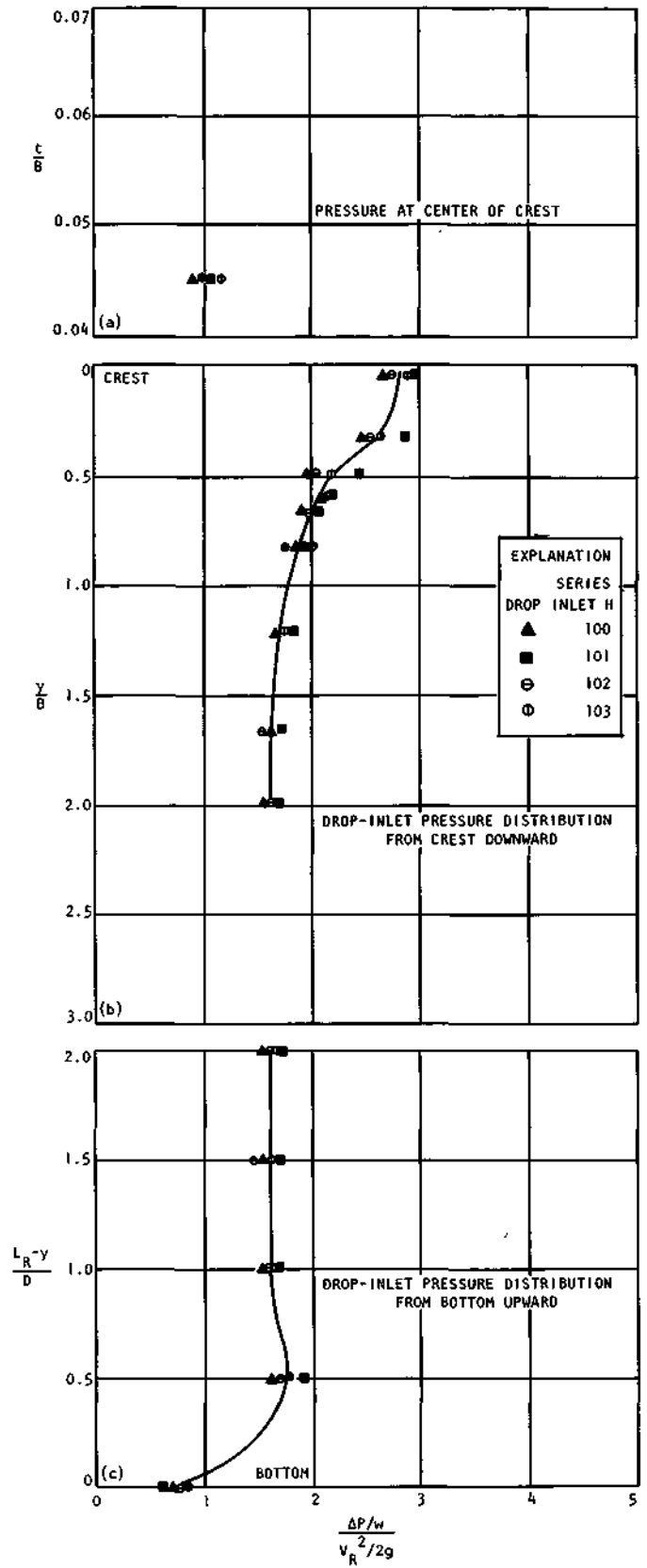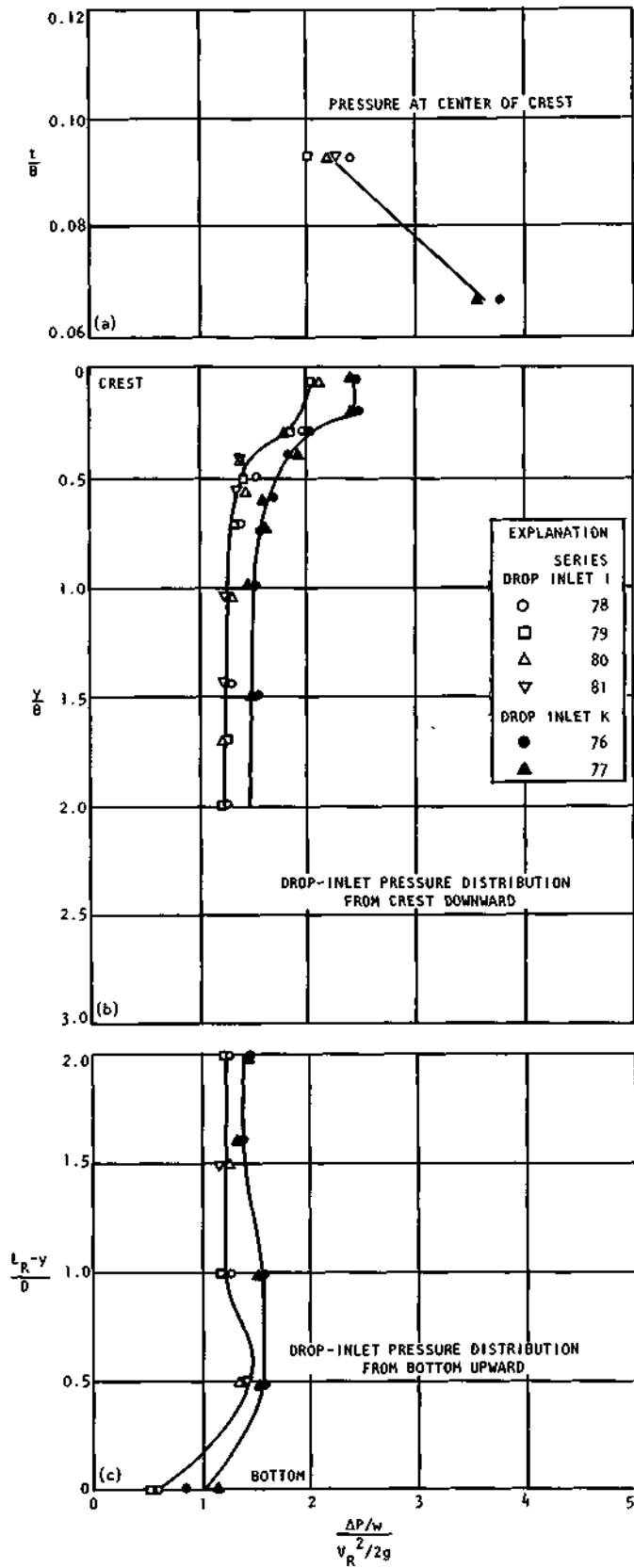
59

Figure 66. Drop-inlet pressure distribution for square drop inlets with quarter-round crest, deep approach, and the spillway flowing full
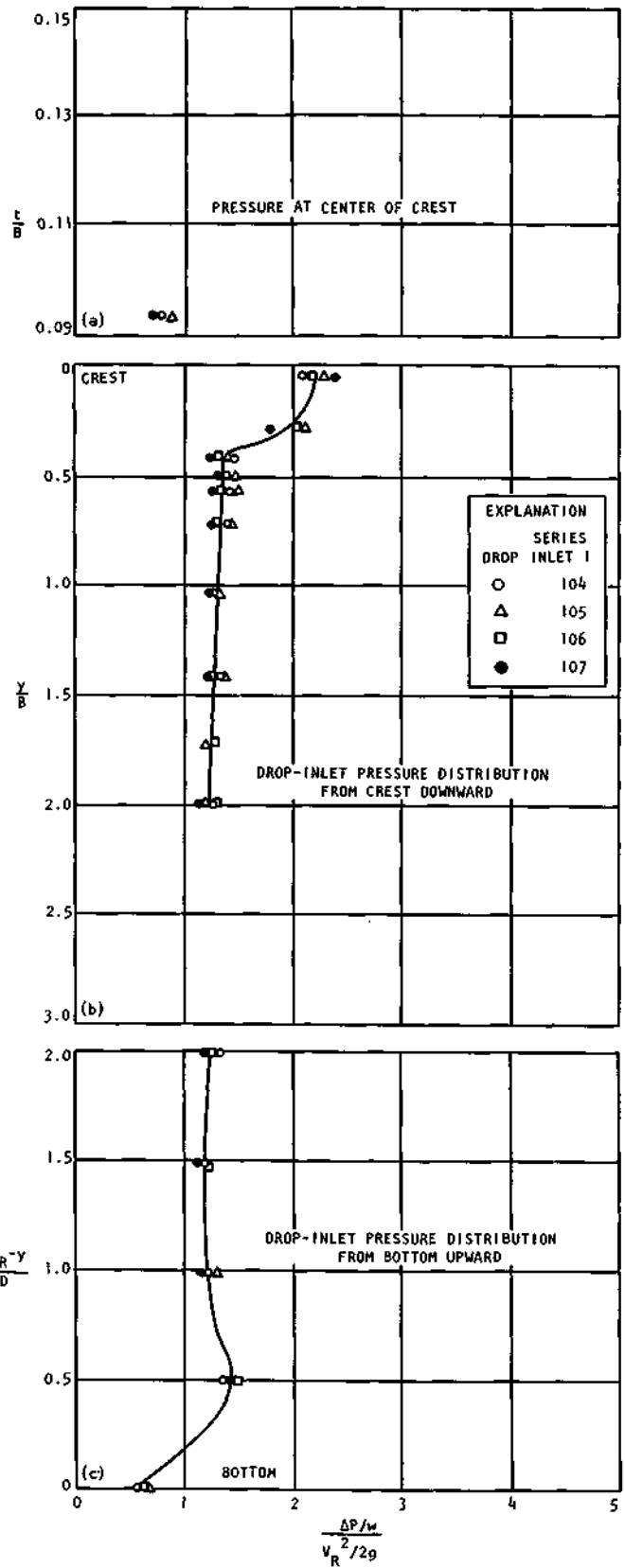
Figure 67. Drop-inlet pressure distribution for drop inlet I with quarter-round crest, flush approach, and the spillway flowing full

60

pressure. However, changing the depth of approach did substantially reduce the crest pressure for the flush approach to a value of $(P/w)/(V_B^2/2g)$ well below that obtained for the deep approach.

For square drop inlets with a quarter-round crest *(see table 1)* the crest pressure $(P/w)/(V_R^2/2g)$ in figure 66a indicates the pressure is dependent upon t/B, although the data are too limited to determine the full effects of t/B, or the rounding of the inside edge of the crest. For the flush approach the crest pressure was determined for only one crest thickness as shown in figure 67a. These limited data show that changing the depth of approach will reduce the crest pressure value of $(\Delta P/w)/(V_B^2/2g)$ obtained for the flush approach to a value well below that obtained for the deep approach.

The vertical pressure distribution in the upper and lower parts of the drop inlet shown in figures 64-67 were measured along a vertical line located on the center of the drop-inlet side. No attempt was made to measure the pressure variation in the horizontal direction across the width of the drop-inlet side. Therefore determination of the force distribution on the drop-inlet sides will be approximate when using the curves in figures 64-67.

The data in figures 64b and 64c (deep approach) for the nondimensional pressure distribution in square drop inlets with square crests and rounded transitions (table 1) scatter about each average curve drawn. However, in each case the single solid curve is representative of the pressure distribution data. The same comments apply to figures 65b and 65c for the flush approach.

A comparison of the pressure distribution curves in figures 64b and 65b for the upper part of square drop inlets with square crests shows these curves are similar although the curves are not identical for any value of y/B. The curves for the flush approach (figure 65b) for corresponding values of y/B give a value of $(\Delta P/w)/(V_B^2/2g)$ that is less than that for the deep approach (figure 64b). This decrease varies from 11 percent at $y/B = 0.25$ to approximately 4-6 percent for y/B greater than 0.4. Therefore, in the upper part of the inlet, changing the depth of approach from deep to flush had the greatest effect on the pressure distribution near the top of the drop inlet.

For the lower part of square drop inlets with square crests a comparison of the pressure distribution curves in figures 64c and 65c shows these curves are similar but not identical. The curve for the flush approach (figure 65c) for corresponding values of $(L_B - y)/D$ gives a value of $(P/w)/(V_B^2/2g)$ that is less than that for the deep approach (figure 64c). The maximum decrease is 12.5 percent at $(L_R - y)/D = 0.5$ and the smallest decrease of about 3 percent is for $(L_B - y)/D$ greater than 1.0. Therefore, in the lower part of the drop inlet, changing the depth of approach from deep to flush had the greatest effect on the pressure distribution at a distance of $(L_B - y)/D = 0.5$ above the bottom of the drop inlet.

For square drop inlets with a rounded crest and square-edged transition (table 1) the data in figures 66b and 66c (deep approach) scatter about each average curve drawn. However in each case the single solid curve is representative

of the pressure distribution data for drop inlets I and K, respectively. Separate average curves are drawn because the data for drop inlet I are consistently less than that for drop inlet K. The reason for this difference is unknown. For the flush approach each curve drawn in figures 67b and 67c for drop inlet I is representative of the data.

A comparison of the pressure distribution curves in figures 66b and 67b for the upper part of the drop inlet shows these curves are similar. The curve in figure 67b for drop inlet I (flush approach) is almost identical to the corresponding curve in figure 66b (deep approach) except for y/B less than 0.5. Therefore, in the upper part of drop inlet I, changing the depth of approach from deep to flush had an effect of ±7 percent on the pressure distribution near the top of the drop inlet. The smaller percentage occurs at $y/B = 0.4$ and the larger percentage is at $y/B = 0.1$.

For the lower part of square drop inlets with rounded crests a comparison of the pressure distribution curves in figure 66c and 67c for drop inlet I shows these curves are essentially identical. Therefore, in the lower part of the drop inlet, changing the depth of approach from deep to flush had very little if any effect on the pressure distribution.

The pressure distribution shown in figures 64, 65, 66, and 67 can be used to determine the pressures in geometrically similar prototype spillways. The procedure to be used is described later in "Hydraulic Loading on Spillway."

Rectangular Drop Inlets

The nondimensional pressure distributions in rectangular drop inlets with quarter-round crests (table 1) and the pressure on their crests are shown in figure 68 for a deep approach. The drop-inlet crest pressure values shown in figure 68a are plotted according to equation 34. The nondimensional pressure distributions on the side and upstream end in the upper part of the drop inlets shown in figure 68b are plotted in accordance with equation 33. The pressure distributions in the lower part of the drop inlets shown in figure 68c are plotted according to equation 31. The data plotted for each series in figure 68 are the average of 8 or more full-flow runs except for series 74 and 83 in which 6 and 7 runs, respectively, were averaged. The dashed curve in figure 68b is for the pressure distribution on the upstream end of drop inlet N where it deviates from the results for drop inlets L and M.

The crest pressure $(P/w)/(V_R^2/2g)$ shown in figure 68a for the side of the rectangular drop inlet was measured at a point in the crest center that was midway between the ends of the drop inlet. The crest pressure for the upstream end was measured at a point in the crest center that was midway between the sides of the drop inlet. The crest pressures on both the side and upstream end show a similar variation with t/B; however, the value of $(P/w)/(V_R^2/2g)$ is greater on the side than on the end for corresponding values of t/B.

The vertical pressure distributions on the drop-inlet side in the upper and lower parts of the drop inlet shown in figures 68a and 68b were measured on a vertical line located midway

between the drop-inlet ends. The corresponding pressure distributions on the drop-inlet upstream end were measured on a vertical line located midway between the drop-inlet sides. No attempt was made to measure the pressure variation in the horizontal direction across the length of the drop-inlet side or across the width of the end. Therefore, determination of the

force distribution on the drop-inlet sides and ends will be approximate when using the curves in figure 68.

The data in figure 68b and 68c for the nondimensional pressure distributions on the side of rectangular drop inlets scatter about the average curves drawn. However, in each case the single solid curve is representative of the data. For the drop-inlet end a single curve is satisfactory in figure 68b when y/B is less than 1.0 and $(L_R - y)/D$ is less than 1.5, but when these have values greater than 1.0 and 1.5, respectively, the data for drop inlet N (dashed curve) show a definite reduction in $(P/w)/(V_R^2/2g)$ as compared with the solid curve. This reduction is a maximum of 39 percent at $y/B = 2.5$. The reason for this difference on the drop-inlet end is unknown.

A comparison of the side and end pressure distribution curves in figure 68b for the upper part of the drop inlet shows these curves to be similar although they do not coincide. At $y/B = 0.15$ the value of $(P/w)/(V_R^2/2g)$ on the end is 32 percent greater than on the side. However, from a y/B of 0.2 to 0.7 where the curves intersect the pressure coefficient on the end varies from about +7 percent at $y/B = 0.5$ to about —9 percent at $y/B = 0.3$ of the pressure coefficient on the side. The pressure coefficient is larger on the side than on the end when y/B is greater than 0.7.

For the lower part of rectangular drop inlets the pressure distribution curves in figure 68c show the pressure coefficient on the drop-inlet side is consistently larger than on the end.

The pressure distributions shown in figure 68 can be used to determine the pressures in geometrically similar prototype spillways. The procedure to be used is described in "Hydraulic Loading on Spillway."

Circular Drop Inlets with Horizontal Antivortex Plate

The effect of the horizontal circular antivortex plate position d/D_R above the inlet crest on the dimensionless pressure in the center of the circular drop-inlet crest, the dimensionless pressure distributions in the drop inlet, and on the bottom of the antivortex plate are shown in figures 69, 70, and 71, respectively.

The dimensionless pressure data on the center of the drop-inlet crest plotted in figure 69 according to equation 37 are the average value for 9 or more full-flow runs. Although there
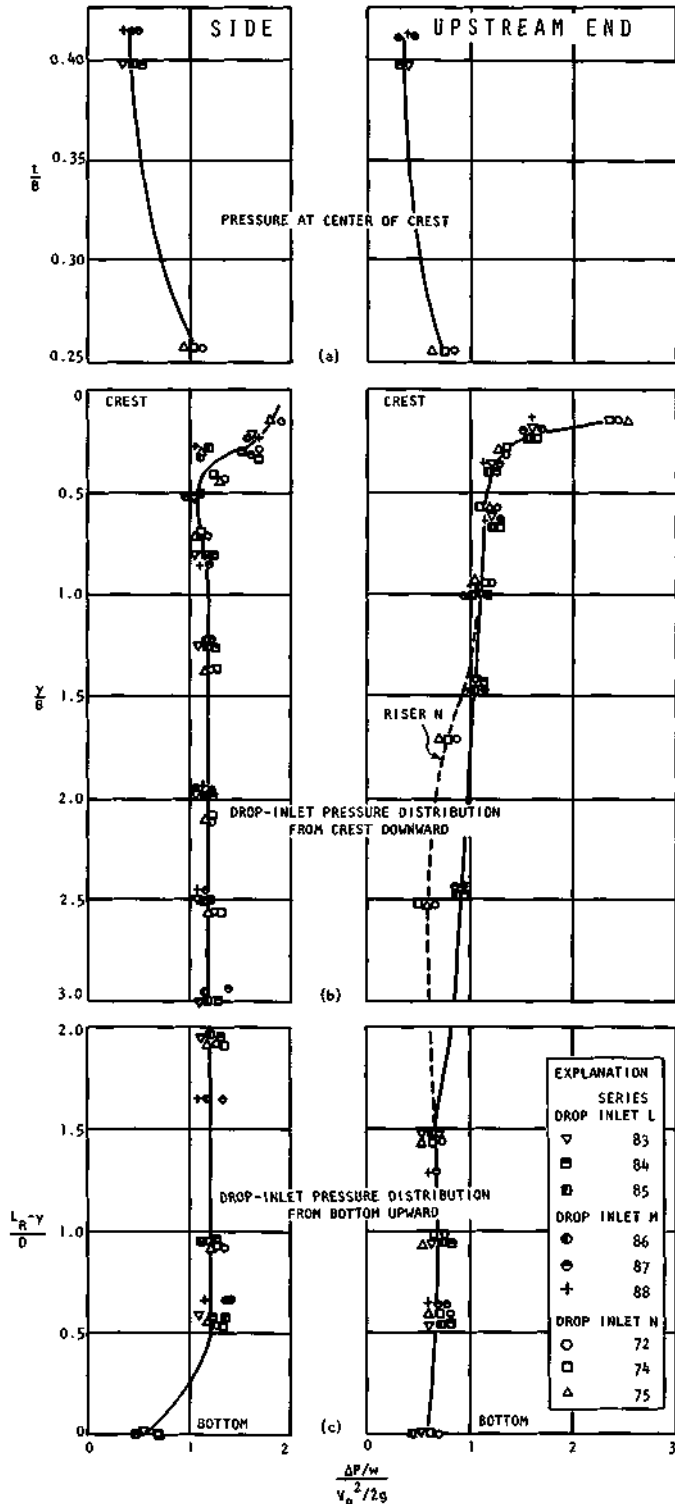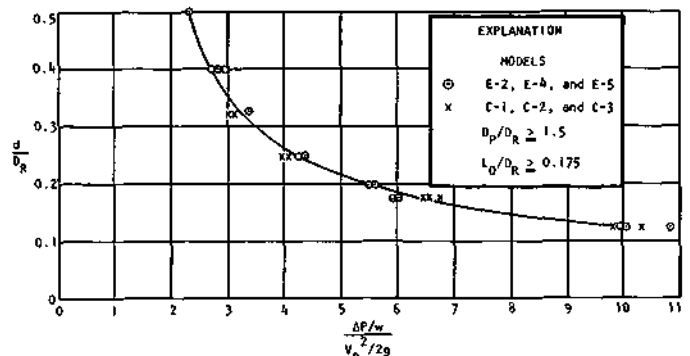
Figure 68. Drop-inlet pressure distribution for side and upstream end of rectangular drop inlets with quarter-round crest, deep approach, and the spillway flowing full

Figure 69. Effect of antivortex plate position on drop-inlet crest pressure

Figure 70. Effect of antivortex plate position on drop-inlet pressure distribution

Figure 71. Effect of antivortex plate position on the plate pressure distribution

cally similar prototypes for all values of d/D_R greater than 0.125.

The nondimensional pressure distributions on the bottom of the antivortex plate for various plate positions d/D_R above the drop-inlet crest are plotted in figure 71 in accordance with equation 38b. The data plotted for each series are the average value for 10 or more full-flow runs. The curves for d/D_R = 0.175, 0.250, and 0.500 are average experimental curves although the data for them are not shown to avoid confusion. The single curve for each d/D_R well represents the pressure distribution. The pressure coefficients $(P/w)/(V_R^2/2g)$ are large when the plate is relatively close $(d/D_R = 0.125)$ to the drop-inlet crest. Increasing the plate clearance rapidly decreases the pressure coefficients until d/D_R = 0.325. When d/D_R is larger than 0.325 the plate pressure distribution rapidly approaches a minimum pressure of approximately zero. The curves shown in figure 71 should enable the designer to determine the pressure distributions on geometrically similar prototypes for all values of d/D_R greater than 0.125.

The pressure distributions shown in figures 69, 70, and 71 can be used to determine pressure distributions in geometrically similar prototype spillways. The procedure to be used is described in "Hydraulic Loading on Spillway."

Local Pressure Deviations in Barrel

Typical average values of the nondimensional pressure coefficient $h_r/(V_B^2/2g)$ for determining the local pressure deviation in the barrel from the established barrel hydraulic grade line (friction grade line) are given in tables 10 and 11 for the deep and flush approaches, respectively. The minimum observed values of the pressure coefficient for the crown piezometer near the barrel entrance are given in tables 2, 3, 4, 6, and 8 for the deep approach, flush approach, antivortex plate, circulation tests, and for the recommended minimum

is some scatter in the data, the single curve well represents the variation in the crest pressure with the antivortex plate position d/D_R. The pressure coefficient $(P/w)/(V_R^2/2g)$ is large when the plate is relatively close $(d/D_R = 0.125)$ to the drop inlet. As the plate clearance is increased the pressure coefficient decreases with its lowest value approaching the value of $(P/w)/(V_R^2/2g)$ shown in figure 62a for drop inlets having the same t/D_R. The curve shown in figure 69 should enable a designer to determine the pressure at the center of a drop-inlet crest on geometrically similar prototypes.

The nondimensional pressure distribution in the drop inlet for various antivortex plate positions d/D_R above the inlet crest are plotted in figures 70a and 70b in accordance with equations 35 and 36. The data plotted for each series are the average value for 10 or more full-flow runs. The curves for d/D_R = 0.175 and 0.250 are average experimental curves although the data for them are not shown to avoid confusion. The single curve for each d/D_R value well represents the pressure distribution to be expected in circular drop inlets with a square-edged crest. The curve identified as "no plate" was obtained without the antivortex plate positioned above the drop inlet. The pressure coefficients $(P/w)/(V_R^2/2g)$ are large when the plate is relatively close $(d/D_R = 0.125)$ to the drop-inlet crest. Increasing the plate clearance decreases the pressure coefficients. For plate clearances larger than d/D_R = 0.325 the drop-inlet pressure distribution rapidly approaches the curve obtained when there was no plate above the drop-inlet crest. The curves shown in figure 70 should enable the designer to determine the pressure distributions in geometri-
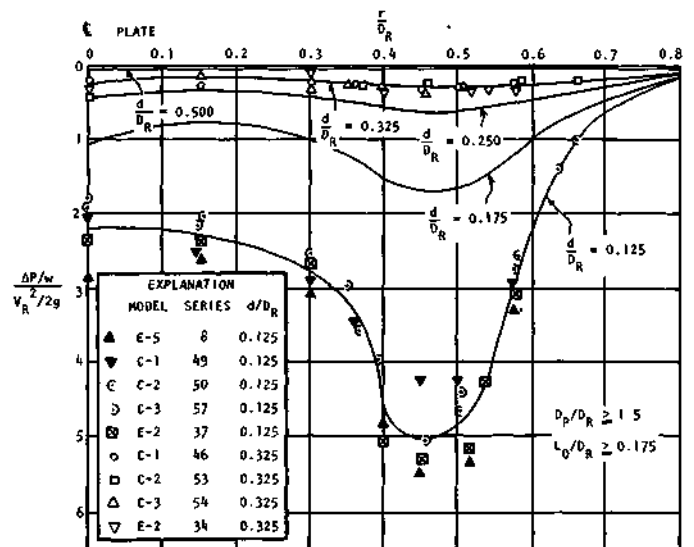
drop-inlet heights, respectively. These values were computed from experimental measurements.

The pressure coefficient values given in tables 10 and 11 show that, regardless of the geometry of the drop inlet or the depth of approach, the largest local pressure head variation in the barrel occurs near the barrel entrance. This is to be expected since the local velocity V of the flow near the barrel entrance will generally have a value different from the velocity V_B obtained farther along the barrel after uniform flow becomes established.

The magnitude of V will depend upon the degree of contraction of the flow near the barrel entrance. The degree of contraction in turn depends upon the geometry of the transition between the drop inlet and the barrel. Therefore, the magnitude of the local velocity is dependent upon this geometry. Because of this dependence upon the transition geometry the local velocity V may be less than, equal to, or larger than V_B.

The effect of the local velocity V on the pressure coefficient $h_n/(V_B^2/2g)$ is evident from an examination of equation 27. The pressure coefficient is positive when V is less than V_B and it is zero when $V = V_B$. When V is greater than V_B the pressure coefficient is negative.

The typical average pressure coefficient values given in tables 10 and 11 show that, regardless of the geometry of the drop inlet or depth of approach, uniform flow is established in the barrel at a distance of approximately $35D$ from the barrel entrance. Although the pressure coefficient in the complete barrel for the circulation and antivortex plate tests are not shown, they were, except for the crown piezometer, the same as the values given in tables 10 and 11 for drop inlets C and E.

The pressure coefficients $h_n/(V_B^2/2g)$ given in tables 2, 3, 4, 6, 8, 10, and 11 can be used with equations 26 and 27 to compute the local pressure or pressure head in the barrel of a prototype spillway.

Hydraulic Loading on Spillway

A prototype drop-inlet spillway must be structurally capable of carrying all loadings imposed on it including the hydraulic loading. There are three types of hydraulic loadings to be considered: 1) the hydrostatic load when no water is flowing into the spillway; 2) the hydraulic loading when the spillway is flowing full of water; and 3) the cavitation loading if the local pressure anywhere in the spillway is small enough for cavitation to develop. The hydrostatic load on the drop inlet can be determined from the well-established hydrostatic principles presented in standard hydraulic and fluid mechanics text books, and the reader should refer to such text books for this computation.

Full Flow

Drop Inlet and Antivortex Plate. The hydraulic load distribution on the drop inlet and on the antivortex plate can be determined with the appropriate nondimensional pressure distributions shown in figures 62-71 when the spillway is flowing full. For example, if the drop inlet is circular with a square crest and has a deep approach, the pressure distributions shown in figure 62 would be used to determine the hydraulic loading. The pressure distributions in figures 62-71 are applicable to prototype spillways that have drop-inlet heights equal to or greater than the relative heights of the models listed in table 1.

The procedure for determining the hydraulic loading on a specific drop-inlet prototype when the spillway is flowing full requires the following steps:

1) Select the figure that is applicable to the prototype geometry from figures 62-70.
2) Draw the prototype drop-inlet height, with the height as the ordinate, to a convenient scale.
3) Plot the pressure distribution shown in part b of the appropriate figure, beginning at the top of the drop inlet.
4) Plot the pressure distribution shown in part c of the figure used for step 3, beginning at the bottom of the drop inlet.
5) Check the two curves plotted in items 3 and 4; they will meet if the drop inlets have the same heights listed in table 1. For taller drop inlets, if the curves do not meet they may be joined by a straight line. The complete curve will represent the nondimensional pressure distribution in the drop inlet.

The nondimensional pressure distribution curve obtained in item 5 may be made dimensional in terms of P by multiplying the abscissa values by the quantity $w(V_R^2/2g)$.

The hydraulic loading on the antivortex plate when the spillway is flowing full can be obtained in a similar manner using the curves shown in figure 71.

Barrel. The hydraulic load distribution in the barrel can be determined using the appropriate nondimensional pressure coefficients given in tables 10 and 11 when the barrel is flowing full. For example, if the drop inlet is geometrically similar to drop inlet model D (table 1) and has a deep approach, the pressure coefficients given in table 10 for this drop inlet would be used. The pressure coefficients given in tables 10 and 11 are applicable to prototype spillways that have drop-inlet heights equal to or greater than the relative heights and drop-inlet proportions listed in table 1.

The procedure for determining the average hydraulic loading distribution in a specific barrel prototype when the barrel is flowing full is:

1) Draw the prototype barrel to a convenient scale showing its slope.
2) Compute the prototype barrel friction grade line for the zone of uniform flow and plot the line in its proper position.
3) Project the straight friction grade line established in item 2 to the barrel entrance. The projected friction grade line should be dashed between the barrel entrance and a distance of 35D along the barrel because this is the part of the barrel in which the hydraulic grade line

deviates from the friction grade line. The two lines coincide for distances along the barrel greater than 35D.

4) Locate along the barrel the piezometer locations given in table 10 or 11. The crown piezometer location for each model is given in table 2. Project these piezometer locations vertically to the friction grade line.

5) Select from table 10 or 11 the column that is appropriate for the prototype drop-inlet geometry. Plot the values of the pressure coefficients in this column for the five piezometers from the crown to 35D; plot these vertically at a convenient scale using the projected friction grade line as a base line. Plot the positive values of $h_n/(V_B^2/2g)$ vertically above the projected friction grade line and plot the negative values vertically below it. A smooth curve connecting the points plotted is the average nondimensional hydraulic grade line in the barrel between the crown piezometer and a distance along the barrel of 35D.

The curve for average nondimensional hydraulic grade line may be made dimensional in terms of h_n by multiplying the ordinate by $V_B^2/2g$. These values in feet of water would be plotted vertically from the projected friction grade line. A smooth curve connecting these points will be the dimensional hydraulic grade line along the barrel from the crown piezometer to the piezometer at a distance of 35D from the barrel entrance. The hydraulic grade line and the friction grade line coincide along the barrel for distances greater than 35D as long as there are no head losses other than the friction head loss in the barrel.

Cavitation

The nondimensional spillway pressure distribution curves for the spillway flowing full do not vary as the head on the spillway increases. Therefore, these curves do not indicate whether cavitation will occur or at what full-flow head the beginning of cavitation is a possibility. The actual minimum pressure in the spillway and the spillway head at which this minimum pressure will occur must be computed to determine if cavitation can occur.

The computation for the minimum pressure must be made separately for the drop inlet and the barrel since the pressure coefficients in the drop inlet, on the drop-inlet crest, or on the antivortex plate are given as $(P/w)/(V_R^2/2g)$ and those in the barrel are given as $h_n/(V_R^2/2g)$.

Drop Inlet and Antivortex Plate. The full-flow head at which the minimum pressure will occur at a specific point in the drop inlet can be determined from an examination of $(P/w)/(V_R^2/2g)$. For convenience the examination is made in terms of pressure head with the datum taken at the location of the point of interest in the drop inlet. This point is at a distance y below the drop-inlet crest *(see figure 8)*. At this point the nondimensional coefficient is a constant. Therefore

$$(P/w)/(V_R^2/2g) = \text{coefficient} \qquad (64)$$

In equation 64, $P = P_1 - P$ where $P_1 = h + y$. Substituting

these values in equation 64 and solving for the pressure head in the drop inlet yields

$$P/w = h + y - (V_R^2/2g) \text{ (coefficient)} \qquad (65)$$

where y is a constant.

The drop-inlet velocity head $V_R^2/2g$ will increase slowly in comparison with the head h, as h increases. In fact, in the model studies for a fivefold increase in h, the drop-inlet velocity head increased less than 12 percent and, therefore, may be considered a constant for this discussion. Since y and $V_R^2/2g$ are constant, the pressure head P/w at the point y in the drop inlet will be a minimum at the smallest full-flow head.

The minimum pressure head in the drop inlet can be computed using equation 65 and the nondimensional pressure distribution curve discussed in item 5 for drop inlets under full flow *(see page 64)*. For this computation the minimum full-flow head h would be a known constant. Therefore, the minimum pressure head will occur at the point in the drop inlet where the value of $[y - (V_R^2/2g) \text{ (coefficient)}]$ is a minimum. The minimum value of this quantity will occur near the point where the pressure coefficient is a maximum. Once the location of the minimum pressure head is determined equation 65 is used to compute the minimum pressure head in the drop inlet.

A similar analysis of equation 64 for the pressure head on the drop-inlet crest yields

$$P/w = h - (V_R^2/2g) \text{ (coefficient)} \qquad (66)$$

where the coefficient is the nondimensional pressure coefficient selected from the figure applicable to the prototype geometry from figures 62-69. The minimum pressure head on the crest occurs, as in the drop inlet, at the smallest full-flow head.

The equation for the pressure head on the antivortex plate, determined from an analysis similar to that for the drop inlet pressure head is

$$P/w = h - d - (V_R^2/2g) \text{ (coefficient)} \qquad (67)$$

where the coefficient is the nondimensional pressure coefficient selected for the point of interest on the plate from figure 71 for the specific plate elevation above the drop-inlet crest. The minimum pressure head at any position on the plate occurs, as in the drop inlet, at the smallest full-flow head. Therefore, the minimum pressure head on the plate will occur at the point where the nondimensional pressure coefficient is largest.

The minimum pressure head in the drop inlet, on the drop-inlet crest, and on the antivortex plate can be computed from equations 65, 66, and 67, respectively. Each of these three pressure heads can, depending upon the magnitudes of the drop-inlet velocity head and the nondimensional pressure coefficient, have a value less than the atmospheric pressure head. That is, the local pressure head would be negative. If the local pressure head has a value about —20 feet of water or less, cavitation is a definite possibility, since no factor of safety is included in equations 65, 66, and 67. Therefore, when the local pressure head is a relatively large negative value, the drop inlet should be redesigned to raise the local pressure head to a cavitation-free value. This may be accomplished by increasing the horizontal dimensions of the drop inlet to reduce the drop-inlet velocity head.

Barrel. The full-flow discharge at which the minimum pres-

sure will occur at a specific location in the barrel can be determined from an examination of equations 26 and 27. For convenience the examination is made in terms of the pressure head at the specific point of interest. Equating the left side of equation 26 to that of equation 27 and solving for P/w, the pressure head at a specific point in the barrel, yields

$$P/w=[h_n/(V_B^2/2g)] \quad (V_B^2/2g) + (\ D-D/2)\cos + (P_0/w) +z_0-z + \qquad h_L \qquad (68)$$

where the barrel pressure coefficient $h_n/(V_B^2/2g)$ is constant. Also, the quantities D, $\cos$, P_0/w, z_0, and z are constant for a particular closed conduit barrel. For a specific drop inlet closed-conduit spillway, a single value of would be selected for design; therefore may be considered constant for this discussion. The term h_L can be expressed as the sum of all the head-loss coefficients between the point in the barrel where the pressure is desired and the barrel exit, times $V_B^2/2g$. This summation of head-loss coefficients will be essentially constant for a specific drop inlet closed-conduit spillway. Therefore, the minimum pressure head P/w at this point will occur when $V_B^2/2g$ is a minimum, which is when the spillway first flows full of water.

The minimum pressure head computed from equation 68 for various points of interest in the barrel may be positive, that is, larger than the atmospheric pressure head, or it may be negative. If the local pressure head is less than atmospheric, cavitation can occur. Therefore it is necessary to compute the minimum pressure head in the barrel. The location of this minimum pressure head in the barrel can be readily determined by considering the position of the hydraulic grade line relative to the barrel.

The position of the hydraulic grade line relative to the barrel depends upon whether the barrel is on a mild or steep slope. The hydraulic grade line and the friction grade line coincide in the zone of established flow; therefore, if the slope of either line is equal to or greater than the barrel slope, the barrel is on a *mild slope.* If, however, the slope of either line is less than the barrel slope, the barrel is on a *steep slope.*

For a barrel on a *mild slope* the pressure head in the barrel will be equal to or greater than the atmospheric pressure head if the nondimensional pressure coefficient $h_n/(V_B^2/2g)$ is positive (model E, table 10), since the hydraulic grade line position will then either coincide with the barrel or be above it. Therefore, cavitation cannot occur for this condition of positive pressure head in the barrel.

However, if the pressure coefficient near the barrel entrance is negative (model L, table 10), the hydraulic grade line would be below the projected friction grade line near the barrel entrance. In this case the hydraulic grade line, depending upon the magnitude of the pressure coefficient and the barrel velocity head, could be below the barrel creating the lowest pressure head in the barrel. The lowest pressure head computed by equation 68, when the hydraulic grade line is below the projected friction grade line, will occur just after the spillway flows full of water and when the pressure coefficient is a minimum. Therefore, the minimum observed pressure coefficient for the crown piezometer located near the barrel entrance should be used rather than the average values given

in tables 10 or 11. The minimum observed pressure coefficient for this crown piezometer used to compute the minimum pressure head should be selected for geometrically similar prototype spillways from the values given in tables 2, 3, 4, 6, or 8. If the computed crown pressure head has a value less than about —20 feet of water, cavitation is a definite possibility.

For a barrel on a *steep slope (see figure 7)* the friction grade line as well as the hydraulic grade line will be below the barrel. The largest distance between the barrel and the friction grade line will occur near the barrel entrance. Therefore, this is the part of the barrel that will always experience the lowest pressure head. The lowest pressure head computed by equation 68 will occur just after the spillway flows full of water and when the pressure coefficient is a minimum. Therefore, the minimum observed pressure coefficient for the crown piezometer located near the barrel entrance should be used rather than the average values given in table 10 or 11. The minimum observed pressure coefficients for this crown piezometer used to compute the minimum pressure head should be selected for geometrically similar prototype spillways from the values given in tables 2, 3, 4, 6, or 8. If this crown pressure head has a value of about —20 feet of water or less, cavitation is a definite possibility.

Comments on Barrel Pressure Head. The pressure head in a prototype spillway barrel can be computed from equation 68. The computed pressure head can, depending upon the position of the hydraulic grade line relative to the barrel, have a value greater than, equal to, or less than the atmospheric pressure head. If the hydraulic grade line is above the barrel, the barrel pressure head is equal to or greater than the atmospheric pressure head, and cavitation cannot occur. Therefore, when considering cavitation the negative pressure head is the one of concern. The negative pressure head in the barrel occurs when the hydraulic grade line position is below the barrel, and the location of the minimum pressure head will be near the barrel entrance. If the minimum local pressure head near the barrel entrance is less than about —20 feet of water, cavitation is a definite possibility since no factor of safety is included in equation 68.

When cavitation possibilities are of concern, the spillway must be redesigned to raise the local pressure head to a cavitation-free value by raising the hydraulic grade line position relative to the barrel. Among the ways this may be accomplished are lowering the barrel, using a rougher barrel, increasing the barrel length, and decreasing the barrel diameter.

Hydraulic Grade Line Location at Barrel Exit

The location of the hydraulic grade line at the barrel outlet for the barrel flowing full and the flow freely discharging from the barrel outlet was computed from experimental measurements. The hydraulic grade line (friction grade line) determined for the barrel in the zone of established flow was extended to the plane normal to the barrel axis at the barrel outlet. The elevation of the hydraulic grade line in this plane was computed. The difference between this elevation and the elevation
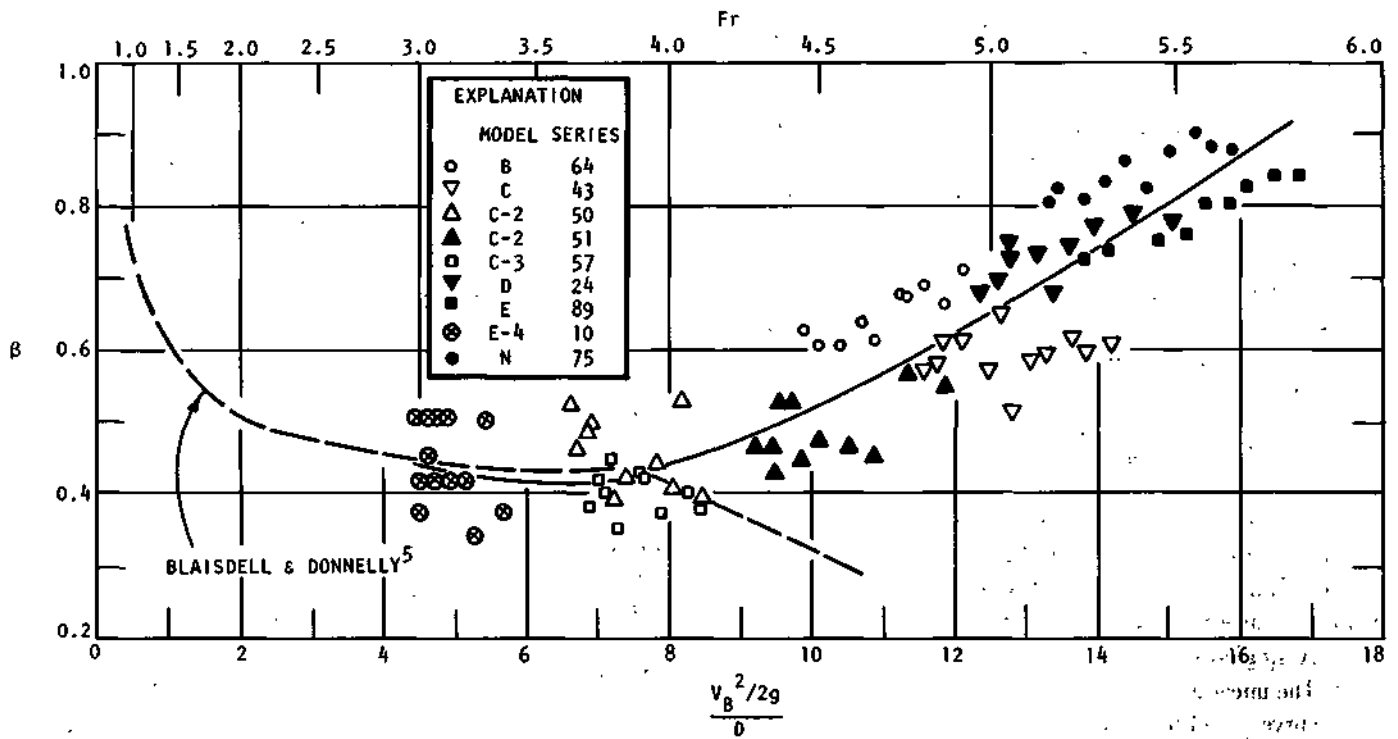
Figure 72. Position of the hydraulic grade line at barrel outlet for the barrel flowing full and discharging freely into the atmosphere

of the barrel invert at the outlet was divided by $D\cos$ to obtain the nondimensional value of . Typical test values of are plotted in figure 72. Although there is some scatter in the data the single solid curve well represents the variation of with $(V_B^2/2g)/D$ or the Froude number, Fr, which is defined as $Fr = V_B/(gD)^{1/2}$.

The dashed curve in figure 72 obtained by Blaisdell and Donnelly[5] is shown for reference. The data for this curve were obtained experimentally for a smooth circular barrel in the same manner as the data for the authors' solid curve. The dashed curve shows a sharp break from the smooth dashed curve at $(V_B^2/2g)/D = 7.8$. Concerning this break Blaisdell and Donnelly state: "The curve defined by the data is quite regular except for the steepest conduit slope. No firm explanation for this deviation is available, although the waste receiver

may have caused a reduction in the pressure at the conduit exit." This would lead one to believe that for this part of their curve the barrel was not discharging freely into the atmosphere. Therefore, the dashed curve for values of $(V_B^2/2g)/D$ greater than 7.8 will be disregarded. The dashed and solid curves are nearly identical for $(V_B^2/2g)/D$ values from 4.4 to 7.8, and from a practical standpoint either curve represents this part of the data.

The position of the extended hydraulic grade line (friction grade line) at the barrel outlet for the barrel flowing full and discharging freely into the atmosphere is shown in figure 72 to be a function of $(V_B^2/2g)/D$ or the Froude number. The smooth dashed and solid curves show that the location of the hydraulic grade line at the barrel exit may be, depending upon the magnitude of $(V_B^2/2g)/D$, above or below the barrel center line.

SUMMARY

The model test results presented in this report can be used to determine the head-discharge curves for geometrically similar prototype spillways. The drop-inlet models listed in table 1 exhibited only weir-flow and • full-flow control when an anti-vortex device was positioned on the drop-inlet crest. None of these drop inlets exhibited orifice or short-tube flow conditions.

The effects of vortices on the spillway performance have been demonstrated. The development of these vortices was a natural flow phenomenon since their formation was neither inhibited nor forced. The spillway discharge or head at which

a vortex will naturally form is unpredictable. The naturally formed vortex can be strong and seriously affect the spillway performance and reduce the spillway capacity, or the vortex can be so weak that it does not affect the spillway performance or capacity.

To determine when an antivortex device on a drop-inlet spillway is required for satisfactory hydraulic performance necessitates plotting, as shown in figure 25, equation 50 for the weir-flow curve, equation 52 for the vortex-envelope curve, and the full-flow curve assuming a vortex is not present. If

67

the full-flow curve intersects the weir curve to the left of the weir curve and vortex-envelope curve intersection, the resulting head-discharge curve will be single-valued and predictable with or without an antivortex device. Conversely, if the full-flow curve intersects the weir curve to the right of the weir curve and vortex-envelope curve intersection, an effective antivortex device is needed to obtain a single-valued and predictable head-discharge curve. If an antivortex device is needed and it is not provided, the head-discharge curve composed of the weir-control curve, the vortex-envelope curve, and the full-flow curve above the vortex-envelope curve will represent the minimum performance that can be expected for a drop-inlet spillway. This method is applicable to similar prototype spillways with the drop-inlet height equal to or greater than the relative heights listed in table 8. The method should also be applicable to the spillway proportions listed in table 9, to the Stillwater prototype, and to the Grave Creek model.

The advantages of fully controlling the vortex formation at the entrance to drop-inlet spillways are:

1) A single-valued head-discharge curve is obtainable.
2) The uncertainties of vortex effects on the head-discharge curve are eliminated.
3) Considerable savings by the construction of lower dams should be possible.

The horizontal circular plate with guide vanes is shown to be an effective antivortex device when the plate is properly positioned above the drop-inlet entrance. This plate can significantly reduce the head necessary for the spillway to prime and flow full of water when compared with the priming head at the usual intersection of the weir- and full-flow curves. This head reduction or lowering of the reservoir level occurs in the normal weir-flow range, and large increases in the spillway discharge are obtained for very small increases in the reservoir elevation. The capacity of the spillway with a circular drop inlet for plate-flow control is given by equation 62.

The capacity of the spillway acting as a weir is given by equation 2 or equation 50. The recommended equation for determining the weir-discharge coefficients, C_w, and their head range limitations are listed in table 7 for the drop-inlet models listed in table 1.

The head-loss coefficients for the spillway flowing full are given in table 2 for the deep approach, in table 3 for the flush approach, in table 4 for the horizontal antivortex plate, in table 6 for the circulation tests, and in table 8 for the recommended minimum drop-inlet heights.

The pressure distribution, hydraulic loading, and cavitation potential in the complete spillway or on the antivortex plate can be determined from the nondimensional pressure coefficients presented.

The nondimensional pressure coefficients for the drop inlets without an antivortex plate are given in figures 62, 64, 66, and 68 for the deep approach, and in figures 63, 65, and 67 for the flush approach. The pressure coefficients for circular drop inlets with an antivortex plate are given in figures 69, 70, and 71.

Typical average nondimensional pressure coefficients for the barrel are given in table 10 for the deep approach and in table 11 for the flush approach. The minimum observed pressure coefficients for a barrel crown piezometer located near the barrel entrance are given in table 2 for the deep approach, in table 3 for the flush approach, in table 4 for the antivortex plate, in table 6 for the circulation tests, and in table 8 for the recommended minimum drop-inlet heights.

Normally developed circulation of the flow around the drop-inlet entrance for the deep and flush approaches has an insignificant effect on the spillway capacity in the weir- and full-flow ranges when the formation of vortices at the drop-inlet entrance is controlled. Therefore, the location in a reservoir of a drop-inlet entrance to a closed-conduit spillway should not affect the spillway performance.

The position of the hydraulic grade line at the barrel exit for the barrel flowing full and discharging freely into the atmosphere varies with $(V_B^2/2g)/D$. The position of the hydraulic grade line at the exit of a smooth barrel can be determined from figure 72.

REFERENCES

1 Blaisdell, Fred W. 1952. *Hydraulics of closed conduit spillways: Part I, Theory and its applications.* U.S. Department of Agriculture, Agricultural Research Service, University of Minnesota, St. Anthony Falls Hydraulic Laboratory. Technical Paper 12, Series B (revised February 1958).

2 Rouse, Hunter. 1946. *Elementary mechanics of fluids.* John Wiley & Sons, Inc., New York, 376 p.

3 Blaisdell, Fred W., and Harold W. Humphreys. 1959. A discussion of "Some Experiments with Emergency Siphon Spillways" by Warren B. McBirney. Proceedings American Society of Civil Engineers Journal of Hydraulics Division v.84(Hy4) :103-108.

4 Rouse, Hunter. 1950. *Fundamental principles of flow* (chapter 1). *In* Engineering Hydraulics, by Hunter Rouse (ed.), John Wiley & Sons, Inc., New York.

5 Blaisdell, Fred W., and Charles A. Donnelly. 1958. *Hydraulics of closed conduit spillways: Part X, The hood inlet.* U.S. Department of Agriculture, Agricultural Research Service, University of Minnesota, St. Anthony Falls Hydraulic Laboratory. Technical Paper 20, Series B.

6 Illinois State Water Survey. 1955. *Hydraulic laboratory research facilities of the Illinois State Water Survey.* Circular 48.

7 Lansford, Wallace M. 1936. *The use of an elbow in a pipe line for determining the rate of flow in the pipe.* University of Illinois Engineering Experiment Station. Bulletin 289.

8 Humphreys, Harold W. 1967. *Circulation-effects on performance of closed-conduit spillways with drop-inlet entrance.* Transactions of the American Society of Agricultural Engineers v.10(1):116-122.

9 Blaisdell, Fred W. 1958. *Hydraulics of closed conduit spillways, II through VII: Results of tests on several forms of the spillway.* U.S. Department of Agriculture, Agricultural Research Service, University of Minnesota, St. Anthony Falls Hydraulic Laboratory. Technical Paper 18, Series B.

10 Blaisdell, Fred W. 1958. *Hydraulics of closed conduit spillways: Part VIII, Miscellaneous laboratory tests; Part IX, Field tests.* U.S. Department of Agriculture, Agricultural Research Service, St. Anthony Falls Hydraulic Laboratory, Technical Paper 19, Series B.

11 Rahm, Lennart. 1953. *Flow problems with respect to intakes and tunnels of Swedish hydro-electric power plants.* Transactions of the Royal Institute of Technology, Stockholm, Sweden, No. 71, p. 103-117.

NOTATIONS

A_0 = area of orifice in square feet

A_B = area of barrel in square feet

A_R = horizontal area of drop inlet in square feet

b = ordinate intercept of plate flow head-discharge curve, nondimensional

B = inside width of square drop inlet or inside width of rectangular drop inlet in feet

c = ratio of horizontal length to width of rectangular drop inlet, nondimensional

C = weir-discharge coefficient in $(feet)^{1/2}$per second, $C = C_w(2g)^{1/2}$

C_w = weir-discharge coefficient, nondimensional

C_0 = orifice-discharge coefficient, nondimensional

C_8 = short-tube discharge coefficient, nondimensional

d = elevation of the bottom of the antivortex plate above the drop-inlet crest in feet

D = barrel diameter in feet

D_{av} = average barrel diameter in feet

Dp = antivortex plate diameter in feet

D_B = circular drop inlet inside diameter in feet

f = Darcy-Weisbach resistance coefficient in barrel, nondimensional

f_R = Darcy-Weisbach resistance coefficient in drop inlet, nondimensional

Fr = Froude number in barrel, nondimensional

g = acceleration of gravity in feet per second per second

h = head on drop-inlet crest in feet

H_E = drop-inlet entrance head loss in feet

h_f = barrel head loss in feet

h_n = local deviation of the hydraulic grade line in the barrel from the projected hydraulic friction grade line in feet

H_8 = head on short tube in feet

H_T = drop-inlet transition head loss in feet

k = ratio of weir crest length to a characteristic drop-inlet dimension. Example, for a circular drop inlet with a square crest, $k = \quad = L_C/D_R$, nondimensional

K_E = drop-inlet entrance head-loss coefficient, nondimensional

K_R = combined drop-inlet entrance and transition head-loss coefficient, nondimensional

K_T = drop-inlet transition head-loss coefficient, nondimensional

L = barrel length in feet

L_c = weir crest length in feet

L_0 = distance antivortex plate overhang extends beyond outside edge of drop inlet in feet

L_R = height of drop inlet in feet

m = slope of plate flow head-discharge curve, nondimensional

P = pressure at a point in the flow in the barrel, in the drop inlet, or on the antivortex plate in pounds per square foot

P_0 = pressure at barrel exit in pounds per square foot

P_1 = reference pressure in reservoir in pounds per square foot

AP = pressure difference at the same elevation between the reference pressure in the reservoir and the pressure in the drop inlet or on the antivortex plate. $P = P_1 — P$ in pounds per square foot

Q = discharge through spillway in cubic feet per second

Q = rate of change in storage in test tank in cubic feet per second

r = radial distance from center of antivortex plate or from vertical axis of vortex in feet

r_1 = radial distance from vertical axis of vortex at the limit of the vortex influence in feet

R = hydraulic radius, ratio of flow area to wetted perimeter, in feet

R_R = Reynolds number in drop inlet, nondimensional

R_B = Reynolds number in barrel, nondimensional

t = drop inlet crest thickness in feet

V = velocity at a point in the flow or tangential velocity of vortex in feet per second

V_1 = tangential velocity of vortex at limit of the vortex influence in feet per second

V_B = average velocity in barrel in feet per second

V_R = average velocity in drop inlet in feet per second

w = unit weight of water in pounds per cubic foot

y = distance vertically downward from drop-inlet crest to a point inside the drop inlet in feet

z = elevation of point in flow or point on vortex surface in feet

Z_1 = elevation of vortex free surface at the limit of the vortex influence in feet

z_0 = elevation of barrel exit center line in feet

Z = elevation of drop-inlet crest above center line of barrel outlet in feet

a = kinetic energy correction factor, nondimensional

= proportional part of barrel diameter above the barrel invert where the hydraulic grade line pierces the plane normal to the barrel axis at the barrel exit, nondimensional

T = circulation constant for a free vortex in feet squared per second

= slope of barrel in degrees

= ratio of drop-inlet horizontal area to the length of the drop-inlet weir crest in feet

v = kinematic viscosity in feet squared per second

= 3.1416

h_L — summation of all head losses between point 'a' in the barrel and barrel exit in feet

ø = function of